This is the peer reviewed author accepted manuscript (post print) version of a published work that appeared in final form in:

Pan, Baizhao, Liu, Feng, Zhuge, Yan, Zeng, Jun Jie, Liao, Jin Jing 2022 'ECCs/UHPFRCCs with and without FRP reinforcement for structural strengthening/repairing: a state-of-the-art review', Construction and Building Materials, vol. 316, pp. 1-30

This output may not exactly replicate the final published authoritative version for which the publisher owns copyright. It is not the copy of record. This output may be used for non-commercial purposes. This version is licensed under a Creative Commons CC-BY-NC-ND 4.0 license ( http://creativecommons.org/licenses/by-nc-nd/4.0/).

The final definitive published version (version of record) is available at: 10.1016/j.conbuildmat.2021.125824

Persistent link to the UniSA Research Outputs Repository: 11541.2/26624

General Rights

Copyright and moral rights for the publications made accessible in the UniSA Research Outputs Repository are retained by the authors and/or other copyright owners and it is a condition of accessing publications that users recognize and abide by the legal requirements associated with these rights.

- Users may download and print one copy for the purpose of private study or research.
- You may not further distribute the material or use it for any profit-making activity or commercial gain
- You may freely distribute the persistent link identifying the publication in the UniSA Research Outputs Repository

If you believe that this document breaches copyright, please contact us and provide details. We will remove access to the work immediately and investigate your claim.

Manuscript (For revision, upload clean version of revised paper) Click here to view linked References

# ECCs/UHPFRCCs with and without FRP Reinforcement for Structural Strengthening/Repairing: A State-of-the-Art Review

Baizhao Pan[a#], Feng Liu[b], Yan Zhuge[c], Jun-Jie Zeng[d#,*], JinJing Liao[e]

[a] Master Student, School of Civil and Transportation Engineering, Guangdong University of Technology, Guangzhou 510006, China.
[b] Professor, School of Civil and Transportation Engineering, Guangdong University of Technology, Guangzhou 510006, China.
[c] Professor, UniSA STEM, University of South Australia, South Australia 5095 Australia.
[d] Professor, School of Civil and Transportation Engineering, Guangdong University of Technology, Guangzhou 510006, China.
[e] Postdoctoral Fellow, School of Civil and Transportation Engineering, Guangdong University of Technology, Guangzhou 510006, China.
[#]Baizhao Pan and Jun-Jie Zeng contributed equally to this work.
*Corresponding author. E-mail: jjzeng@gdut.edu.cn (Jun-Jie Zeng).

**Abstract:** High-performance cementitious composites, such as engineered cementitious composites (ECCs) with strong tensile strain-hardening behavior or ultra-high performance fiber-reinforced cementitious composites (UHPFRCCs) with excellent compressive behavior, have been widely used in civil engineering. In cases that UHPFRCC strengthening layer without internal reinforcement has an inferior average ultimate tensile stress to UHPFRCC strengthening layer with internal reinforcement, fiber-reinforced polymer (FRP) bar/grid can be adopted as internal tension reinforcement. This paper presents a state-of-the-art comprehensive review on the characteristics and application of high-performance cementitious composites with and without FRP grid reinforcement. This review discusses the feasibility of application of ECC/UHPFRCC to structural strengthening/repairing, and concludes that FRP grid-reinforced ECC/UHPFRCC exhibits better potential than ECC/UHPFRCC in improving mechanical performance of composite structures. Finally, the application prospect and future research on FRP grid-reinforced ECC/UHPFRCC are identified.

**Keywords:** engineered cementitious composites (ECCs), ultra-high performance fiber-reinforced cementitious composites (UHPFRCCs), fiber-reinforced polymer (FRP), FRP grid-reinforced ECC/UHPFRCC

**Contents**


1. Introduction
2. ECCs and UHPFRCCs: Raw material, Characteristic and Application
    - 2.1 Raw material and Mechanical Properties of ECCs
    - 2.2 Raw material and Mechanical Properties of UHPFRCCs
        - 2.2.1 UHPC
        - 2.2.2 UHP-ECC
    - 2.3 Bond behavior between ECCs/UHPFRCCs and concrete substrate
        - 2.3.1 ECC-to-concrete interface
        - 2.3.2 UHPFRCC-to-concrete interface
    - 2.4 Durability of ECC/UHPFRCCs
    - 2.5 Applications of ECCs and UHPFRCCs
        - 2.5.1 RC beams strengthened with ECCs/UHPFRCCs
        - 2.5.2 RC columns strengthened with ECCs/UHPFRCCs
        - 2.5.3 ECC/UHPFRCC permanent formwork
        - 2.5.4 Repairing structures using ECCs/UHPFRCCs
        - 2.5.5 Structural elements
3. FGREM/FGRUM: Application and Mechanical Behavior
    - 3.1 Flexural Strengthening
        - 3.1.1 Flexural behavior of RC beams strengthened with FGREM
        - 3.1.2 The analytical models for flexural capacity
    - 3.2 Shear Strengthening
        - 3.2.1 Shear behavior of RC beams strengthened with FGREM/FGRUM
        - 3.2.2 Existing predictive models for shear capacity
    - 3.3 Confined Concrete Column
        - 3.3.1 Axial behavior of concrete columns confined with FGREM/FGRUM
        - 3.3.2 Existing peak stress models
    - 3.4 Comparison on ECC and UHPFRCC on effects of strengthening
    - 3.5 Novel FRP-ECC/UHPFRCC composite structures
    - 3.6 Theoretical Models for FRP-ECC/UHPFRCC Strengthened Structures
4. Conclusions
5. Future Research Opportunities

## 1. Introduction

Fiber-reinforced polymer (FRP) composites are a kind of high performance material with superior durability and mechanical properties [1-6], and has been widely used in civil engineering. Externally-bonded FRP strengthening system is one of the most common techniques for strengthening reinforced concrete (RC) structures. However, externally-bonded FRP strengthening systems have some disadvantages [7,8]: 1) a relatively poor bond performance between the concrete substrate and the FRP layer; 2) a poor behavior of epoxy resin at high temperature, especially when the temperature is higher than the glass transition temperature; 3) incompatibly of epoxy resins with the substrate material.

In recent years, researchers have proposed fabric-reinforced cementitious matrix (FRCM) strengthening systems to be the alternative to externally-bonded FRP strengthening systems. FRCM is a class of cementitious composites with dry fiber textiles or FRP/fiber textile grids embedded in cementitious matrix (see Fig.1). Many experimental studies have been carried out to confirm the effectiveness of FRCM strengthening systems for flexural and shear strengthening of RC beams [9-15] and confinement of RC columns [16-19]. Moreover, it has been proved that the strengthening efficiency of resin-impregnated FRP grid-reinforced cementitious matrix (FGRCM) is much better than that of un-impregnated fiber textile-reinforced cementitious matrix [10,20]. The excellent strengthening efficiency of FGRCM is mainly due to improved bond between the concrete substrate and strengthening systems provided by mechanical interlocking effect of the bidirectional FRP strips in grids.

Engineered cementitious composites (ECCs), also known as ultra-high toughness cementitious composites (UHTCCs), is a class of high-performance fiber-reinforced cementitious composites (HPFRCCs). Owing to the addition of fibers, ECCs can exhibit a large tensile strain capacity ranging from 3% to 8%, with the advantages of high fracture toughness, high tensile strength, high cracking resistance and superior durability [21-30]. Structures strengthened/repaired with ECC have an excellent corrosion resistance because invasion of corrosive media is effectively postponed due to the protection of the durable ECC jackets, which generally experience favorite multiple microcracking under tension [31-33]. However, ECCs have a relatively low compressive strength closed to that of conventional concrete. Recently, some advanced ultra-high performance fiber-reinforced cementitious composites (UHPFRCCs) were developed to improve the compressive strength of fiber-reinforced concrete while maintaining the high tensile strength and ductility, such as ultra-high

performance concrete (UHPC) and ultra-high performance engineered cementitious composite (UHP-ECC). Both UHPC and UHP-ECC generally has a compressive strength over 120 MPa [34-37], and a tensile strength over 7 MPa [35,37-40]. With the advantages of ultra-high compressive strength coupled with excellent tensile properties and high durability, UHPFRCCs is a promising material for creating a lightweight and durable permanent formwork [41,42] or strengthening RC structures [43]. Recently, FRP grid-reinforced ECC matrix and FRP grid-reinforced UHPFRCC matrix, which are abbreviated as "FGREM" and "FGRUM", respectively, have been proposed as efficient FGRCM strengthening systems or to form novel composite structures with an excellent long-term mechanical behavior. Instead of common mortar, ECCs/UHPFRCCs with multiple cracking behavior are applied as cementitious matrix to reduce the stress concentration and suppress the debonding between strengthening layer and concrete substrate, which contributes to a high strengthening efficiency. Moreover, the FRP grid is efficient in enhancing both the tensile strength and fracture toughness of FGRCM composites [44-46].

In recent years, some studies have focused on strengthening structural members using FGREM/FGRUM composites and developing novel FGRUM composite structures. Currently, it has been demonstrated that the flexure or shear capacities of RC beams [47-49] and axial performance of RC columns [50-52] can be effectively improved after strengthening with FGREM/FGRUM layers. This paper presents a state-of-the-art review on the current studies that investigate the characteristics and applications of ECCs/UHPFRCCs as well as FGREM/FGRUM composites (referred to as FRP-reinforced high-performance cementitious composites) in strengthening structures or constructing new composite structures. Finally, further research opportunities and application prospects associated with FRP-reinforced high-performance cementitious composites are identified.

## 2. ECCs and UHPFRCCs: Raw material, Characteristic and Application

Based on the packing density method, to obtain dense packing thus improving the performance of cementitious matrix, ECCs and UHPFRCCs are produced by removing the coarse aggregate, replacing a portion of cement with mineral admixtures, and adding superplasticizers to achieve a relatively low water-binder ratio generally ranged from 0.14 to 0.30 [23-25,35,36]. Additionally, various fibers are added into the mix to enhance the tensile performance. The basic characteristics of ECCs and UHPFRCCs are mainly determined by the mixing proportion and the properties of raw materials. The raw materials and mechanical properties of

ECCs/UHPFRCCs are reviewed in detail, and the bond performance between ECCs/UHPFRCCs and concrete substrate as well as structural applications of ECCs/UHPFRCCs are also introduced below.

### 2.1 Raw material and Mechanical Properties of ECCs

The ECC is usually obtained by mixing a certain proportion of Portland cement, fly ash, fine sand, water and water reducer as well as a certain volume ratio of fibers. Some typical mixing proportions and corresponding mechanical properties of ECCs are shown in Table 1. It has been confirmed that the mechanical properties of ECCs are mainly influenced by fly ash-binder ratios (FA/B), water-binder ratios (W/B), sand-binder ratios (S/B), fiber types and fiber volume fraction [26,53-55]. Note that FA/B, W/B and S/B mean the mass ratio of fly ash, water and sand to binder (including cement and mineral admixtures), respectively.

Fly ash is the most common mineral admixture that replacing a portion of cement to improve the qualities of the ECCs including fire resistance [55-57], freeze–thaw resistance [58], fiber-to-matrix interfacial bonding and matrix toughness [55]. When the mass percentage of fly ash in cementitious composites exceeds 50% (FA/B≥0.5), it is called as high-volume fly ash (HVFA). By the comparison on mechanical properties of specimen with mixing proportion of M1, M2 and M3 (see Table 1), it is found that the compressive strength of ECC decreases while the tensile strain capacity is enhanced by increasing FA/B. As the HVFA increases, the reduction of compressive strength is due to the increase of porosity in ECC matrix [59], while the increase of tensile ductility is caused by the decline of fiber-to-matrix interfacial chemical bonding and matrix toughness [53,60]. Moreover, W/B and S/B are key factors affecting the mechanical properties of ECCs. ECC with higher S/B and lower W/B, (e.g., specimen M6 and M13 shown in Table 1), exhibits a higher compressive strength because of a larger matrix density, but a poorer tensile ductility caused by increasing matrix toughness and fiber-to-matrix interfacial bonding [53]. Overall, a low FA/B, a low W/B or a high S/B contributes to a higher compressive strength of ECC, while a high tensile strain capability may not be achieved. Oppositely, increasing FA/B and W/B and reducing the S/B are in favor of improving ECC's strain-hardening and multiple cracking behavior.

Polyvinyl alcohol (PVA) or polypropylene (PP) fibers are usually used to improve the tensile performance of ECCs. With the addition of PVA or PP fibers, the tensile strength and ultimate tensile strain of ECCs can reach more than 6 MPa and 2%, respectively [54,61]. The oiled PVA

fibers are the most commonly utilized fibers in producing ECC due to their good dispersibility, proper interfacial properties [62] and higher tensile strength than PP fibers [26,63]. With the oiled surface, PVA fiber-to-matrix interfacial bonding is weakened aiming to improving the tensile ductility of ECC [53], and the tensile failure of PVA-ECC is governed by fiber being pulled out from matrix. Different from oiled PVA fibers, PP fibers exhibit strong chemical bonding to cementitious matrix [61], thus PP-ECCs usually fail by fiber rupture before fiber pullout. Similar to PVA and PP fibers, polyethylene (PE) fibers have also been adopted to produce PE-ECC [63]. The PE fiber-to-matrix interface was tailored using plasma treatment to enhance the tensile strength and ductility of ECC [64].

The tensile and compressive performance of ECC are related to the fiber contents. Lin et al. [61] found that when the PVA fiber volume fraction increased from 1.0% to 2.0%, the tensile strength and tensile strain capacity of the ECC were enhanced by about 71% and 103%, respectively. It was mainly due to the higher fiber pullout resistance and fiber bridging capacity with the higher fiber content. However, when volume fraction was increased from 2.0% to 2.5%, the tensile and compression strength of ECC were decreased by 26% and 18%, respectively. The reduction of strength can be attributed to the initial defects in the matrix caused by uneven fiber distribution, as well as the large porosity caused by excessive fibers [61]. So, an optimum fiber volume fraction of 2% is commonly applied to make PVA-ECC [51,55,64]. The compressive and flexural strength of PP-ECC increased with fiber content increasing from 0% to 2%, and a flexural hardening behavior was observed for PP-ECC containing 2% fiber while a softening behavior occurred when the fiber content dropped to 1% [66]. With the increase of fiber content from 1% to 2%, PE-ECC's tensile strength and strain capacity increased approximately linearly [67].

The typical tensile stress-strain curve of ECC can be divided into three stage (see Fig.2): 1) linear elasticity; 2) strain-hardening and 3) fracture failure. In the linear elasticity stage, the first crack occurs in ECC when tensile stress reaches the initial cracking strength ($f_{t0}$). With the increase of tensile stress, ECC exhibits strain-hardening behavior with the appearance of multiple small cracks. Finally, the ECC fracture failure occurs on the occurrence of a main crack with fiber pullout or rupture at the main crack surface. Under uniaxial compression, the compressive stress-strain curve of ECC exhibits a near-linear ascending stage and a near-bilinear strain-softening stage [65,66]. The compressive strength of ECC is comparable to that of normal strength concrete (NSC) while the compressive strain capacity of ECC is better than

that of NSC. Zhou et al. [66] found that the peak strain of ECC under uniaxial compression was between 0.004 and 0.005 (approximately twice that of NSC's peak strain).

## 2.2 Raw materials and Mechanical Properties of UHPFRCCs

The UHPFRCCs typically consist of high-grade Portland cement, fine aggregate, mineral admixtures, water, high-range water-reducing admixture (HRWR), and high-volume fractions of fibers. Generally, UHPFRCCs exhibit high tensile and compressive strength (over 7 MPa and 120 MPa, respectively), as well as superior durability due to its dense micro-structure and the addition of fibers. Recently, some advanced UHPFRCCs have been developed, including UHPC and UHP-ECC.

### 2.2.1 UHPC

The mix components of UHPC generally include sand (used as fine aggregate), water, Portland cement, fine mineral powders (used as mineral admixtures), superplasticizer and steel fibers [35,67,68]. To achieve an ultra-high compressive strength, a low water-binder ratio (usually ranges from 0.14 to 0.20) is usually maintained, and polycarboxylates were found to be the most effective superplasticizers for UHPC with such low W/B [67]. Courtial et al. [69] reported that the belite phase content strongly decreased when the dosage of polycarboxylate increased from 1.8% to 2% because of the activation of the hydration reaction of belite. Moreover, ultra-fine mineral admixtures (e.g., silica fume, granulated blast furnace slag, fly ash, and limestone powder) are added in mixture to ensure a highly dense matrix and a low porosity of UHPC [35,67,68,70]. Particularly, silica fume with particle sizes ranging from 0.1 to 0.7μm is commonly used to significantly reduce the porosity and defects in the UHPC matrix [45,67,71]. It was also found that the optimal silica fume content was between 20% and 30% of cement mass for the best fiber-to-matrix bond performance [71]. Moreover, the usage of superplasticizer can significantly decrease the required W/B for a sufficient workability, and thus effectively reduce the porosity and enhance the strength. The quartz/natural sands with diameters of less than 0.6 mm are usually used as fine aggregate [45,67], which can significantly restrain the growth of micro-cracks during the initial crack development of UHPC [67]. The S/B of UHPC is usually controlled from 0.8 to 1.0 [34,45,72,73].

Steel fibers are the most commonly adopted reinforcement fibers in UHPC matrix because of their high tensile strength and stiffness [67]. When a load acts on UHPC, the stress on matrix is transferred to the fibers through the fiber-to-matrix interface. The working mechanism of the

fibers in matrix is shown in Fig. 3, demonstrating the function of fibers in preventing the development of cracks. Under tensile loading, the debonding between fiber and matrix occurs when initial crack appears in the matrix (see Fig.3a). As the stress increases, the crack width is enlarged, and the matrices on both sides of the crack are connected to each other by the fiber bridging effect (see Fig.3b). UHPC usually exhibits the failure mode of fiber pullout (see Fig.3c) due to the relatively low bond strength between steel fiber and matrix [73]. If the fiber-to-matrix interfacial bonding is strong enough to prevent the fiber pullout, fiber rupture (see Fig.3d) will occur. Therefore, the tensile performance of UHPC is mainly affected by the fiber-to-matrix bonding behavior. Steel fibers with a longer length can achieve a higher tensile strength and strain capacity of UHPC due to the higher fiber pullout load carrying capacity and slip capacity provided by the larger fiber-to-matrix bond area [35]. Relation between steel fiber volume ratio and compressive and flexural strengths of UHPC are shown in Fig. 4. It has been confirmed that flexural and compressive strength of UHPC almost increase linearly with the increasing fiber volume ratio from 0% to 3% [38,68,73]. The bond stress between fiber and matrix is reduced with an increase of fiber content, which contributes to suppressing propagation of cracks and thus resulting in the increase of strength. For cost saving, the steel fiber volume ratio is usually taken as 1.0 % to 2.0% [45,74]. Recently, synthetic fibers, e.g., barchip fibers, polypropylene fibers and nylon fibers, have been confirmed to be promising substitutes for steel fibers [75,76].

As shown in Fig. 5, the typical tensile stress-strain curve of UHPC can be divided into three stages: a linear elastic stage, a strain-hardening stage and a strain softening stage. In the linear elastic stage, the first cracking occurs when the tensile stress achieves the initial crack strength ($f_{t0}$). As the stress increases, UHPC exhibits a strain-hardening behavior with the tensile strain capacity ($\varepsilon_{tu}$) less than 1% [35,45,74]. The poor tensile ductility is attributed to low W/B and high S/B of UHPC. After the peak stress ($f_{tu}$), UHPC exhibits an obvious strain-softening behavior.

### 2.2.2 UHP-ECC

Recently, UHP-ECC, a novel cementitious material combining the advantages of ECC and UHPC, have been developed and studied. The difference between UHPC and UHP-ECC is that UHP-ECC exhibits a tensile strain-hardening behavior. A low W/B ranging from 0.14 to 0.18 is utilized to generate a homogenous cementitious matrix with dense micro-structures, resulting in a high compressive strength of UHP-ECC [36,37,40]. The blending materials of UHP-ECC

consist of high-grade Portland cement and mineral admixtures. The reactive powders, e.g., ground granulated blast furnace slag (GGBFS), limestone powder (LP) and silica fume (SF), are usually adopted as mineral admixtures to fill the pores in matrix for achieving a high strength and a high toughness of the matrix [36,37,77-79]. The content percentage of mineral admixtures in cementitious composites is usually above 50% [36,40]. Furthermore, a relative low S/B ranged from 0.29 to 0.30 was usually utilized [36,40,77,79] aiming to improve the tensile ductility. To achieve a high tensile strength and a high tensile rupture strain, polyethylene (PE) fibers with a high tensile strength and a high aspect ratio are used as reinforcing fibers in UHP-ECC [40]. The tensile performance of UHP-ECC is mainly decided by the fiber aspect ratio ($L_f/d_f$) and fiber volume ratio ($V_f$). The initial cracking stress, tensile strength and tensile strain capacity of UHP-ECC would increase with the rise of fiber reinforcement index ($V_f \cdot L_f/d_f$) which typically ranges from 7.5 to 18 [40,79].

The tensile stress-strain curves of UHP-ECC exhibit the same three-staged behavior as that of ECC (see Fig. 2). The comparison on typical tensile stress-strain curve of UHPC [74] and that of UHP-ECC [40] is shown in Fig. 6. The UHP-ECC has a greater initial cracking strength than UHPC. After the first cracking, UHP-ECC exhibits a strong strain-hardening behavior with the ultimate tensile strain up to 8%, while the tensile strain capacity of UHPC is very poor. A bilinear constitutive model with great agreement to the experimental tensile stress-strain curve of UHP-ECC has been purposed by Yu et al. [40]. Under uniaxial compression, the compressive stress-strain curve of UHP-ECC has the same shape as that of a normal ECC [79,80]. The general mechanical properties of ECC, UHPC and UHP-ECC are summarized in Table 2, indicating that UHP-ECC not only has a higher compressive strength that is comparable to UHPC, but also higher tensile strength and tensile strain capacity than those of ECC.

### 2.3 Bond behavior between ECCs/UHPFRCCs and concrete substrate

Recently, ECC/UHPFRCC layers have been used to repair or strengthen the existing RC structures. The key issue of this repair/strengthening technology is the interfacial bonding behavior between the ECC/UHPFRCC layer and the concrete substrate. Many factors affect the bond behavior of ECC/UHPFRCC-to-concrete, including the construction method of ECC/UHPFRCC, the surface roughness of concrete substrate, the surface treatment of the overlays and the strength of concrete, etc. Currently, five different bonding strength test techniques including slant shear test, splitting tensile test, pull-off test, shear test (single-surface

or bi-surface), and flexural test (three-point or four-point) are usually used to analyze the bond strength between ECC/UHPFRCC and concrete (see Fig. 7) [81,82].

### 2.3.1 ECC-to-concrete interface

The construction method of ECC includes prefabrication, spraying and casting-in-place. Usually, to achieve stronger interfacial bonding, except for the necessary rough surface, the bonding materials are also important. For example, the cast-in-place ECC repair/strengthening system is connected with existing concrete substrate through the primer (e.g., cement paste), while the prefabricated one is bonded to substrate using bonding agents (e.g., mortar), which is shown in Fig. 8a and Fig. 8b. Proper primers or thin bonding agents contribute to the excellent interfacial bonding by strengthening the mechanical interlocking or cohesion between ECC and concrete [82-85]. Among them, the epoxy resin adhesive between ECC and concrete could significantly improve the FRP-ECC-concrete interfacial bonding behavior due to the strong cohesive force on the interfaces [85]. The relations between interfacial bond strengths and roughness of concrete substrate surface/strength of old concrete are summarized in Fig. 9. With increasing concrete strength or increasing surface roughness up to 4mm, the bond strengths increased obviously for both the cast-in-place and prefabricated ECC-to-concrete interfaces. However, when the surface roughness was increased to 5 mm, the increase in bond strengths became inconspicuous, even decrease in bond strength was reported in some studies. Wang et al. [82-84] concluded that the surface roughness around 4 mm had the optimum effect on improving the bond strength of interfaces. In most instances, the cast-in-place ECC has a higher bond strength compared with the prefabricated ECC (see Fig. 9).

For spraying ECC repair/strengthening systems, the interfacial bonding behavior between spraying ECC and concrete substrate has been studied by conducting splitting tensile tests [86] and interfacial shear tests [86,87]. It was found that the usage of primer has a marginal effect on enhancing the bond strengths of spraying ECC-to-concrete interface [86]. The spraying ECC and existing concrete are usually connected to each other only by the surface-to-surface contact (see Fig. 8c), and the shear bond strength is mainly resulted from friction and mechanical interlocking. Thus, the higher roughness of concrete substrate surface will lead to stronger friction and mechanical interlock effect that enhancing the shear bond strength of spraying ECC-to-concrete interface [86,87]. Moreover, the construction method of downward spraying ECC is recommended because of the positive effect of gravity on the bond behavior [86]. Tian et al. [87] also found that the spraying ECC generally had a lower interfacial shear strength

compared with the casting ECC.

Overall, the typical variables affecting the various bond strengths between prefabricated/cast-in-place/spraying ECC and concrete are summarized in Table 3. Among them, the proper roughness of concrete substrate and sufficient curing age (above 28 days) are the important parameters to ensure effective interfacial bonding [82-84,88,89]. The increase of concrete strength results in a higher bond strength [82-84], which is mainly due to the high strength concrete suppressing the development of cracks on the interface. As for prefabricated layers, increasing the roughness of prefabricated ECC surface is an effective method to improve interfacial bonding [82-84]. Furthermore, a higher ECC strength contributes to higher interfacial shear bond strength [87].

### 2.3.2 UHPFRCC-to-concrete interface

A number of slant shear tests, splitting tensile tests and direct shear tests have been conducted to evaluate the bond strength of UHPC-to-concrete interfaces. It has been confirmed that surface preparation of concrete substrate, strength of concrete, wettability of concrete substrate and curing age of UHPC have significant influences on the bond strength of UHPC-to-concrete interfaces. The surface preparation for concrete substrate can be divided into three categories: mechanical connector (MC) preparation, roughness degree (RD) preparation and bonding agent (BA) preparation [81]. There are seven surface RD preparation technologies commonly used, namely smooth surface (SM), rough surface achieved by exposing coarse aggregates (R), post-installed rebar (PR), sand blasting (SB), wire brushing (WB), drilling holes (DH) and grooving (GR). Three common failure modes were found, including interfacial debonding, partial interfacial debonding and concrete substrate failure. The failure modes are dependent on the UHPC-to-concrete interfacial bond strength: when the bond strength is low, the interfacial debonding occurs; when the bond strength is high, the partial interfacial debonding occurs; when the bond strength is ultra-high, the concrete substrate failure occurs.

The relations between shear bond strength and different variables and corresponding failure modes under bi-surface shear tests are concluded in Table 4. The shear bond strength of UHPC-to-concrete interface is sensitive to the surface roughness of concrete substrate, so the proper RD preparation is very important. Valikhani et al. [90] investigated the shear bond strength of cast-in-place UHPC-to-concrete interface using the mechanical connectors to restrict the relative slip between UHPC and concrete substrates. It was found that the shear bond strength

was enhanced by 40% to 255% due to the addition of mechanical connectors. When the BA surface preparation was used, the bond strength between UHPC and concrete reduced because the UHPC surface and concrete surface were separated by bonding agent which decreased the cohesion between the two materials [91,92]. Zhang et al. [93] compared the shear bond strength under various RD preparation including R, SM, DH, GR and PR, and confirmed that the R preparation for concrete substrate surface had the most significant effect on improving the interfacial bond strength. Except for the surface treatment, the adequate curing age (above 28 days) of UHPC is necessary for the growth of interfacial bond strength [93,94]. Additionally, the adequate wetting of concrete substrate [94,95] contribute to the increase of bond strength.

To find out the reliable surface preparation, the slant shear bond strengths and the splitting tensile strengths under various surface preparation for concrete substrate are compared in Fig. 10. Zhang et al. [92] found that the rough surface (R), combination of rough surface with drilling holes (R+DH) and combination of rough surface with grooving (R+GR) had very close effect on enhancing UHPC-to-concrete bonding strength. Tayeh et al. [96-98] reported that the highest slant shear bond strength could be achieved by the SB surface, and the same result was found by Jafarinejad et al. [99] and Carbonell Muñoz et al. [94]. Tayeh et al. [96-98] also found that the SB preparation was the most effective method on increasing splitting tensile strength, while Carbonell Muñoz et al. [94] declared that GR preparation was better than SB preparation. There is no unified conclusion on the best surface preparation, whereas according to the existing studies, the WB and DH surface preparation have a relatively poor effect (see Fig. 10).

### 2.4 Durability of ECCs/UHPFRCCs

Durability of construction materials is highly important for the long-term behavior of civil engineering structures. The durability of cementitious materials can be evaluated by many aspects, such as freeze-thaw resistance, chemical attack resistance, abrasion resistance, fire resistance and etc. [70,100]. The durability of ECC/UHPC is introduced below from the four significant aspects mentioned above.

The fire resistant of ECC/UHPC is affected by the behavior of matrix, fiber and fiber-to-matrix interface under high temperatures. The mechanical properties of concrete subjected to elevated temperatures usually degrade accompanied with spalling failure of matrix caused by the excessive internal tensile stress. Şahmaran et al. [56] found that the explosive spalling failure of ECC matrix was suppressed due to the addition of PVA fibers. The residual mechanical

properties of ECC under temperatures ranging from 200 to 600 ℃ was significantly enhanced with the increase of fly ash content [56]. However, the degeneration of fiber properties under high temperatures would lead to the decrease or disappearance of the strain-hardening capacity. Bhat et al. [101] found that ECC lost its strain-hardening behavior and excellent ductility for temperature above 300 ℃ due to the decomposition of PVA fibers. Zhang et al. [102] reported that the tensile properties of ECC suddenly decreased at 200 ℃ due to the strength loss of PVA fibers and the increase of matrix toughness. It was also found that the fiber-to-matrix interfacial bond, which contributed to the high ductility of ECC, was reduced at 200 ℃. Moreover, the compressive strength and stiffness of ECC exhibited a linear declination when temperature was above 200 ℃ [103].

UHPC has an excellent fire resistance characterized by the high residual mechanical properties and an excellent spalling resistance. The loss of compressive strength for UHPC begins at the temperature ranging from 350 to 400 ℃, and when reaching 800 ℃, the UHPC strength dropped to zero [104]. A study reported that 30% to 50% strength loss was observed for UHPC when temperature was higher than 1000 ℃ [105]. The damage on steel fibers is much less than that of PVA or PP fibers under elevated temperatures because of the higher melting point of steel fibers, which helps maintain the high tensile performance of UHPC effectively after exposure to elevated temperatures. The steel fibers can improve not only the residual mechanical properties but also the spalling resistance of heat-damaged UHPC. According to current statistics, the spalling temperature of UHPC with steel fibers ranged from 260 ℃ to 550 ℃ [104]. The excellent spalling resistance of UHPC is owe to the strong fiber bridging effect.

To compare the fire resistance of ECC and UHPC, the effect of temperature on mass loss [56,102,103,106,107], relative compressive strength [56,102,103,106,108-111], relative tensile strength [57,102,111-115] and relative stiffness [56,103,107,108,110,116] on ECC/UHPC is illustrated in Fig. 11. After 200 ℃, the mass loss rate of UHPC was lower than that of ECC (see Fig.11a), indicating that less damage on UHPC matrix under high temperatures. In most cases, compared with ECC, UHPC has a lager relative compressive strength at 200 ℃~800 ℃ (see Fig.11b) but a lower relative stiffness after 400 ℃ (see Fig.11d). Moreover, it should be noted that the relative tensile strength of ECC could be above 1.0 at 50℃~200℃ (see Fig.11c). When the FA/B reached above 80% [57,102], the HVFA accelerated hydration process and pozzolanic reaction thus leading to a stronger fiber-to-matrix interfacial bonding, which resulted in the enhancement of tensile strength under 50℃~200℃.

The relative dynamic elastic modulus and mass loss of matrix are usually used to evaluate the freeze-thaw resistance. The larger relative dynamic modulus and less matrix mass loss rate after more freeze-thaw cycles indicate a higher freeze-thaw resistance. The addition of PVA fiber, fly ash and slag contributes to the high freeze-thaw resistance of ECC. The ECC with PVA fiber survived after 300 freeze-thaw cycles with a mass loss rate less than 8% [117] while premature failure of ECC without fibers occurred, indicating that PVA fiber could prevent the damage of matrix under freeze-thaw cycles. By mixing fly ash and slag in matrix, the relative dynamic elastic modulus of ECC could be above 100% after water or salt 200 freeze-thaw cycles [118].

UHPC has a more superior freeze-thaw resistance than ECC. Wang et al. [119] found that the mass loss rate of UHPC was only 0.62% after 1500 freeze-thaw cycles. With proper hot or steam curing for UHPC, the relative dynamic elastic modulus of UHPC subjected to 1000 or 1500 freeze-thaw cycles could reach over 100% [120]. Fig. 12 shows the comparison on the freeze-thaw resistance between ECC and UHPC. After 300 freeze-thaw cycles, the mass loss rate of ECC has reached about 8% [117], while UHPC had a much lower mass loss rate (under 0.3%) even after 700 freeze-thaw cycles [121]. In addition, the relative dynamic modulus of ECC without slag was less than 90% [118] after 200 freeze-thaw cycles while the relative dynamic modulus of UHPC subjected to 600 freeze-thaw cycles could reach over 100% [121]. The excellent freeze-thaw resistance of UHPC mainly benefits from its dense microstructures.

The chemical attack resistance, especially the salt corrosion resistance, is very important to the concrete structures serving in harsh environment. Liu et al. [122] reported that the ECC exposed to long-term sulfate and mixed sulfate-chloride environment had higher compressive and tensile strength than of those exposed to water. The increase of strength was due to some hydration products filled the pores thus leading to the decrease of porosity in ECC. Despite of the reduction of tensile ductility under sulfate and sulfate-chloride environment, ECC can still exhibit the strain-hardening behavior that are characterized by multiple cracking development and tensile strain capacity above 2%. The superior salt corrosion resistance of UHPC mainly involves in two aspects: high residual compressive strength and high permeability resistance. UHPC has superior chloride ion permeability resistance, inhibiting the penetration of chloride ions into the concrete, and thus restrain the corrosion of steel fibers or reinforcement [70]. Ye et al. [123] found the percentage of compressive strength of UHPC after exposure to various

corrosive solutions to the original value ranged from 42% to 98%, among which strong acid solution caused the greatest damage to UHPC. A study reported that the mass and compressive strength of UHPC were reduced by less than 9.2% after exposure to various concentrations of sulphuric acid, sodium chloride, and sulphate solution for 60 days [124].

The abrasion resistance of concrete is a key durability property for structures bearing friction loading, especially for the bridge decks. The addition of PVA fibers could effectively improve the abrasion resistance of ECC. Abid et al. [125] found that the smaller abrasive mass loss occurred in ECC with the larger PVA fiber volume ratio. However, when PVA fiber content exceeded 3%, the decline of abrasion resistance was observed because of the large void ratio caused by excessive fiber [126]. Mohamed et al. [127] reported that the abrasion mass loss of ECC tended to follow a negative correlation with the compressive strength, indicating that the denser matrix leaded to the higher abrasion resistance. Lee et al. [128] compared the abrasion resistance of NSC, HSC, and UHPC and concluded that UHPC had the highest abrasion resistance. The excellent abrasion resistance of ECC/UHPC mainly relies on the compactness of matrix and fiber bridging capabilities.

## 2.5 Applications of ECCs and UHPFRCCs

With excellent tensile properties and high durability, ECC and UHPFRCCs are promising material in strengthening/repairing RC structures, making permanent formworks and structural elements and etc.

### 2.5.1 RC beams strengthened with ECCs/UHPFRCCs

Fig. 13 shows the four existing ECC/UHPC strengthening forms: C-sided, T-sided, 2-sided and 3-sided strengthening. C-sided strengthening means that the ECC/UHPC is located at the compressive zone. T-sided strengthening means that the ECC/UHPC is located at the tensile zone, which is commonly used to enhance the flexure behavior of RC beams. 2-sided strengthening means that the ECC/UHPC is placed on both sides of the cross section to improve the shear behavior of members. 3-sided strengthening is the combination of T-sided and 2-sided strengthening providing both shear and flexure strengthening for members.

The T-sided and 3-sided ECC layers are usually adopted in strengthening RC beams. Shang et al. [129] reported that the 3-sided stirrups-reinforced ECC layers effectively enhanced the shear load capacity, stiffness and ductility of fire damaged RC beams. However, the interfacial

debonding between ECC layers and concrete substrate was observed. Similar debonding failure also occurred in some FRP-ECC composite strengthening systems. Wu and Li [130] investigated the flexure behavior of RC beams strengthened with T-sided CFRP-ECC hybrid layer. The results showed that the strengthening effectiveness of CFRP-ECC hybrid layer was limited due to the premature debonding between ECC and concrete. Subsequently, Hou et al. [32] found that the T-sided BFRP bar-reinforced ECC layer incorporating the steel bolts at the end could effectively mitigate the ECC-to-concrete interfacial debonding. Overall, the bond behavior between ECC layer and concrete significantly impacts the strengthening efficiency. It has been confirmed that the addition of mechanical connectors (e.g., shear studs and bolts) can significantly enhance the interfacial bonding [32,131]. For fully utilization of ECC, mechanical connectors are recommended to be installed in ECC strengthening systems (see Fig. 14). The function of mechanical connectors is to prevent interfacial separation, meanwhile the FRP/steel reinforcement is utilized to enhance the strengthening effect [132-134]. However, RC beams strengthened with such ECC strengthening systems need further studies, especially in the design of mechanical connector (number and location) and the optimal reinforcement ratio in ECC layer.

Recently, many studies have focused on the flexural behavior of strengthened RC beams/slabs with UHPC layer, with the effects of key parameters, such as strengthening forms, thickness of UHPC layer ($t_u$), reinforcement ratio of UHPC layer ($\rho_u$), reinforcement ratio of RC beam ($\rho_s$) and surface treatment for concrete substrate, being investigated. The findings are summarized in Table 5. Among them, the proper surface treatment is the most important factor to achieve an effective strengthening. It has been confirmed that the combination of roughness degree (RD) preparation and epoxy bonding agent [135-137], as well as adding mechanical connectors [135,138] can ensure the sufficient interfacial bonding for an effective strengthening. The T-sided strengthening enhances the ultimate moment through the tensile contribution provided by UHPC layer located in the tensile zone, and thus the increases of $t_u$ and $\rho_u$ lead to the more increase in flexure capacities of composite members [135-137,139]. Nevertheless, the increase of $\rho_s$ may reduce the strengthening effect of UHPC layer [136].

Fig. 15 depicts the typical failure modes observed in RC beams strengthened with T-sided UHPC layer. The ideal failure is governed by concrete crushing [140] (see Fig. 15a), under which the compressive strength of NSC and tensile strength of UHPC are fully utilized.

Without internal reinforcement of UHPC and a strong interfacial bonding, the premature rupture of UHPC layer associated with partial debonding occurs [135] (see Fig.15b), thus the UHPC layer is separated into two parts and lose its function. Without an end anchorage system, the large concentrated load at support may break the concrete cover, causing UHPC layer being peeled off [135] (see Fig.15c), which is regarded as special interfacial debonding failure.

As for C-sided configuration, the strengthening effect of UHPC is approximate to that of NSC [138,141], indicating that high strength concrete is not necessary when strengthening in the compressive zone. Compared with the C-sided and T-sided strengthening, the 3-sided one was the most effective method on enhancing the flexural capacity of composite beams owing to the larger cross-sectional area of UHPC and the perfect bonding between U-shaped jacket and concrete [141,142], but it may also lead to a less ductility due to the brittleness of UHPC and a higher cost. Overall, the T-sided UHPC layer is the most cost-effective flexural strengthening form.

### 2.5.2 RC columns/joints strengthened with ECCs/UHPFRCCs

ECC jackets have been proposed to strengthen RC columns/joints. Zhang et al. [143] used the ECC jackets with steel reinforcement to strengthen the RC columns and found that the composite columns exhibited more excellent ductility hysteresis response, plastic deformation ability and energy dissipation compared with RC columns. The same result was also concluded by Deng et al. [144]. Similarly, ECC jackets are also effective for seismic strengthening for beam-column joints. Esmaeeli et al. [145] reported that the lateral load capacity and energy dissipation capacity of RC beam-column joints were significantly increased with the presence of the 4-sided CFRP-ECC hybrid jackets. Except using ECC jackets, replacing the conventional concrete with ECC in the joint region is an effective method to improving the cyclic behavior of joints [146]. It was found that the ECC strengthening layer could enhance the lateral load capacity and the energy dissipation, and alleviate the pinching behavior of conventional RC beam-column joints [148]. The excellent seismic strengthening effect of ECC is owe to the excellent mechanical properties of ECC. On the one hand, with high tensile strength and strong strain-hardening behavior of ECC, the crack development in ECC jackets is effectively restrained and the effective confinement provided by the jackets for core concrete can be achieved, which contributes to high load bearing capacities. On the other hand, the rotational capacity of plastic hinge in composite members is improved due to the high compressive and tensile strain capabilities of ECC, thus enhancing the lateral deformation

capacity.

Compared with the ECC jackets, the UHPC jackets are more suitable for strengthening RC columns with high axial compression ratio due to the ultra-high compressive strength of UHPC. Due to the extra axial contribution offered by UHPC jackets, the load carrying capacities of UHPC-strengthened columns are higher than those of GFRP-confined columns [147,148]. With a higher strength and elastic modulus than ECC, UHPC exhibits satisfactory effects on seismic strengthening of columns [149] or joints [150], especially in terms of enhancing the lateral stiffness and the load carrying capacity. The composite action of UHPC jackets and core concrete directly affects the seismic/axial performance of composite columns or joints, so the UHPC-to-concrete interfacial bonding and construction method of UHPC are key issues for a reliable strengthening. Dadvar et al. [148] reported that the longitudinal grooving surface treatment was more effective in enhancing load carrying capacities and energy absorption of UHPC jacket-strengthened RC columns compared to the sand blasting and horizontal grooving. Notably, without sufficient lateral reinforcement inside jacket to provide confinement, separation between UHPC jacket and concrete core may occur due to the large lateral dilation under high axial load [149]. So, Tian et al. [151] used high-strength steel spiral stirrup to provide continuous sufficient confinement and successfully avoided the detachment of the UHPC jacket from the concrete core under loading. Furthermore, it should be pointed out that the segmental prefabrication method caused discontinuity of the prefabricated jackets, thus significantly reducing the strengthening efficiency [149]. Thus, the problem of joint splicing for segmental prefabricated jackets needs to be addressed to improve the continuity of jackets and achieve an effective assembled strengthening. Alternatively, the research focus can be shifted to developing integral assembled jackets.

### 2.5.3 ECCs/UHPFRCCs permanent formwork

With the superior durability and tensile properties, ECC and UHPC show great potential on making U-shaped permanent formwork for RC beams. Note that the permanent formwork can also be regarded as a strengthening layer for RC beams. The roughness of prefabricated ECC/UHPC surface contributes to the good interfacial bonding to concrete substrate, so the proper treatment for formwork surface is necessary. Li et al. [152] and Huang et al. [153] firstly designed the assembled ECC formwork with distributed grooves on the inner surface. Subsequently, Qiao et al. [154] developed the ECC permanent formworks with three different surface treatments (SM, SB and GR) and embedded L-shaped reinforcement (see Fig. 16a).

The experimental results showed that the GR surface led to the best ductility of strengthened beam because of the best interfacial bonding, followed by the SB surface and SM surface. Similarly, Zhang et al. [155] compared the ECC formworks using three different surface treatments (SM, shear keys on the surface and using steel bars as mechanical connectors). It was found that the surface with shear keys exhibited the highest interfacial bonding thus resulting in a stable strengthening effect. They also proposed a predictive model for shear capacity of concrete beams strengthened with U-shaped ECC permanent formwork. It should be mentioned that the effect of ECC thickness on angle of critical inclined crack has been accounted for in their model. However, different formwork surface treatment caused different shear behavior of composite beams, so their model had some limitations because the influence of surface treatment was not considered in the equation.

Currently, few studies have focused on U-shaped UHPC permanent formworks for RC beams. To author's best knowledge, only Dong et al. [41] purposed the U-shaped UHPC permanent formworks with or without pre-embedded half of BFRP stirrup for seawater sea-sand concrete (SWSSC) beams. The former (see Fig. 16b) exhibited better cracking resistance than the latter (see Fig. 16c) because the pre-embedded stirrup limited the relative slippage between UHPC and SWSSC and improved the interfacial bonding. Similar to ECC formworks, the key issue of developing novel UHPC formworks is how to achieve a good interfacial bonding. Thus, development of U-shaped UHPC formworks with different types of surface treatment and their corresponding strengthening effects are of great concern in future research.

Several researchers have devoted to developing novel ECC permanent formworks for concrete columns. Li et al. [156] developed a PP-ECC formwork to strengthen the NSC column (namely hybrid ECC-NSC column shown in Fig. 17a). The results showed that the hybrid ECC-NSC column with sufficient confinement (decided by the ECC thickness and the transverse reinforcement ratio) delivered the most excellent deformability compared with RC or reinforced PP-ECC columns. It should be highlighted that they considered the confinement contributions from the stirrups and ECC when analyzing the confining effect of hybrid column. Zhang et al. [157] used precast PP-ECC permanent formwork to strengthen the plastic hinges region of RC columns (see Fig. 17b) subjected to the combination of axial and unilateral cyclic load. It was found that the RC columns reinforced with PP-ECC in the plastic hinge region exhibited higher load carrying capacity, ductility and energy dissipation capacity than RC columns under cyclic loading. Pan et al. [158] studied the seismic behavior of ECC formwork

reinforced short rectangular concrete column (see Fig. 17c), reporting that a proper ECC thickness (selected as the depth of compression zone) was required to obtain a cost-effective flexural behavior of composite columns.

Recently, some UHPC formworks for RC columns have been invented. Tian et al. [50] studied the axial behavior of RC column reinforced with pure UHPC formwork (see Fig. 18a). To further enhance the strengthening effect of formwork, they used the stainless steel (SS) grid-reinforced UHPC formwork to strengthen RC columns (see Fig. 18b). Subsequently, Zeng et al. [159] proposed the FRP-UHPC tubular formwork to strengthen the RC columns (namely concrete-filled FRP-UHPC tube column shown in Fig. 18c). The typical axial load-strain curves of concrete columns confined with above UHPC formworks are shown in Fig. 19. The axial load-strain curve of the column confined with pure or SS-grid-reinforced UHPC formwork can be divided into 5 stages by the feature points: 1) a linear ascending stage; 2) a post-peak descending stage; 3) a strength recovery stage; 4) a secondary descending stage; 5) a strain softening stage. The axial load-strain curve of concrete-filled FRP-UHPC tube column exhibits linear ascending behavior and post-peak descending behavior, and subsequently performs a strength recovery behavior (confinement type II) or a strain softening behavior (confinement type I). In the linear ascending stage, the distinct reduction of stiffness is not found in concrete columns confined with UHPC formwork because the axial contribution of UHPC layer is dominant. After the peak load, the sudden strength loss occurs due to the brittleness of UHPC and insufficient lateral confinement. The ratio of residual strength to peak strength is determined by the ratio of the cross-sectional area of UHPC formwork to that of the overall column ($\rho_{uc}$). The larger $\rho_{uc}$ means more significant axial contribution of UHPC formwork, thus leading to more strength loss caused by the brittle behavior of UHPC. So, the thicker the UHPC formwork was, the more significant strength loss after the peak load was observed [50,159]. After the strength loss, the confinement effect of UHPC formwork begins to function, thus leading to strength recovery until the steel fibers being pullout from UHPC matrix or the fracture of the reinforcement in the formwork. It should be noted that the strain softening will occur instead of strength recovery if the confinement is not strong enough, which is shown in Fig .17b (the axial load-strain curve of confinement type I). In conclusion, the confinement level greatly affects the post-peak behavior of composite columns. The addition of internal FRP grids [50] or external FRP jackets [159] for UHPC formwork has been proved to be the effective approach to provide strong confinement.

### 2.5.4 Repairing structures with ECCs/UHPFRCCs

Different from the strengthening technology introduced in section 2.5.1, ECC/UHPFRCC repairing RC structures are constructed by replacing certain portion of concrete in RC members with ECC/UHPFRCC, which means no increase in cross-sectional area (see Fig. 20). Kobayashi and Rokugo [33] firstly purposed using ECC as the repair material for corroded RC members. They reported that no secondary corrosion was observed on the rebar in the corroded beams repaired with ECC because ECC's multiple micro-cracking behavior reduced the penetration of chloride ions. The ECC patching could contribute to the strength recovery of corroded beams with less than 10% mass loss of steel reinforcement. Hou et al. [31] reported that using ECC to replace the damaged concrete could effectively recover the flexure strength of corroded RC beams with corrosion ratios less than 11.2%, but it was suggested to add extra reinforcement when corrosion ratios were above 13.9%. So, if the corrosion loss is relatively large, external or internal reinforcement for ECC repair system is recommended. Thus, Hu et al. [160] proposed a RC beam repaired with ECC layer bonding with CFRP strips, namely hybrid CFRP-ECC retrofitted RC beam. It was found that the hybrid CFRP-ECC repair system could recover up to 114.7% of initial flexure capacity. Similarly, Kobayashi and Rokugo [33] used fiber net as internal reinforcement of ECC and obtained the good recovery capacity for beams subjected to severe corrosion.

ECC/UHPC-NSC composite members render structures with higher durability, larger spans, lighter weights, and lower maintenance costs. The main design variables of composite beam include ECC/UHPC layer thickness (height replacement ratio) and the reinforcement ratio. Fig. 21 show the relation between the ECC/UHPC height replacement ratio (the ratio of layer thickness to the effective height of beam) and increase in flexural capacity (compared with the beam with zero height replacement ratio). With increasing height replacement ratio, more increase in flexural capabilities can be obtained [161]. The increase in flexure capacity varied from 0 to 47% for ECC-NSC composite beams with height replacement ratio of 0.15 to 0.6 [161-163] and ranged from 0 to 90% for UHPC-NSC composite beams with height replacement ratio of 0.05 to 0.7 [164,165]. The failure of composite beam with low and high reinforcement ratio is govern by the rupture of reinforcement (tensile failure) and concrete crushing (compressive failure), respectively. With the increase of height replacement ratio, the ductility essentially remains unchanged in the case of tensile failure, while decreases in the case of compressive failure [161]. However, Qin et al. [163] found that the ductility of ECC-NSC composite beam subjected to compressive failure was enhanced with increasing height

replacement ratio, which was in contrary to the Ge et al.'s conclusion [161]. Therefore, the relation between ductility and height replacement ratio of ECC/UHPC-NSC composite members need to be further studied.

Please note that ECCs/UHPFRCCs have also been used with other structural purposes [155-160], whereas they are in within scope of this review.

## 3. FGREM/FGRUM: Mechanical Behavior and Application

Currently, the FRCM systems can be divided into two major categories: cementitious matrix reinforced with dry fiber sheets/textiles and cementitious matrix reinforced with resin-impregnated fiber (FRP) grid. It has been proved that the FRP grid-based systems was more effective than dry fiber textiles-based systems on shear strengthening of RC beams [10]. The ineffectiveness of dry FRP fabric is mainly due to poor bonding between the FRP without impregnating resin and the matrix [49], which leads to less efficiency of FRCM systems than FRP jackets [166]. It has been confirmed that the epoxy impregnation could highly enhance the bond strength between FRP fabric and cementitious materials [167]. Using ECC/UHPC as the matrix in FRCM helps overcome the disadvantages of poor crack resistance and the low ductility of traditional FRCM, and to achieve a fully utilization of high tensile strength of the FRP. Based on the application of ECC/UHPC introduced in section 2.5 and the advantages of FRP grid, FGREM and FGRUM were proposed to further promote the development of ECC/UHPC strengthening and FRCM strengthening. The existing studies on the application of FGREM/FGRUM are reviewed below.

### 3.1 Flexural Strengthening

#### 3.1.1 Flexural behavior of RC beams strengthened with FGREM

Some studies have focused on FGREM-strengthened RC beams. Using ECC as matrix for FRP grid to form the FGREM may reduce the stress concentration and suppress the interfacial debonding between the strengthening layer and the concrete substrate. The reinforcement ratio of FRP grid and the reinforcement ratio of RC beam are important factors affecting the strengthening efficiency. Zheng et al. [168] first studied the flexural behavior of RC beams strengthened with T-sided FGREM layers and found that the cracking resistance, yield and ultimate loads of RC beams were enhanced due to the effective strengthening provided by FGREM layers. Afterwards, Yang et al. [49] reported that the ultimate load capacity would be enhanced with a larger cross-sectional area of FRP grid, but significantly decreased due to the

steel reinforcement ratio increment. The results indicated that the enhancement effect of FRP grid on flexure capacity was determined by the ratio of tensile stiffness of FRP grid to steel reinforcement. Usually, to prevent the plate end debonding, proper end anchorage systems should be used in cast-in-place FGREM layers, such as steel bolts [168] and U-wrapped CFRP anchorages [49]. As for prefabricated FGREM layers, using epoxy as bonding agent could completely suppress both the interfacial debonding and plate end debonding, thus resulting in better strengthening effect than cast-in-place systems [49].

### 3.1.2 The analytical models for flexural capacity

The common flexural failure modes of RC beams strengthened with T-sided FGREM layer can be divided into two cases [49,168]: 1) the concrete crushing (CC) occurs prior to the rupture of FRP grid after the yield of steel reinforcement; 2) the rupture of FRP grid (RG) occurs prior to the concrete crushing after the yield of steel reinforcement. To predict the flexural capacity of RC beams strengthened with T-sided FGREM layer, some assumptions and simplifications, as proposed by the authors of this paper, are listed below: i) Plane section assumption; ii) No interfacial debonding between strengthening layer and concrete substrate; iii) The bond between the FRP grid and the cementitious matrix is prefect; iv) The ultimate and peak compressive strain of NSC are assumed to be 0.0033 and 0.002, respectively; v) The stress-strain relationship of steel bars is elastic-perfectly plastic; vi) The tensile contribution of NSC and epoxy resin is ignored; vii) The tensile contribution of ECC is considered. Similar approaches have also been adopted in existing studies (e.g., [49,170])

The analytical models for flexural capacity are shown in Table 6, which are proposed based on a cross-section analysis. The comparison between experimental results [49,168] and predictions of the proposed models is depicted in Fig. 22. It is indicated that the model predictions are relatively conservative but show good agreement with experimental results. However, due to the lack of the experimental data on flexural strengthening with T-sided FGREM layer, the accuracy of the proposed model needs further verification.

## 3.2 Shear Strengthening

### 3.2.1 Shear behavior of RC beams strengthened with FGREM/FGRUM

Some studies have been conducted to confirm the effectiveness of 2-sided bonded FGREM layer in shear strengthening of RC beams with the variables of shear span ratio, the reinforcement ratio of FRP grids and FRP type being investigated, as shown in Table 7. Zheng

et al. [169] found that the shear capacities of RC beams were greatly improved by the 2-sided FGREM strengthening and the partial debonding between concrete and FGREM layer induced by diagonal cracks was also observed. With increasing FRP grid's thickness, more shear contribution offered by FGREM was obtained, but the FRP grids with a large thickness (5 mm) resulted in a lower effective strain than those with a small thickness (3 mm). Yang et al. [170] compared the strengthening efficiency of cast-in-place and prefabricated FGREM. It was found that the prefabricated FGREM using epoxy as bonding agent led to a higher utilization rate of FRP's tensile strength, and thus enhanced the strengthening effectiveness. They also reported that BFRP grids were more effective than CFRP grids on shear strengthening. Guo et al. [171] highlighted that both the vertical and horizontal grids could provide shear contribution. Furthermore, it was found that the shear contribution of FRP grids reduced with increasing shear span ratio [170,171].

The FGREM/FGRUM have been successfully applied in strengthening corrosion-damaged structures. Zheng et al. [47] confirmed the effectiveness of FGREM on shear strengthening for RC beams with corrosion-damaged stirrups. It was also found that the BFRP grid exhibited a lager effective strain at limit state compared to CFRP grid, indicating the better strengthening efficiency of basalt-FGREM than carbon-FGREM. Chen et al. [48] investigated the shear behavior of corroded RC beams strengthened with U-shaped FGRUM jackets and found that the FGRUM jackets effectively improved the shear capacity and the crack control behavior of the beams. The good interfacial bonding between the CFRP grid and the UHPC jacket led to an excellent composite action. However, under the same corrosion level, the shear contribution provided by FRP grids reduced slightly with increasing layers of FRP grids.

### 3.2.2 Existing predictive models for shear capacity

The failure of shear-strengthened RC beams using FRCM composites is usually governed by premature debonding of the FRCM strengthening layers. In the case of debonding failure, the effectiveness of FRCM strengthening systems is very close to that of FRP jackets [172]. Therefore, some models for predicting shear capacity of FRCM systems have been proposed based on the effective stress determined by the models of FRP strengthening systems. Among them, Chen and Teng's model [173] is one of the most accurate models for predicting the shear contribution of the FRP jackets, which was also available for predicting the shear contribution of the FGRCM jackets. In this model, the effective stress of FGRCM jacket is mainly determined by the available bond length ($L_{max}$), the effective bond length ($L_e$), the axial

stiffness ($\rho_f E_f$) of FRP grids, and the concrete compressive strength ($f_c$). Subsequently, Tetta et al. [174] modified the Chen and Teng's model by introducing some correction factors and proposed two modified models on the basis of Chen and Teng's model. It should be highlighted that the above three models are only available for strengthened beams failed by interfacial debonding of FGRCM layers. Sometimes, the strengthened beams may fail from the rupture of FGRCM jackets [175]. In this case, Tetta et al. [174] suggested using the ultimate strength of FRP ($f_{fu}$) instead of effective stress to calculate the shear contribution of FGRCM jacket. To develop a design-oriented model, the effective tensile strain in FRCM is limited to be less than 0.004 conservatively based on the ACI code [176]. Recently, a novel model for shear contribution of FGRCM has been proposed by Guo et al. [171]. In their model, the shear contribution of the vertical and horizontal grids was considered. The effective strain of vertical grids ($\varepsilon_{u,ver}$) was determined by the ratio of cross-sectional area to the spacing of FRP grids. The effective strain of horizontal grids ($\varepsilon_{u,hor}$) was defined as $\varepsilon_{u,ver}$ multiplied by a comparison coefficient ($k$) which was related to the shear span ratio of the beams. Without considering the shear resistance of horizontal grids, Cai et al. [177] proposed a model with an effective strain of vertical grids related to the mortar thickness, the shear span ratio and the ratio of tensile strength of mortar to concrete through regression analysis. However, the experimental data used for regression analysis were very few (only 5 data), and the regression coefficient was 0.79 (not close to 1.00), so their model had some limitations. The models mentioned above are summarized in Table 8.

The shear capacity of RC beams strengthened with FGREM jackets can be calculated by Eq. (1).

$$V = V_c + V_s + V_{ecc} + V_f \quad (1)$$

where $V_c$, $V_s$, $V_{ecc}$, $V_f$ is the shear contribution of the concrete, the steel stirrups, the ECC and the FRP grid, respectively. The $V_s$ can be expressed as follow:

$$V_s = \frac{2 f_{yv} A_{sv} d}{s} \quad (2)$$

where $f_{yv}$ is the yield strength of stirrups; $A_{sv}$ is the cross-sectional area of single-leg stirrup; $d$ is the effective depth of beam; $s$ is the stirrup spacing. In the existing studies, the partial debonding between FGREM layer and concrete substrate always occurs before the rupture of FRP grid [47,171], so the tensile strength of grid could not be fully utilized. The $V_f$ can be calculated according to ACI 549.4R-20 [171], Guo et al.'s model [166] or Cai et al.'s model

[172]. The $V_{ecc}$ and $V_c$ can be calculated according to the JSCE code [178,179] (for Guo et al.'s model [166] and ACI 549.4R-20 [171]) or the Chinese code [180] (for Cai et al.'s model [172]), as shown in Table 9. The comparison between experimental results (see Table 7) and model predictions are depicted in Fig. 23. The Guo et al.'s model [166] shows better agreement with the experimental results compared with ACI 549.4R-20 [171] and Cai et al.'s model [172]. However, for BFRP grid-reinforced ECC strengthening systems, the predictions from the three models are all conservative, especially for the BFRP grid with low elastic modulus. Note that both the Guo et al.'s [166] and Cai et al.'s model [172] were proposed based on the carbon-FGREM strengthening, thus the effective strain of BFRP grids may be underestimated.

## 3.3 Confined Concrete Column

### 3.3.1 Axial behavior of FGREM/FGRUM-confined concrete columns

Recently, FGREM/FGRUM has been successfully used to confine short cylindrical concrete columns, as shown in Table 10. AL-Gemeel and Zhuge [177-178] have investigated compressive behavior of circular and square columns strengthened with basalt FGREM. They found that the load carrying capacity and the ductility of concrete columns can be enhanced by basalt textile-reinforced ECC, whereas it was found that using textile reinforced mortar may result in a lower ultimate axial stain due to the cracking of the mortar caused by premature failure of the textile. Yan et al. [64] strengthened the concrete-filled steel-tube (CFST) columns using carbon-FGREM with number of FRP grid layers as the main variable. It was found that the confined CFST columns had a higher peak stress than unconfined CFST columns, meanwhile the confined CFST columns exhibited an excellent ductility due to the progressive failure instead of the brittle failure observed in FRP sheet-confined columns. With increasing grid layer number, the confined CFST columns exhibited improved ductility. Chen et al. [181] studied the compressive behavior of concrete column confined with basalt-FGREM, and reported that the FGREM composites were more effective on confining concrete columns than textile reinforced mortar, which was also documented in other literatures [52]. Increasing the number of grid layers and decreasing the grid spacing have obvious effect on improving the peak load of confined columns. Moreover, FGREM jackets were proved to be effective on enhancing peak load and ductility of square concrete columns [51], but the non-uniform confining effect of FGREM was not analyzed and the confinement model for FGREM-confined square columns has not been proposed yet.

Currently, there is few studies on FGRUM-confined columns. Only Tian et al. [50] investigated

the axial behavior of RC columns confined with FGRUM jacket. It was found that the CFRP grid can provide a sufficient lateral confinement to increase the peak load and ductility of the RC column. Compared with the pure/SS-grid-reinforced UHPC formwork, the FGRUM formwork provided stronger confinement which suppressed the brittle behavior and reduced the stress degradation after the peak load.

### 3.3.2 Existing predictive models for peak stress

The axial stress-strain behavior of FRCM-confined columns is affected by many factors including the type of fabric, the characteristic of cementitious matrix, and the fiber-to-matrix interfacial bonding. The poor tensile properties of matrix and weak fiber-to-matrix interfacial bonding are responsible for the post-peak softening behavior of FRCM-confined columns [18] (see the red solid curve in Fig. 24), indicating the weak confinement provided by FRCM. Conversely, the FGREM/FGRUM composites could effectively restrain the development of cracks and maintain the structural integrity due to the excellent tensile properties of ECC/UHPC and superior bond performance between FRP grid and ECC/UHPC, thus resulting in the post-peak ascending curve (see the blue solid curve in Fig. 24), which indicates the effective confinement provided by FGREM/FGRUM. Some predictive models for peak stress of FRCM-confined concrete have been proposed. Ombres et al. [182] established a model by regression analysis based on a database of 152 experimental results of different types of FRCM. A design-oriented model was presented in ACI 549.4R-20 [176], where the effective tensile strain of FRP was kept below 0.012. It should be noted that the confinement provided by cementitious matrix was not considered in the above two models. Recently, Chen et al. [181] proposed a novel model accounting for the lateral confining stress provided by FRP grid and cementitious matrix (see Fig. 25). Table 11 summarizes the aforementioned peak strength models.

The comparison on predictive and experimental results of peak stress is shown in Table 12. To evaluate the axial contribution provided by the confinement of FGREM/FGRUM jackets, the axial contribution of ECC/UHPC layer was estimated by $P_{ue} = 0.9 f_{eu} A_{eu}$, where $f_{eu}$ and $A_{eu}$ are the compressive strength and the cross-sectional area of the ECC/UHPC, respectively. As for the CFST columns confined with FGREM, the predictive results obtained by Ombres et al.'s model [177] and the ACI code [171] have good agreements with the experimental results, but those from Chen et al.'s model [176] overestimate the confinement effect of FGREM. Additionally, Chen et al.'s model [176] has a higher accuracy in predicting the peak stress of

FGREM/FGRUM-confined NSC columns than the other two models [171,177].

### 3.4 Comparison of ECC and UHPFRCC on effects of strengthening

As introduced in chapter 2, the tensile properties of ECC and UHPFRCC are greatly different, thus causing different strengthening effects by using ECC and UHPFRCC. The flexural and shear contribution of strengthening layers are positively correlated to their tensile strength, and thus higher flexural or shear capacities of composite members can be obtained when using the UHPFRCC strengthening layers than the ECC strengthening layer because UHPFRCC generally has a higher tensile strength than that of ECC. For example, the flexural capacity of RC beams was enhanced by 47.8% (specimen C3B) [32] after strengthening with T-sided BFRP bars-reinforced ECC layer, and increased by 57% when using the T-sided UHPC layer without any additional reinforcement (specimen BEAM-2 shown in Table 5) [135]. It can be concluded that the UHPC strengthening is more effective than ECC strengthening in term of increasing load carrying capabilities. Nevertheless, the poor tensile strain capabilities and the high brittleness under compression of UHPFRCC lead to reduction of ductility of UHPFRCC strengthened beams. Strengthening with 3-sided UHPC jackets greatly decreased the deformation capacities of beams, resulting in original ductile failure turning into brittle failure [142]. Conversely, with excellent tensile ductility, 3-sided ECC strengthening was effective on improving the ductility of strengthened beams [129].

### 3.5 Novel FRP-ECC/UHPFRCC structures

Currently, some researchers have proposed FRP grid-reinforced ECC/UHPC plates (i.e., referred to as FRP-ECC/UHPC composite plates) combining the advantages of FRP grid and ECC/UHPC, which is depicted in Fig. 26. FRP grid-reinforced ECC/UHPC plates can not only be used for strengthening structures, but also be used for composite structural elements. The typical tensile stress-strain curves of FRP-ECC/UHPC composites are shown in Fig. 27. Before first cracking, the FRP grid has insignificant effect on tensile performance. After the first cracking, the composite plates exhibited multiple cracking behavior until the fracture of the FRP grid. The addition of the FRP grid can highly improve the ultimate tensile strength of the composite plates.

The FRP-ECC composite plates have a large tensile strength which can be more than two times higher that of pure ECC due to the tensile contribution of FRP gird. Zheng et al. [46] found that no debonding between BFRP grid and ECC was observed in their tests, indicating a good

FRP-to-ECC interfacial bonding. Recently, the mechanical properties of FRP-UHPC composite plates have also been studied. Meng et al. [44] firstly studied the flexural behavior of FRP-UHPC composite plates and found that the composite plates exhibited excellent flexural capacities and deformation capacities. Subsequently, Ye et al. [45] studied the uniaxial tensile and flexural performances of FRP-UHPC composite plates. They concluded that the combination of steel fibers and FRP grids were most effective on enhancing the tensile and flexural capacities of the composite plates. On one hand, the steel fibers with bridging effect could prevent the UHPC cover from peel-off, and to restrain the relative slippage between FRP grid and UHPC matrix because of some fibers passing through the grid openings.

The application prospects of FRP-UHPC (also called FGRUM) composites are illustrated in Fig. 28. Based on the superior mechanical properties of FRP-UHPC composite plates, the authors have proposed a novel thin-walled FRP-UHPC composite box girder consisting of FRP grid, FRP bars and box-shaped UHPC matrix. Obviously, the combination of FRP and UHPC can not only ensure the excellent mechanical performance but also highly enhance the durability of the structures. Therefore, the FRP-UHPC composite box girder is a promising flexural member that are applicable in highway bridges and prefabricated submarine immersed tube. Furthermore, the FGRUM composites are potential strengthening materials for enhancing the axial and seismic performance of bridge piers, meanwhile providing shear and flexural strengthening for bridge abutment girders.

### 3.6 Theoretical Models for FRP-ECC/UHPFRCC Strengthened Structures

In this section, theoretical models for FRP-ECC/UHPFRCC strengthened structures are summarized. The analytical models based on a cross-section analysis for flexural capacity of ECC/UHPFRCC strengthened beams are summarized in Table 6. The comparisons have shown that predicted values of conservative. Also, models for predicting shear capacity of FRCM strengthened beams under shear have been proposed, as can be seen in Tables 8-9. The validations presented in Section 3.2 show that the models are in various accuracies. Additionally, Table 11 summarizes the peak strength models for ECC/UHPFRCC strengthened RC columns and the validation results are given in Table 12. Particularly, further studies on theoretical models for FRP- ECC/UHPFRCC strengthened RC members are necessary.

## 4. Conclusions

This paper presents a state-of-the-art comprehensive review on the components, basic

characteristics and applications of ECC/UHPFRCC with and without FRP reinforcements in structural strengthening/repairing. The applications and mechanical behaviors of FRP-ECC/UHPFRCC composites were further introduced. Several key conclusions can be drawn:

(1) Reducing FA/B ratios and W/B ratios and increasing S/B ratios of ECC contribute to a higher compressive strength but lead to a lower tensile strain capability. Common fibers utilized in ECC are PVA and PP fibers, and the PVA fibers with volume fraction of 2% are more widely used.

(2) Low W/B ratios (from 0.14 to 0.20) and high S/B ratios (from 0.8 to 1.0) contribute to a higher compressive strength but lead to a poor tensile ductility of UHPC. The steel fibers with volume fraction ranging from 1.0% to 2.0% are commonly applied to enhance the tensile properties of UHPC.

(3) UHP-ECC has low W/B ratios (from 0.14 to 0.18) to achieve a higher compressive strength, and low S/B ratios (from 0.29 to 0.30) to improve the tensile ductility. PE fibers are commonly used as reinforcing fibers in UHP-ECC. The tensile performance of UHP-ECC is enhanced with increasing fiber reinforcement index.

(4) The roughness around 4 mm of concrete substrate and the usage of primer (for cast in place ECC) or bonding agent (for prefabricated ECC) effectively enhanced the ECC-to-concrete interfacial bonding. Mechanical connector (e.g., shear studs) and SB or R surface preparation for concrete substrate are effective on enhancing UHPC-to-concrete interfacial bonding.

(5) ECC and UHPFRCC exhibit superior freeze-thaw resistance, chemical attack resistance, abrasion resistance and fire resistance. Generally, the freeze-thaw and fire resistance of UHPFRCC are better than those of ECC.

(6) The T-sided and 3-sided ECC strengthening can effectively enhance the flexural and shear behavior of RC beams, respectively. Compared with C-sided and 3-sided strengthening, T-sided UHPFRCC layers are more cost-effective for flexural strengthening. The mechanical connectors located at the interface can suppress the premature debonding between UHPFRCC/ECC layer and concrete. Furthermore, UHPFRCC/ECC layers should be moderately reinforced to prevent the premature failure in the strengthening layer.

(7) The 4-sided ECC/UHPFRCC jackets show great potential in seismic strengthening of RC columns or beam-column joints. The interfacial bonding between the NSC and the ECC/UHPFRCC plays a key role in improving the seismic performance of composite members. Sufficient reinforcement inside the jackets is required to provide a strong confinement for the core of the column to prevent the interfacial detachment. Moreover,

the integrity and continuity of prefabricated jackets is important for a good composite action between the jacket and the core concrete.

(8) The formwork surface treatment has a great influence on the strengthening efficiency of U-shaped ECC/UHPFRCC formwork for strengthening RC beams. How to quantify the effect of different surface treatments on strengthening efficiency has become a key issue.

(9) The ECC/UHPFRCC permanent formwork can effectively provide confinement for RC columns to enhance the load capacity and ductility. Whether the confinement provided by formwork is strong enough (which is depend on the ECC/UHPFRCC layer thickness, the transverse reinforcement type and the transverse reinforcement ratio) becomes the most key issue to develop an efficient formwork.

(10) The ECC/UHPFRCC-NSC composite beams exhibit higher load carrying capability, ductility and energy absorption capability than NSC beams. But there are some contradictions on the relation between ductility and height replacement ratio in existing studies.

(11) The T-sided FGREM layers can effectively improve the flexural behavior of RC beams. The proposed predictive model for flexural capacities of FGREM strengthened RC beams is accurate in predicting the flexural capacities of the specimens in the existing experimental studies.

(12) The 2-sided FGREM layers can effectively improve the shear behavior of RC beams. The Guo et al.'s model considering the shear contribution of bidirectional strips shows the best agreement with the experimental results of carbon-FGREM strengthened RC beams. However, for basalt-FGREM strengthening, the results from all existing models are conservative.

(13) FGREM/FGRUM-confined columns exhibit higher peak stress and ductility than unconfined column. The Chen et al.'s model considering both the confinement from the FRP grid and the cementitious matrix provides more accurate predictions on the peak stresses of FGREM/FGRUM-confined NSC columns.

(14) The FGREM/FGRUM composites exhibit superior tensile and flexural performance combining the advantages of the FRP grid and the ECC/UHPFRCC, making them promising candidates in strengthening/repairing existing RC structures or constructing novel composite structures.

## 5. Further Research Opportunities

On one hand, there are some deficiencies or limitations in the existing studies on

ECC/UHPFRCC with and without FRP reinforcement. On the other hand, in order to widely exploit the advantages of FGREM/FGRUM composites and promote the applications of FGREM/FGRUM composites in engineering structures, it is necessary to gain a comprehensive insight to the load carrying capacities and the ductility of strengthened/composite members with FGREM/FGRUM composites subjected to various forms of loading. Future research needs are identified and discussed below based on the above state-of-the-art review:

(1) Although it is found that the addition of mechanical connectors has a satisfactory effect on preventing the interfacial debonding, future efforts can also focus on the optimum design of mechanical connectors, especially the impact of the number and location of mechanical connectors on the strengthening effect.

(2) To further promote the assembled seismic strengthening technology, the issue of joint splicing for segmental prefabricated ECC/UHPFRCC jackets needs to be addressed to enhance the continuity of prefabricated jackets. The impact of different types of preparation for substrate surface (e.g., SB, R and GR surface) and the transverse reinforcement ratio inside the jacket on the efficiency of seismic strengthening needs to be investigated.

(3) Existing studies on 2-sided and 3-sided ECC/UHPFRCC strengthening are still limited. Effectiveness of 2-sided or 3-sided ECC/UHPC layers on shear strengthening of RC beams needs to be further studied, especially the impact of surface treatment for the concrete substrate and the reinforcement ratio of UHPFRCC layers on the strengthening efficiency.

(4) The surface treatment of precast U-shaped ECC/UHPFRCC formwork is the key to obtain a sufficient bond strength and thus ensure an excellent strengthening effect. More studies are required to quantify the impact of various surface treatments on the strengthening efficiency of U-shaped ECC/UHPFRCC formwork.

(5) The influences of ECC/UHPFRCC layer thickness, the transverse reinforcement types (e.g., steel stirrups, FRP spirals and FRP grid), and the transverse reinforcement ratio on the confinement efficiency of ECC/UHPFRCC permanent formworks need to be studied.

(6) The relation between the ductility and the replacement ratio of ECC/UHPFRC-NSC composite members need to be further studied to clarify the contradictions in existing research.

(7) The studies on flexural strengthening with T-sided FGREM layer is still very limited, so the accuracy of the proposed model for predicting the flexural capabilities of strengthened RC beams with FGREM needs further verifications.

(8) The shear strength models for RC beams with FRP-ECC strengthening should consider the impact of shear span ratio, the ratio of cross-sectional area to spacing of FRP grids, the

ECC thickness, and the ratio of tensile strength of ECC to concrete on the effective strain of FRP grids at ultimate state.

(9) The predictive model for ultimate compressive strain of FGREM/FGRUM-confined NSC columns should be developed.

(10) UHP-ECC strengthened/repaired RC structures and UHP-ECC permanent formwork are worth further development and continuous investigation in the future.

## Acknowledgements

The authors acknowledge the financial support received from the Key Special Project for Introduced Talents Team of Southern Marine Science and Engineering Guangdong Laboratory (Guangzhou) (GML2019ZD0503), the Hong Kong Innovation and Technology Fund (No. ITS/077/18FX), the Guangzhou Science and Technology Department (No. 201904010163), the Natural Science Foundation of Guangdong Province (No. 2019A1515011637, 2021A0505060008), the University of Macau (File no. UMMTP2020-MYSP-003), as well as the Association for Promotion of Science and Technology of Macau and the Office of China National Postdoctoral Council (File no. AM2020002).

## References

[1] M.A. Ali, E. El-Salakawy.Seismic Performance of GFRP-Reinforced Concrete Rectangular Columns.Journal of Composites for Construction,2016, 20 (3).

[2] M. Bazli, X.-L. Zhao, Y. Bai, R.K. Singh Raman, S. Al-Saadi, A. Haque.Durability of pultruded GFRP tubes subjected to seawater sea sand concrete and seawater environments.Construction and Building Materials,2020, 245.

[3] B. Benmokrane, A. Sanni Bakouregui, H.M. Mohamed, D. Thébeau, O.I. Abdelkarim.Design, Construction, and Performance of Continuously Reinforced Concrete Pavement Reinforced with GFRP Bars: Case Study.Journal of Composites for Construction,2020, 24 (5).

[4] Y. Duo, X. Liu, Y. Liu, T. Tafsirojjaman, M. Sabbrojjaman.Environmental impact on the durability of FRP reinforcing bars.Journal of Building Engineering,2021, 43.

[5] T. Liu, X. Liu, P. Feng.A comprehensive review on mechanical properties of pultruded FRP composites subjected to long-term environmental effects.Composites Part B: Engineering,2020, 191.

[6] J.-J. Zeng, W.-Y. Gao, Z.-J. Duan, Y.-L. Bai, Y.-C. Guo, L.-J. Ouyang.Axial compressive behavior of polyethylene terephthalate/carbon FRP-confined seawater sea-sand concrete in circular columns.Construction and Building Materials,2020, 234.

[7] Y.A. Al-Salloum, H.M. Elsanadedy, S.H. Alsayed, R.A. Iqbal.Experimental and Numerical Study for the Shear Strengthening of Reinforced Concrete Beams Using Textile-Reinforced Mortar.Journal of Composites for Construction,2012, 16 (1): 74-90.

[8] P.J. Burke, L.A. Bisby, M.F. Green.Effects of elevated temperature on near surface mounted and externally bonded FRP strengthening systems for concrete.Cement and Concrete Composites,2013, 35 (1): 190-199.

[9] Z.R. Aljazaeri, M.A. Janke, J.J. Myers.A novel and effective anchorage system for enhancing the flexural capacity of RC beams strengthened with FRCM composites.Composite Structures,2019, 210: 20-28.

[10] R. Azam, K. Soudki, J.S. West, M. Noël.Strengthening of shear-critical RC beams: Alternatives to externally bonded CFRP sheets.Construction and Building Materials,2017, 151: 494-503.

[11] A.C.H. Giese, D.N. Giese, V.F.P. Dutra, L.C.P. Da Silva Filho.Flexural behavior of reinforced concrete beams strengthened with textile reinforced mortar.Journal of Building Engineering,2021, 33.

[12] J.H. Gonzalez-Libreros, C. Sabau, L.H. Sneed, C. Pellegrino, G. Sas.State of research on shear strengthening of RC beams with FRCM composites.Construction and Building Materials,2017, 149: 444-458.

[13] J.H. Gonzalez-Libreros, L.H. Sneed, T. D'antino, C. Pellegrino.Behavior of RC beams strengthened in shear with FRP and FRCM composites.Engineering Structures,2017, 150: 830-842.
[14] Z.C. Tetta, T.C. Triantafillou, D.A. Bournas.On the design of shear-strengthened RC members through the use of textile reinforced mortar overlays.Composites Part B: Engineering,2018, 147: 178-196.
[15] T.G. Wakjira, U. Ebead.A shear design model for RC beams strengthened with fabric reinforced cementitious matrix.Engineering Structures,2019, 200.
[16] P. Colajanni, F. De Domenico, A. Recupero, N. Spinella.Concrete columns confined with fibre reinforced cementitious mortars: Experimentation and modelling.Construction and Building Materials,2014, 52: 375-384.
[17] F. Faleschini, M.A. Zanini, L. Hofer, K. Toska, D. De Domenico, C. Pellegrino.Confinement of reinforced concrete columns with glass fiber reinforced cementitious matrix jackets.Engineering Structures,2020, 218.
[18] A. Napoli, R. Realfonzo.Compressive strength of concrete confined with fabric reinforced cementitious matrix (FRCM): Analytical models.Composites Part C: Open Access,2020, 2.
[19] L. Ombres.Concrete confinement with a cement based high strength composite material.Composite Structures,2014, 109: 294-304.
[20] T. Blanksvard, B. Taljsten, A. Carolin.Shear Strengthening of Concrete Structures with the Use of Mineral-Based Composites.Journal Of Composites for Construction,2009, 13 (1): 25-34.
[21] S.F.U. Ahmed, H. Mihashi.A review on durability properties of strain hardening fibre reinforced cementitious composites (SHFRCC).Cement & Concrete Composites,2007, 29 (5): 365-376.
[22] H.D. Li, S.L. Xu, C.K.Y. Leung.Tensile and flexural properties of ultra high toughness cemontious composite.Journal Of Wuhan University Of Technology-Materials Science Edition,2009, 24 (4): 677-683.
[23] V.C. Li, S.X. Wang, C. Wu.Tensile strain-hardening behavior of polyvinyl alcohol engineered cementitious composite (PVA-ECC).Aci Materials Journal,2001, 98 (6): 483-492.
[24] H.Z. Liu, Q. Zhang, C.S. Gu, H.Z. Su, V.C. Li.Influence of microcrack self-healing behavior on the permeability of Engineered Cementitious Composites.Cement & Concrete Composites,2017, 82: 14-22.
[25] H.R. Pakravan, M. Jamshidi.Tensile properties of strain-hardening cementitious composites containing polyvinyl-alcohol fibers hybridized with polypropylene fibers.Journal Of Central South University,2018, 25 (1): 51-59.
[26] K. Yu, L. Li, J. Yu, Y. Wang, J. Ye, Q. Xu.Direct tensile properties of engineered cementitious composites: A review.Construction and Building Materials,2018, 165: 346-362.
[27] A. Alyousif, M. Lachemi, G. Yildirim, G.H. Aras, M. Sahmaran.Influence of Cyclic Frost Deterioration on Water Sorptivity of Microcracked Cementitious Composites.Journal of Materials in Civil Engineering,2016, 28 (4).
[28] Y. Al-Najjar, S. Yesilmen, M. Al-Dahawi, M. Sahmaran, G. Yildirim, M. Lachemi, L. Amleh.Physical and Chemical Actions of Nano-Mineral Additives on Properties of High-Volume Fly Ash Engineered Cementitious Composites.Aci Materials Journal,2016, 113 (6): 791-801.
[29] M. Sahmaran, O. Anil, M. Lachemi, G. Yildirim, A.F. Ashour, F. Acar.Effect of Corrosion on Shear Behavior of Reinforced Engineered Cementitious Composite Beams.Aci Structural Journal,2015, 112 (6): 771-782.
[30] O. Ozturk, G. Yildirim, U.S. Keskin, H. Siad, M. Sahmaran.Nano-tailored multi-functional cementitious composites.Composites Part B-Engineering,2020, 182.
[31] L. Hou, J. Wang, T. Huang, C. Shen, F. Aslani, D. Chen.Flexural behaviour of corroded reinforced concrete beams repaired with ultra-high toughness cementitious composite.Construction and Building Materials,2019, 211: 1127-1137.
[32] W. Hou, Z.-Q. Li, W.-Y. Gao, P.-D. Zheng, Z.-X. Guo.Flexural behavior of RC beams strengthened with BFRP bars-reinforced ECC matrix.Composite Structures,2020, 241.
[33] K. Kobayashi, K. Rokugo.Mechanical performance of corroded RC member repaired by HPFRCC patching.Construction and Building Materials,2013, 39: 139-147.
[34] K. Ragalwar, W.F. Heard, B.A. Williams, D. Kumar, R. Ranade.On enhancing the mechanical behavior of ultra-high performance concrete through multi-scale fiber reinforcement.Cement and Concrete Composites,2020, 105.
[35] D.-Y. Yoo, N. Banthia.Mechanical properties of ultra-high-performance fiber-reinforced concrete: A review.Cement and Concrete Composites,2016, 73: 267-280.
[36] K.-Q. Yu, J.-T. Yu, J.-G. Dai, Z.-D. Lu, S.P. Shah.Development of ultra-high performance engineered cementitious composites using polyethylene (PE) fibers.Construction and Building Materials,2018, 158: 217-227.
[37] K.-Q. Yu, W.-J. Zhu, Y. Ding, Z.-D. Lu, J.-T. Yu, J.-Z. Xiao.Micro-structural and mechanical properties of ultra-high performance engineered cementitious composites (UHP-ECC) incorporation of recycled fine powder (RFP).Cement and Concrete Research,2019, 124.
[38] S.-T. Kang, Y. Lee, Y.-D. Park, J.-K. Kim.Tensile fracture properties of an Ultra High Performance Fiber Reinforced Concrete (UHPFRC) with steel fiber.Composite Structures,2010, 92 (1): 61-71.
[39] K.-Q. Yu, J.-G. Dai, Z.-D. Lu, C.-S. Poon.Rate-dependent tensile properties of ultra-high performance engineered cementitious composites (UHP-ECC).Cement and Concrete Composites,2018, 93: 218-234.

[40] K.-Q. Yu, Z.-D. Lu, J.-G. Dai, S.P. Shah.Direct Tensile Properties and Stress–Strain Model of UHP-ECC.Journal of Materials in Civil Engineering,2020, 32 (1).
[41] Z. Dong, G. Wu, X.-L. Zhao, H. Zhu, X. Shao.Behaviors of hybrid beams composed of seawater sea-sand concrete (SWSSC) and a prefabricated UHPC shell reinforced with FRP bars.Construction and Building Materials,2019, 213: 32-42.
[42] B. Shan, D.-D. Lai, Y. Xiao, X.-B. Luo.Experimental research on concrete-filled RPC tubes under axial compression load.Engineering Structures,2018, 155: 358-370.
[43] Y. Zhu, Y. Zhang, H.H. Hussein, G. Chen.Flexural strengthening of reinforced concrete beams or slabs using ultra-high performance concrete (UHPC): A state of the art review.Engineering Structures,2020, 205.
[44] W. Meng, K.H. Khayat, Y. Bao.Flexural behaviors of fiber-reinforced polymer fabric reinforced ultra-high-performance concrete panels.Cement and Concrete Composites,2018, 93: 43-53.
[45] Y.-Y. Ye, S.T. Smith, J.-J. Zeng, Y. Zhuge, W.-M. Quach.Novel ultra-high-performance concrete composite plates reinforced with FRP grid: Development and mechanical behaviour.Composite Structures,2021, 269.
[46] Y.-Z. Zheng, W.-W. Wang, K.M. Mosalam, Z.-F. Zhu.Mechanical behavior of ultra-high toughness cementitious composite strengthened with Fiber Reinforced Polymer grid.Composite Structures,2018, 184: 1-10.
[47] A. Zheng, S. Li, D. Zhang, Y. Yan.Shear strengthening of RC beams with corrosion-damaged stirrups using FRP grid-reinforced ECC matrix composites.Composite Structures,2021, 272.
[48] C. Chen, H. Cai, L. Cheng.Shear Strengthening of Corroded RC Beams Using UHPC–FRP Composites.Journal of Bridge Engineering,2021, 26 (1).
[49] X. Yang, W.-Y. Gao, J.-G. Dai, Z.-D. Lu, K.-Q. Yu.Flexural strengthening of RC beams with CFRP grid-reinforced ECC matrix.Composite Structures,2018, 189: 9-26.
[50] H. Tian, Z. Zhou, Y. Zhang, Y. Wei.Axial behavior of reinforced concrete column with ultra-high performance concrete stay-in-place formwork.Engineering Structures,2020, 210.
[51] A.N. Al-Gemeel, Y. Zhuge.Experimental investigation of textile reinforced engineered cementitious composite (ECC) for square concrete column confinement.Construction and Building Materials,2018, 174: 594-602.
[52] A.N. Al-Gemeel, Y. Zhuge.Using textile reinforced engineered cementitious composite for concrete columns confinement.Composite Structures,2019, 210: 695-706.
[53] Z. Pan, C. Wu, J. Liu, W. Wang, J. Liu.Study on mechanical properties of cost-effective polyvinyl alcohol engineered cementitious composites (PVA-ECC).Construction and Building Materials,2015, 78: 397-404.
[54] S. Sasmal, G. Avinash.Investigations on mechanical performance of cementitious composites micro-engineered with poly vinyl alcohol fibers.Construction and Building Materials,2016, 128: 136-147.
[55] M. Singh, B. Saini, H.D. Chalak.Performance and composition analysis of engineered cementitious composite (ECC) – A review.Journal of Building Engineering,2019, 26.
[56] M. Şahmaran, E. Özbay, H.E. Yücel, M. Lachemi, V.C. Li.Effect of Fly Ash and PVA Fiber on Microstructural Damage and Residual Properties of Engineered Cementitious Composites Exposed to High Temperatures.Journal of Materials in Civil Engineering,2011, 23 (12): 1735-1745.
[57] J. Yu, J. Lin, Z. Zhang, V.C. Li.Mechanical performance of ECC with high-volume fly ash after sub-elevated temperatures.Construction and Building Materials,2015, 99: 82-89.
[58] M. Şahmaran, E. Özbay, H.E. Yücel, M. Lachemi, V.C. Li.Frost resistance and microstructure of Engineered Cementitious Composites: Influence of fly ash and micro poly-vinyl-alcohol fiber.Cement and Concrete Composites,2012, 34 (2): 156-165.
[59] M. Şahmaran, M. Lachemi, K.M.A. Hossain, V.C. Li.Internal curing of engineered cementitious composites for prevention of early age autogenous shrinkage cracking.Cement and Concrete Research,2009, 39 (10): 893-901.
[60] M. Sahmaran, M. Lachemi, K.M.A. Hossain, R. Ranade, V.C. Li.Influence of Aggregate Type and Size on Ductility and Mechanical Properties of Engineered Cementitious Composites.Aci Materials Journal,2009, 106 (3): 308-316.
[61] J.-X. Lin, Y. Song, Z.-H. Xie, Y.-C. Guo, B. Yuan, J.-J. Zeng, X. Wei.Static and dynamic mechanical behavior of engineered cementitious composites with PP and PVA fibers.Journal of Building Engineering,2020, 29.
[62] M.F. Arain, M. Wang, J. Chen, H. Zhang.Study on PVA fiber surface modification for strain-hardening cementitious composites (PVA-SHCC).Construction and Building Materials,2019, 197: 107-116.
[63] B. Felekoglu, K. Tosun-Felekoglu, R. Ranade, Q. Zhang, V.C. Li.Influence of matrix flowability, fiber mixing procedure, and curing conditions on the mechanical performance of HTPP-ECC.Composites Part B: Engineering,2014, 60: 359-370.
[64] Y. Yan, H. Liang, Y. Lu, Y. Huang.Behaviour of concrete-filled steel-tube columns strengthened with high-strength CFRP textile grid-reinforced high-ductility engineered cementitious composites.Construction and Building Materials,2021, 269.
[65] S.L. Xu, X.R. Cai.Experimental Study and Theoretical Models on Compressive Properties of Ultrahigh Toughness Cementitious Composites.Journal Of Materials In Civil Engineering,2010, 22 (10): 1067-1077.

[66] J. Zhou, J. Pan, C.K.Y. Leung.Mechanical Behavior of Fiber-Reinforced Engineered Cementitious Composites in Uniaxial Compression.Journal of Materials in Civil Engineering,2015, 27 (1).
[67] C. Shi, Z. Wu, J. Xiao, D. Wang, Z. Huang, Z. Fang.A review on ultra high performance concrete: Part I. Raw materials and mixture design.Construction and Building Materials,2015, 101: 741-751.
[68] R. Yu, P. Spiesz, H.J.H. Brouwers.Mix design and properties assessment of Ultra-High Performance Fibre Reinforced Concrete (UHPFRC).Cement and Concrete Research,2014, 56: 29-39.
[69] M. Courtial, M.N. De Noirfontaine, F. Dunstetter, M. Signes-Frehel, P. Mounanga, K. Cherkaoui, A. Khelidj.Effect of polycarboxylate and crushed quartz in UHPC: Microstructural investigation.Construction and Building Materials,2013, 44: 699-705.
[70] J. Li, Z. Wu, C. Shi, Q. Yuan, Z. Zhang.Durability of ultra-high performance concrete – A review.Construction and Building Materials,2020, 255.
[71] Y.-W. Chan, S.-H. Chu.Effect of silica fume on steel fiber bond characteristics in reactive powder concrete.Cement and Concrete Research,2004, 34 (7): 1167-1172.
[72] D.-Y. Yoo, J.-H. Lee, Y.-S. Yoon.Effect of fiber content on mechanical and fracture properties of ultra high performance fiber reinforced cementitious composites.Composite Structures,2013, 106: 742-753.
[73] Z. Wu, C. Shi, W. He, L. Wu.Effects of steel fiber content and shape on mechanical properties of ultra high performance concrete.Construction and Building Materials,2016, 103: 8-14.
[74] B.-T. Huang, J.-G. Dai, K.-F. Weng, J.-X. Zhu, S.P. Shah.Flexural Performance of UHPC–Concrete–ECC Composite Member Reinforced with Perforated Steel Plates.Journal of Structural Engineering,2021, 147 (6).
[75] H. Bahmani, D. Mostofinejad, S.A. Dadvar.Mechanical Properties of Ultra-High-Performance Fiber-Reinforced Concrete Containing Synthetic and Mineral Fibers.Aci Materials Journal,2020, 117 (3): 155-168.
[76] H. Bahmani, D. Mostofinejad, S.A. Dadvar.Effects of Synthetic Fibers and Different Levels of Partial Cement Replacement on Mechanical Properties of UHPFRC.Journal Of Materials In Civil Engineering,2020, 32 (12).
[77] Y. Ding, K.-Q. Yu, J.-T. Yu, S.-L. Xu.Structural behaviors of ultra-high performance engineered cementitious composites (UHP-ECC) beams subjected to bending-experimental study.Construction and Building Materials,2018, 177: 102-115.
[78] K. Yu, Y. Wang, J. Yu, S. Xu.A strain-hardening cementitious composites with the tensile capacity up to 8%.Construction and Building Materials,2017, 137: 410-419.
[79] L. Li, Z. Cai, K. Yu, Y.X. Zhang, Y. Ding.Performance-based design of all-grade strain hardening cementitious composites with compressive strengths from 40 MPa to 120 MPa.Cement and Concrete Composites,2019, 97: 202-217.
[80] K. Yu, L. Li, J. Yu, J. Xiao, J. Ye, Y. Wang.Feasibility of using ultra-high ductility cementitious composites for concrete structures without steel rebar.Engineering Structures,2018, 170: 11-20.
[81] A.I.B. Farouk, S.I. Haruna.Evaluation of Bond Strength between Ultra-High-Performance Concrete and Normal Strength Concrete: An Overview.Jurnal Kejuruteraan,2020, 32 (3): 41-51.
[82] B. Wang, Q. Li, F. Liu, S. Xu, H. Zhou, K. Tan.Comparison of Cast-In-Situ and Prefabricated UHTCC Repair Systems under Bending.Journal of Materials in Civil Engineering,2018, 30 (1).
[83] B. Wang, S. Xu, F. Liu.Evaluation of tensile bonding strength between UHTCC repair materials and concrete substrate.Construction and Building Materials,2016, 112: 595-606.
[84] B. Wang, Q. Li, F. Liu, J. Wang, S. Xu.Shear bond assessment of UHTCC repair using push-out test.Construction and Building Materials,2018, 164: 206-216.
[85] L. Sui, M. Luo, K. Yu, F. Xing, P. Li, Y. Zhou, C. Chen.Effect of engineered cementitious composite on the bond behavior between fiber-reinforced polymer and concrete.Composite Structures,2018, 184: 775-788.
[86] S. Xu, F. Mu, J. Wang, W. Li.Experimental study on the interfacial bonding behaviors between sprayed UHTCC and concrete substrate.Construction and Building Materials,2019, 195: 638-649.
[87] J. Tian, X. Wu, Y. Zheng, S. Hu, Y. Du, W. Wang, C. Sun, L. Zhang.Investigation of interface shear properties and mechanical model between ECC and concrete.Construction and Building Materials,2019, 223: 12-27.
[88] M. Sahmaran, H.E. Yücel, G. Yildirim, M. Al-Emam, M. Lachemi.Investigation of the Bond between Concrete Substrate and ECC Overlays.Journal of Materials in Civil Engineering,2014, 26 (1): 167-174.
[89] G. Yildirim, M. Sahmaran, M.K.M. Al-Emam, R.K.H. Hameed, Y. Al-Najjar, M. Lachemi.Effects of Compressive Strength, Autogenous Shrinkage, and Testing Methods on Bond Behavior of High-Early-Strength Engineered Cementitious Composites.Aci Materials Journal,2015, 112 (3): 409-418.
[90] A. Valikhani, A.J. Jahromi, I.M. Mantawy, A. Azizinamini.Effect of mechanical connectors on interface shear strength between concrete substrates and UHPC: Experimental and numerical studies and proposed design equation.Construction and Building Materials,2021, 267.
[91] A. Valikhani, A.J. Jahromi, I.M. Mantawy, A. Azizinamini.Experimental evaluation of concrete-to-UHPC bond strength with correlation to surface roughness for repair application.Construction and Building Materials,2020, 238.
[92] Y. Zhang, P. Zhu, Z. Liao, L. Wang.Interfacial bond properties between normal strength concrete substrate and ultra-high performance concrete as a repair material.Construction and Building Materials,2020, 235.

[93] Y. Zhang, C. Zhang, Y. Zhu, J. Cao, X. Shao.An experimental study: various influence factors affecting interfacial shear performance of UHPC-NSC.Construction and Building Materials,2020, 236.
[94] M.a.C. Munoz, D.K. Harris, T.M. Ahlborn, D.C. Froster.Bond Performance between Ultrahigh-Performance Concrete and Normal-Strength Concrete.Journal Of Materials In Civil Engineering,2014, 26 (8).
[95] A.A. Semendary, D. Svecova.Factors affecting bond between precast concrete and cast in place ultra high performance concrete (UHPC).Engineering Structures,2020, 216.
[96] B.A. Tayeh, B.H.A. Bakar, M.a.M. Johari, Y.L. Voo.Evaluation of Bond Strength between Normal Concrete Substrate and Ultra High Performance Fiber Concrete as a Repair Material.Procedia Engineering,2013, 54: 554-563.
[97] B.A. Tayeh, B.H. Abu Bakar, M.A. Megat Johari.Characterization of the interfacial bond between old concrete substrate and ultra high performance fiber concrete repair composite.Materials and Structures,2012, 46 (5): 743-753.
[98] B.A. Tayeh, B.H. Abu Bakar, M.A. Megat Johari, Y.L. Voo.Mechanical and permeability properties of the interface between normal concrete substrate and ultra high performance fiber concrete overlay.Construction and Building Materials,2012, 36: 538-548.
[99] S. Jafarinejad, A. Rabiee, M. Shekarchi.Experimental investigation on the bond strength between Ultra high strength Fiber Reinforced Cementitious Mortar & conventional concrete.Construction and Building Materials,2019, 229.
[100] H. Ma, C. Yi, C. Wu.Review and outlook on durability of engineered cementitious composite (ECC).Construction and Building Materials,2021, 287.
[101] P.S. Bhat, V. Chang, M. Li.Effect of elevated temperature on strain-hardening engineered cementitious composites.Construction and Building Materials,2014, 69: 370-380.
[102] Z. Zhang, J.-C. Liu, X. Xu, L. Yuan.Effect of sub-elevated temperature on mechanical properties of ECC with different fly ash contents.Construction and Building Materials,2020, 262.
[103] X.Y. Shang, Z.D. Lu.Impact of High Temperature on the Compressive Strength of ECC.Advances In Materials Science And Engineering,2014, 2014.
[104] M. Abid, X.M. Hou, W.Z. Zheng, R.R. Hussain.High temperature and residual properties of reactive powder concrete - A review.Construction And Building Materials,2017, 147: 339-351.
[105] A.Q. Sobia, M.S. Hamidah, I. Azmi, S.F.A. Rafeeqi.Elevated temperature resistance of ultra-high-performance fibre-reinforced cementitious composites.Magazine Of Concrete Research,2015, 67 (17): 923-937.
[106] W. Zheng, H. Li, Y. Wang.Compressive behaviour of hybrid fiber-reinforced reactive powder concrete after high temperature.Materials & Design,2012, 41: 403-409.
[107] S. Sanchayan, S.J. Foster.High temperature behaviour of hybrid steel–PVA fibre reinforced reactive powder concrete.Materials and Structures,2015, 49 (3): 769-782.
[108] W. Zheng, H. Li, Y. Wang.Compressive stress–strain relationship of steel fiber-reinforced reactive powder concrete after exposure to elevated temperatures.Construction and Building Materials,2012, 35: 931-940.
[109] G.F. Peng, Y.R. Kang, Y.Z. Huang, X.P. Liu, Q. Chen.Experimental Research on Fire Resistance of Reactive Powder Concrete.Advances In Materials Science And Engineering,2012, 2012.
[110] Y.-S. Tai, H.-H. Pan, Y.-N. Kung.Mechanical properties of steel fiber reinforced reactive powder concrete following exposure to high temperature reaching 800°C.Nuclear Engineering and Design,2011, 241 (7): 2416-2424.
[111] W. Zheng, B. Luo, Y. Wang.Compressive and tensile properties of reactive powder concrete with steel fibres at elevated temperatures.Construction and Building Materials,2013, 41: 844-851.
[112] V. Mechtcherine, F.D. Silva, S. Muller, P. Jun, R.D. Toledo.Coupled strain rate and temperature effects on the tensile behavior of strain-hardening cement-based composites (SHCC) with PVA fibers.Cement And Concrete Research,2012, 42 (11): 1417-1427.
[113] J.J. Luo, Z.W. Cai, K.Q. Yu, W.J. Zhu, Z.D. Lu.Temperature impact on the micro-structures and mechanical properties of high-strength engineered cementitious composites.Construction And Building Materials,2019, 226: 686-698.
[114] W.Z. Zheng, H.Y. Li, Y. Wang, H.Y. Xie: Tensile properties of steel fiber-reinforced reactive powder concrete after high temperature, Chen S.F., Jiang B.,editor,Materials Science And Engineering Application Ii,2012: 270-276.
[115] H.Y. Li, G. Liu.Tensile Properties of Hybrid Fiber-Reinforced Reactive Powder Concrete After Exposure to Elevated Temperatures.International Journal Of Concrete Structures And Materials,2016, 10 (1): 29-37.
[116] S. Pourfalah.Behaviour of engineered cementitious composites and hybrid engineered cementitious composites at high temperatures.Construction And Building Materials,2018, 158: 921-937.
[117] M. Sahmaran, E. Ozbay, H.E. Yucel, M. Lachemi, V.C. Li.Frost resistance and microstructure of Engineered Cementitious Composites: Influence of fly ash and micro poly-vinyl-alcohol fiber.Cement & Concrete Composites,2012, 34 (2): 156-165.

[118] Y.S. Liu, X.M. Zhou, C.B. Lv, Y.Z. Yang, T.A. Liu.Use of Silica Fume and GGBS to Improve Frost Resistance of ECC with High-Volume Fly Ash.Advances In Civil Engineering,2018, 2018.
[119] Y. Wang, M.-Z. An, Z.-R. Yu, S. Han, W.-Y. Ji.Durability of reactive powder concrete under chloride-salt freeze–thaw cycling.Materials and Structures,2016, 50 (1): 18.
[120] T.M. Ahlborn, D.K. Harris, D.L. Misson, E.J. Peuse.Characterization of Strength and Durability of Ultra-High-Performance Concrete Under Variable Curing Conditions.Transportation Research Record,2011 (2251): 68-75.
[121] B. Graybeal.Material Property Characterization of Ultra-High Performance Concrete.FHWA-HRT-06-103,2006: 1-176.
[122] H.Z. Liu, Q. Zhang, V. Li, H.Z. Su, C.S. Gu.Durability study on engineered cementitious composites (ECC) under sulfate and chloride environment.Construction And Building Materials,2017, 133: 171-181.
[123] Q. Ye, J. Zhu.Investigation on durability of reactive powder concrete.New Building Materials,2006: 33-36.
[124] R. Reju, G. Jacob. Investigations on the chemical durability properties of Ultra High Performance Fibre Reinforced Concrete. 2012: 181-185.
[125] S.R. Abid, M.S. Shamkhi, N.S. Mahdi, Y.H. Daek.Hydro-abrasive resistance of engineered cementitious composites with PP and PVA fibers.Construction and Building Materials,2018, 187: 168-177.
[126] C. Wu, Y. Pan, T. Ueda.Characterization of the abrasion resistance and the acoustic wave attenuation of the engineered cementitious composites for runway pavement.Construction and Building Materials,2018, 174: 537-546.
[127] M.K. Ismail, A.a.A. Hassan, M. Lachemi.Abrasion Resistance of Self-Consolidating Engineered Cementitious Composites Developed with Different Mixture Compositions.Aci Materials Journal,2019, 116 (1): 27-38.
[128] M.-G. Lee, Y.-C. Wang, C.-T. Chiu.A preliminary study of reactive powder concrete as a new repair material.Construction and Building Materials,2007, 21 (1): 182-189.
[129] X.-Y. Shang, J.-T. Yu, L.-Z. Li, Z.-D. Lu.Shear strengthening of fire damaged RC beams with stirrup reinforced engineered cementitious composites.Engineering Structures,2020, 210.
[130] C. Wu, V.C. Li.CFRP-ECC hybrid for strengthening of the concrete structures.Composite Structures,2017, 178: 372-382.
[131] F. Yuan, M. Chen, J. Pan.Flexural strengthening of reinforced concrete beams with high-strength steel wire and engineered cementitious composites.Construction and Building Materials,2020, 254.
[132] C.-C. Hung, Y.-S. Chen.Innovative ECC jacketing for retrofitting shear-deficient RC members.Construction and Building Materials,2016, 111: 408-418.
[133] X.-Y. Shang, J.-T. Yu, L.-Z. Li, Z.-D. Lu.Strengthening of RC Structures by Using Engineered Cementitious Composites: A Review.Sustainability,2019, 11 (12).
[134] B. Wang, S. Xu.Textile reinforced engineered cementitious composites (TR-ECC) overlays for the strengthening of RC beams.Proc. Asia-Pacific Conf. on FRP in Structures,2009.
[135] H.M. Tanarslan.Flexural strengthening of RC beams with prefabricated ultra high performance fibre reinforced concrete laminates.Engineering Structures,2017, 151: 337-348.
[136] P.R. Prem, A.R. Murthy.Acoustic emission and flexural behaviour of RC beams strengthened with UHPC overlay.Construction and Building Materials,2016, 123: 481-492.
[137] A. Ramachandra Murthy, B.L. Karihaloo, D.S. Priya.Flexural behavior of RC beams retrofitted with ultra-high strength concrete.Construction and Building Materials,2018, 175: 815-824.
[138] Y. Zhang, Y. Zhu, M. Yeseta, D. Meng, X. Shao, Q. Dang, G. Chen.Flexural behaviors and capacity prediction on damaged reinforcement concrete (RC) bridge deck strengthened by ultra-high performance concrete (UHPC) layer.Construction and Building Materials,2019, 215: 347-359.
[139] S.A. Paschalis, A.P. Lampropoulos, O. Tsioulou.Experimental and numerical study of the performance of ultra high performance fiber reinforced concrete for the flexural strengthening of full scale reinforced concrete members.Construction and Building Materials,2018, 186: 351-366.
[140] P.R. Prem, A.R. Murthy, M. Verma.Theoretical modelling and acoustic emission monitoring of RC beams strengthened with UHPC.Construction and Building Materials,2018, 158: 670-682.
[141] A.P. Lampropoulos, S.A. Paschalis, O.T. Tsioulou, S.E. Dritsos.Strengthening of reinforced concrete beams using ultra high performance fibre reinforced concrete (UHPFRC).Engineering Structures,2016, 106: 370-384.
[142] M.A. Al-Osta, M.N. Isa, M.H. Baluch, M.K. Rahman.Flexural behavior of reinforced concrete beams strengthened with ultra-high performance fiber reinforced concrete.Construction and Building Materials,2017, 134: 279-296.
[143] Y. Zhang, M. Deng, T. Li, Z. Dong.Strengthening of flexure-dominate RC columns with ECC jackets: Experiment and analysis.Engineering Structures,2021, 231.
[144] M. Deng, Y. Zhang, Q. Li.Shear strengthening of RC short columns with ECC jacket: Cyclic behavior tests.Engineering Structures,2018, 160: 535-545.

[145] E. Esmaeeli, J.a.O. Barros, J. Sena-Cruz, L. Fasan, F.R. Li Prizzi, J. Melo, H. Varum.Retrofitting of interior RC beam–column joints using CFRP strengthened SHCC: Cast-in-place solution.Composite Structures,2015, 122: 456-467.
[146] W. Nadir, A.Y. Ali, M.M.A. Kadhim.Structural behavior of hybrid reinforced concrete beam-column joints under cyclic load: State of the art review.Case Studies In Construction Materials,2021, 15.
[147] S.A. Dadvar, D. Mostofinejad, H. Bahmani.Strengthening of Reinforced Concrete Columns with Combined Ultra-High-Performance Fiber-Reinforced Concrete and Glass Fiber-Reinforced Polymer Jacketing.Aci Structural Journal,2021, 118 (5): 285-297.
[148] S.A. Dadvar, D. Mostofinejad, H. Bahmani.Strengthening of RC columns by ultra-high performance fiber reinforced concrete (UHPFRC) jacketing.Construction and Building Materials,2020, 235.
[149] Y. Shao, C.-W. Kuo, C.-C. Hung.Seismic performance of full-scale UHPC-jacket-strengthened RC columns under high axial loads.Engineering Structures,2021, 243.
[150] A.A. Bahraq, M.A. Al-Osta, M.I. Khan, S. Ahmad.Numerical and analytical modeling of seismic behavior of beam-column joints retrofitted with ultra-high performance fiber reinforced concrete.Structures,2021, 32: 1986-2003.
[151] H. Tian, Z. Zhou, Y. Wei, L. Zhang.Experimental and numerical investigation on the seismic performance of concrete-filled UHPC tubular columns.Journal of Building Engineering,2021, 43.
[152] Q.-H. Li, B.-T. Huang, S.-L. Xu.Development of assembled permanent formwork using ultra high toughness cementitious composites.Advances in Structural Engineering,2016, 19 (7): 1142-1152.
[153] B.-T. Huang, Q.-H. Li, S.-L. Xu, C.-F. Li.Development of reinforced ultra-high toughness cementitious composite permanent formwork: Experimental study and Digital Image Correlation analysis.Composite Structures,2017, 180: 892-903.
[154] Z. Qiao, Z. Pan, W. Xue, S. Meng.Experimental study on flexural behavior of ECC/RC composite beams with U-shaped ECC permanent formwork.Frontiers of Structural and Civil Engineering,2019, 13 (5): 1271-1287.
[155] R. Zhang, P. Hu, X. Zheng, L. Cai, R. Guo, D. Wei.Shear behavior of RC slender beams without stirrups by using precast U-shaped ECC permanent formwork.Construction and Building Materials,2020, 260.
[156] F. Li, Z. Feng, K. Deng, Y. Yu, Z. Hu, H. Jin.Axial behavior of reinforced PP-ECC column and hybrid NSC-ECC column under compression.Engineering Structures,2019, 195: 223-230.
[157] R. Zhang, Q. Meng, Q. Shui, W. He, K. Chen, M. Liang, Z. Sun.Cyclic response of RC composite bridge columns with precast PP-ECC jackets in the region of plastic hinges.Composite Structures,2019, 221.
[158] Z. Pan, Y. Zhu, Z. Qiao, S. Meng.Seismic behavior of composite columns with steel reinforced ECC permanent formwork and infilled concrete.Engineering Structures,2020, 212.
[159] J.-J. Zeng, S.-P. Chen, K.-D. Peng, J.-G. Dai.Novel FRP micro-bar reinforced UHPC Permanent Formwork for Circular Columns: Concept and Compressive Behavior,2020.
[160] B. Hu, Y. Zhou, F. Xing, L. Sui, M. Luo.Experimental and theoretical investigation on the hybrid CFRP-ECC flexural strengthening of RC beams with corroded longitudinal reinforcement.Engineering Structures,2019, 200.
[161] W.-J. Ge, A.F. Ashour, X. Ji, C. Cai, D.-F. Cao.Flexural behavior of ECC-concrete composite beams reinforced with steel bars.Construction and Building Materials,2018, 159: 175-188.
[162] W. Ge, A.F. Ashour, D. Cao, W. Lu, P. Gao, J. Yu, X. Ji, C. Cai.Experimental study on flexural behavior of ECC-concrete composite beams reinforced with FRP bars.Composite Structures,2019, 208: 454-465.
[163] F. Qin, Z. Zhang, Z. Yin, J. Di, L. Xu, X. Xu.Use of high strength, high ductility engineered cementitious composites (ECC) to enhance the flexural performance of reinforced concrete beams.Journal of Building Engineering,2020, 32.
[164] M. Safdar, T. Matsumoto, K. Kakuma.Flexural behavior of reinforced concrete beams repaired with ultra-high performance fiber reinforced concrete (UHPFRC).Composite Structures,2016, 157: 448-460.
[165] L. Hussein, L. Amleh.Structural behavior of ultra-high performance fiber reinforced concrete-normal strength concrete or high strength concrete composite members.Construction and Building Materials,2015, 93: 1105-1116.
[166] E. Tzoura, T.C. Triantafillou.Shear strengthening of reinforced concrete T-beams under cyclic loading with TRM or FRP jackets.Materials and Structures,2014, 49 (1-2): 17-28.
[167] S.L. Xu, M. Kruger, H.W. Reinhardt, J.K. Ozbolt.Bond characteristics of carbon, alkali resistant glass, and ararnid textiles in mortar.Journal Of Materials In Civil Engineering,2004, 16 (4): 356-364.
[168] Y.-Z. Zheng, W.-W. Wang, J.C. Brigham.Flexural behaviour of reinforced concrete beams strengthened with a composite reinforcement layer: BFRP grid and ECC.Construction and Building Materials,2016, 115: 424-437.
[169] Y.-Z. Zheng, W.-W. Wang, K.M. Mosalam, Q. Fang, L. Chen, Z.-F. Zhu.Experimental investigation and numerical analysis of RC beams shear strengthened with FRP/ECC composite layer.Composite Structures,2020, 246.
[170] X. Yang, W.-Y. Gao, J.-G. Dai, Z.-D. Lu.Shear strengthening of RC beams with FRP grid-reinforced ECC matrix.Composite Structures,2020, 241.

[171] R. Guo, Y. Ren, M. Li, P. Hu, M. Du, R. Zhang.Experimental study on flexural shear strengthening effect on low-strength RC beams by using FRP grid and ECC.Engineering Structures,2021, 227.
[172] R. Guo, Y. Pan, L. Cai, S. Hino.Study on design formula of shear capacity of RC beams reinforced by CFRP grid with PCM shotcrete method.Engineering Structures,2018, 166: 427-440.
[173] J.F. Chen, J.G. Teng.Shear capacity of FRP-strengthened RC beams: FRP debonding.Construction And Building Materials,2003, 17 (1): 27-41.
[174] Z.C. Tetta, T.C. Triantafillou, D.A. Bournas.On the design of shear-strengthened RC members through the use of textile reinforced mortar overlays.Composites Part B-Engineering,2018, 147: 178-196.
[175] Z.C. Tetta, L.N. Koutas, D.A. Bournas.Shear strengthening of concrete members with TRM jackets: Effect of shear span-to-depth ratio, material and amount of external reinforcement.Composites Part B: Engineering,2018, 137: 184-201.
[176] ACI 549.4R-20, Guide to Design and Construction of Externally Bonded Fabric-Reinforced Cementitious Matrix and Steel-Reinforced Grout Systems for Repair and Strengthening Concrete Structures.American Concrete Institute,2020.
[177] L. Cai, Q. Liu, R. Guo.Study on the shear behavior of RC beams strengthened by CFRP grid with epoxy mortar.Composite Structures,2021, 275.
[178] Japan Society of Civil Engineers (JSCE): Recommendations for Design and Construction of High Performance Fiber Reinforced Cement Composites with Multiple Fine Cracks (HPFRCC),2008.
[179] Japan Society of Civil Engineers (JSCE): Concrete Library 101: Repair Reinforcement Guidelines for Concrete Structures using Continuous Fiber sheet,2000.
[180] Code for design of concrete structures: GB 50010-2010.Beijing: China Architecture & Building Press,2010.
[181] X. Chen, Y. Zhuge, A. Nassir Al-Gemeel, Z. Xiong.Compressive behaviour of concrete column confined with basalt textile reinforced ECC.Engineering Structures,2021, 243.
[182] L. Ombres, S. Mazzuca.Confined Concrete Elements with Cement-Based Composites: Confinement Effectiveness and Prediction Models.Journal of Composites for Construction,2017, 21 (3).

Click here to view linked References

# TABLES AND FIGURES

## TABLE CAPTIONS

**Table 1.** Typical mixing proportion and corresponding mechanical properties of ECCs

**Table 2.** Comparison on general mechanical properties of ECC, UHPC and UHP-ECC

**Table 3.** The summary of variables affecting the bond strengths of ECC-to-concrete interface

**Table 4.** The summary of variables affecting the shear bond strength of UHPC-to-concrete interface

**Table 5.** Database for strengthened RC beams/slabs with an UHPC layer

**Table 6.** Analysis models for flexure-strengthened RC beams using T-sided FGREM

**Table 7.** Database for shear-strengthened RC beams using 2-sided FGREM layers in existing experimental studies

**Table 8.** Existing analysis models for shear-strengthened RC beams using FGRCM

**Table 9.** The design formulas for shear contribution of ECC and concrete

**Table 10.** Database for confined short cylindrical columns with FGREM/FGRUM jackets

**Table 11.** Existing strength prediction models of short cylindrical columns confined with FGRCM jackets

**Table 12.** Results of the peak stress of the confined short cylindrical columns from models and experiments

**Table 1.** Typical mixing proportions and corresponding mechanical properties of ECCs

| Reference | Mixture ID | Mixing proportion (kg/m3) | | | | | | W/B | FA/B | S/B | Mechanical properties | | |
|---|---|---|---|---|---|---|---|---|---|---|---|---|---|
| | | OPC | Fly ash | Sand | Water | PVA Fiber (VF) | Water reducer | | | | Compressive strength (MPa) | Tensile strain capacity (%) | Tensile strength (MPa) |
| Pan et al. [53] | M1 | 1.0 | 1.2 | 0.79 | 0.66 | 1.3% | 0.0054 | 0.30 | 0.55 | 0.36 | 42 | 0.33 | - |
| | M2 | 1.0 | 1.8 | 1.01 | 0.84 | 1.3% | 0.0052 | 0.30 | 0.64 | 0.36 | 34 | 0.48 | - |
| | M3 | 1.0 | 2.4 | 1.22 | 1.02 | 1.3% | 0.0050 | 0.30 | 0.71 | 0.36 | 28 | 0.51 | - |
| | M6 | 1.0 | 1.8 | 1.01 | 0.78 | 1.3% | 0.0083 | 0.28 | 0.64 | 0.36 | 45 | 0.17 | - |
| | M7 | 1.0 | 1.8 | 1.01 | 0.90 | 1.3% | 0.0045 | 0.32 | 0.64 | 0.36 | 33 | 0.50 | - |
| | M12 | 1.0 | 2.4 | 1.02 | 1.02 | 1.3% | 0.0050 | 0.30 | 0.71 | 0.30 | 25 | 0.65 | - |
| | M13 | 1.0 | 2.4 | 1.43 | 1.02 | 1.3% | 0.0050 | 0.30 | 0.71 | 0.42 | 42 | 0.16 | - |
| Lin et al. [61] | 1.0% PVA | 1.0 | 2.33 | 1.20 | 0.78 | 1.0% | 0.0470 | 0.23 | 0.70 | 0.36 | 61 | 1.13 | 4.44 |
| | 1.5% PVA | 1.0 | 2.33 | 1.20 | 0.78 | 1.5% | 0.0470 | 0.23 | 0.70 | 0.36 | 65 | 1.76 | 7.54 |
| | 2.0% PVA | 1.0 | 2.33 | 1.20 | 0.78 | 2.0% | 0.0470 | 0.23 | 0.70 | 0.36 | 62 | 2.29 | 7.60 |
| | 2.5% PVA | 1.0 | 2.33 | 1.20 | 0.78 | 2.5% | 0.0470 | 0.23 | 0.70 | 0.36 | 46 | 3.30 | 6.27 |

Note: OPC—— Ordinary Portland cement; VF —— Volume fraction; W/B —— Water-to-binder ratio; FA/B —— Flay ash-to-binder ratio; S/B —— Sand-to-binder ratio.

**Table 2.** Comparison on general mechanical properties of ECC, UHPC and UHP-ECC

| Cementitious material | Compressive strength (MPa) | Tensile strength (MPa) | Ultimate tensile strain (%) |
|---|---|---|---|
| ECC | 20~60 | 3~7 | 2~8 |
| UHPC | 120~200 | 7~10 | 0.1~0.8 |
| UHP-ECC | 120~200 | 10~18 | 6~10 |

**Table 3.** Summary of variables affecting the bond strengths of ECC-to-concrete interface

| Strength type | Variable | | | | | | | |
|---|---|---|---|---|---|---|---|---|
| | Construction method of ECC | RC | SC | RP | Primer | Bonding agent | ES | Curing age |
| SBS | Prefabrication | + | + | + | - | + | O | + |
| | Cast-in-place | + | + | - | + | - | + | + |
| | Spraying | + | O | - | + | - | + | + |
| TBS | Prefabrication | + | + | + | - | + | O | + |
| | Cast-in-place | + | + | - | + | - | O | + |
| FBS | Prefabrication | + | + | + | - | + | O | + |
| | Cast-in-place | + | + | - | + | - | O | + |
| STB | Cast-in-place | + | + | - | + | - | O | + |
| | Spraying | + | O | - | + | - | O | + |
| SSB | Cast-in-place | + | + | - | + | - | O | + |

Note: "+" indicates the positive relationship between variables and bond strengths; "O" means that the relationship between variables and bond strengths is still unclear; "-" means that there is no relationship between variables and bond strengths; RC — The roughness of concrete substrate surface; SC — The strength of concrete substrate; RP — The roughness of prefabricated ECC surface; ES — The strength of ECC; SBS — The shear bond strength; TBS — The tensile bond strength; FBS — The flexure bond strength; STB — The splitting tensile strength; SSB — The slant shear bond strength.

**Table 4.** Summary of variables affecting the shear bond strength of UHPC-to-concrete interface

| Reference | Variable | | | | Bond strength (MPa) | Failure mode |
|---|---|---|---|---|---|---|
| | SP | CU (Day) | SC (MPa) | WC | | |
| Valikhani et al. [90] | SM | 28 | 35 | Dry | 1.26 | ID |
| | SM+MC | | | | 1.77~ 4.47 | PD |
| | SB | | | | 2.86 | ID |
| | SB+MC | | | | 4.25~ 8.05 | PD |
| Valikhani et al. [91] | SM | 28 | 35 | Dry | 2.80 | PD |
| | SM+BA | | | | 2.40 | ID |
| | SB | | | | 6.30 | CF |
| | SB+MC | | | | 7.40 | CF |
| | SB+BA | | | | 3.20 | PD |
| Zhang et al. [93] | R | 28 | 55.14 | Saturated | 6.55 | CF |
| | SM | | | | 4.24 | PD |
| | DH | | | | 5.93 | PD |
| | GR | | | | 5.50 | PD |
| | PR | | | | 6.12 | PD |
| | R | 2 | 55.14 | Saturated | 3.06 | ID |
| | R | 3 | | | 5.96 | PD |
| | R | 7 | | | 6.28 | PD |
| | R | 180 | | | 6.74 | CF |
| | R | 28 | 34.25 | Saturated | 4.54 | PD |
| | R | 28 | 46.77 | Saturated | 5.21 | PD |
| | R | 28 | 55.14 | Dry | 4.35 | PD |
| | R | 28 | 55.14 | Wet | 5.71 | PF |

Note: SP — The surface preparation of concrete substrate; CU — The curing age of UHPC; SC — The strength of concrete; WC — The wettability of concrete substrate; ID — Interfacial debonding; PD — Partial interfacial debonding; CF — Concrete substrate failure; SM — Smooth surface; MC — Mechanical connector; SB — Sand blasting; BA — Bonding agent; R — rough surface; DH — Drilling holes; GR — grooving; PR — post-installed rebar.

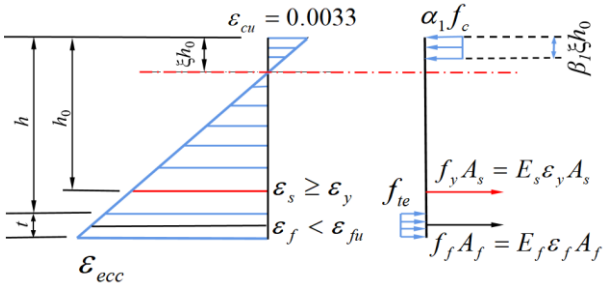
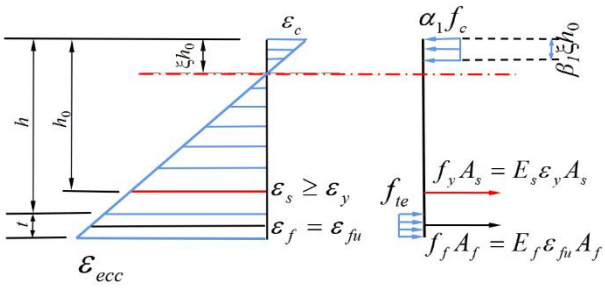
**Table 5.** Database for strengthened RC beams/slabs with an UHPC layer

| Reference | Specimen ID | Beam | | | UHPC | | | | | Surface treatment (roughness) | Result | |
|---|---|---|---|---|---|---|---|---|---|---|---|---|
| | | $H \times B$ (mm×mm) | $f_c$ (MPa) | $\rho_s$ (%) | Strengthening form | $t_u$ (mm) | $f_{c,u}$ (MPa) | VF (%) | $\rho_u$ (%) | | $M_u/M_c - 1$ (%) | Failure mode |
| Lampropoulos et al. [141] | ST_UHPFRC_TS | 250 × 150 | 39.5 | 0.60 | T-sided | 50 | 164 | 3 | 0 | RD (2~3mm) | 31 | CC |
| | ST_UHPFRC_CS | | | | C-sided | | | | | | 28 | CC |
| | ST_UHPFRC_3SJ | | | | 3-sided | | | | | | 178 | UC |
| Tanarslan [135] | BEAM-2 | 250 × 150 | 20.4 | 0.90 | T-sided | 30 | 200 | 3 | 0 | RD+BA | 57 | UR |
| | BEAM-3 | | | | | | | | 0 | MC | 32 | UR |
| | BEAM-4 | | | | | | | | 3.35 | RD+BA | 116 | DB* |
| | BEAM-5 | | | | | | | | 3.35 | MC | 107 | CC |
| Prem and Murthy [136] | A2 | 200 × 100 | 35 | 0.57 | T-sided | 15 | 170 | 2 | 0 | RD (2~3mm) +BA | 23.50 | CC |
| | A3 | | | 0.57 | | 20 | | | | | 34.80 | CC |
| | B2 | | | 0.90 | | 15 | | | | | 11.57 | CC |
| | B3 | | | 0.90 | | 20 | | | | | 18.45 | CC |
| | C2 | | | 1.30 | | 15 | | | | | 10.60 | CC |
| | C3 | | | 1.30 | | 20 | | | | | 15.12 | CC |
| Paschalis et al. [139] | Average U1,2 | 200 × 150 | 30.9 | 0.75 | T-sided | 50 | 136.5 | 3 | 0 | RD (2~2.5mm) | 1.5 | UR |
| | Average UB1,2 | | | | | | | | 2.10 | | 90 | CC |
| Ramachandra | RB5 | 200 × 100 | 35 | 0.80 | T-sided | 10 | 122.5 | 2 | 0 | RD (3mm) +BA | 8.5 | CC |

| | | | | | | | | | | | | |
|---|---|---|---|---|---|---|---|---|---|---|---|---|
| Murthy et al. [137] | RB6 | | | | | 12 | | | | | 13.0 | CC |
| | RB7 | | | | | 15 | | | | | 19.6 | CC |
| Al-Osta et al. [142] | RC-SB-BOTSJ | 230 × 140 | 54 | 0.49 | T-sided | 30 | 128 | 2 | 0 | RD (2mm) | 16 | CC |
| | RC-SB-2SJ | | | | 2-sided | | | | | RD (2mm) | 46 | CC |
| | RC-SB-3SJ | | | | 3-sided | | | | | RD (2mm) | 89 | UC |
| | RC-EP-BOTSJ | | | | T-sided | | | | | BA | 8 | CC |
| | RC-EP-2SJ | | | | 2-sided | | | | | BA | 36 | CC |
| | RC-EP-3SJ | | | | 3-sided | | | | | BA | 85 | UC |
| Zhang et al. [138] | N-UC | 280 × 2000 | 60.2 | 0.73 | T-sided | 50 | 130 | 3.5 | 4.16 | RD (1~4mm) +MC | 98 | CC |
| | H-UC-1 | | | | T-sided | | 140 | | | | 85 | CC |
| | H-UC-2 | | | | C-sided | | 140 | | | | 27 | CC |

Note: $H$ and $B$ — The height and width of the beam; $f_c$ — The compressive strength of concrete; $\rho_s$ — The reinforcement ratio of RC member; $t_u$ — The thickness of UHPC layer; $f_{c,u}$ — The compressive strength of UHPC; VF — The volume fraction of steel fiber; $\rho_u$ — The reinforcement ratio of UHPC layer; $M_u$ — The ultimate moment of strengthened RC beam; $M_c$ — The ultimate moment of RC beam; RD — Roughness degree preparation for concrete surface; BA — Bonding agent (epoxy adhesion) ; MC — Mechanical connector; CC — The concrete crushing; UC — The UHPC crushing; UR — The rupture of UHPC layer; DB* — The interfacial debonding near the support.

**Table 6.** Analysis models for flexure-strengthened RC beams using T-sided FGREM

| Failure mode | Model | Diagrammatic sketch |
|---|---|---|
| CC | $\frac{\varepsilon_f}{\varepsilon_{cu}} = \frac{\varepsilon_f}{0.0033} = \frac{h-\xi h_0+t/2}{\xi h_0}$<br>$\frac{\varepsilon_{ecc}}{\varepsilon_{cu}} = \frac{\varepsilon_{ecc}}{0.0033} = \frac{h-\xi h_0+t}{\xi h_0}$<br>$f_f = E_f\varepsilon_f$<br>$\alpha_1 f_c \beta_1 \xi b h_0 = f_y A_s + f_f A_f + f_{te} t b$<br>Ultimate moment:<br>$M_u = f_y A_s\left(h_0 - \frac{\beta_1\xi h_0}{2}\right) + f_f A_f\left(h - \frac{\beta_1\xi h_0}{2} + \frac{t}{2}\right) +$<br>$f_{te} t b\left(h - \frac{\beta_1\xi h_0}{2} + \frac{t}{2}\right)$ |  |
| RG | $\frac{\varepsilon_c}{\varepsilon_{fu}} = \frac{\xi h_0}{h-\xi h_0+t/2}$<br>$\frac{\varepsilon_{ecc}}{\varepsilon_{fu}} = \frac{h-\xi h_0+t}{h-\xi h_0+t/2}$<br>$f_{fu} = E_f\varepsilon_{fu}$<br>$\alpha_1 f_c \beta_1 \xi b h_0 = f_y A_s + f_{fu} A_f + f_{te} t b$<br>Ultimate moment:<br>$M_u = f_y A_s\left(h_0 - \frac{\beta_1\xi h_0}{2}\right) + f_{fu} A_f\left(h - \frac{\beta_1\xi h_0}{2} + \frac{t}{2}\right) +$<br>$f_{te} t b\left(h - \frac{\beta_1\xi h_0}{2} + \frac{t}{2}\right)$ |  |

Note: CC — Concrete crushing; RG — FRP grid rupture; $\varepsilon_f$, $\varepsilon_{ecc}$ and $\varepsilon_s$ — The tensile strain of FRP grid, ECC edge and steel reinforcement, respectively; $\varepsilon_c$— The compressive strain of concrete at the top of compression zone; $\varepsilon_{cu}$ — The ultimate compressive strain of concrete; $\varepsilon_y$ — The yield strain of steel reinforcement; $\varepsilon_{fu}$— The ultimate tensile strain of FRP grid; $A_s$ and $A_f$ — The cross-sectional area of steel reinforcement and FRP grid, respectively; $E_s$ and $E_f$ — The elastic modulus of steel reinforcement and FRP grid, respectively; $f_c$ — The compressive strength of concrete; $f_y$ — The yield strength of steel reinforcement; $f_f$ and $f_{fu}$ — The tensile stress and ultimate tensile strength of FRP grid, respectively; $f_{te}$ — The tensile strength of ECC; $h, h_0$ and $b$ — The height, effective height and width of RC beam; $t$ — The thickness of FGREM layer; $\xi$ — The ratio of the height of compression zone to effective height of beam; $\alpha_1$ and $\beta_1$ — The coefficient of equivalent rectangular stress block of cconcrete.

**Table 7.** Database for shear-strengthened RC beams using 2-sided FGREM layers

| Reference | Specimen ID | Beam | | | | | | FRP grid | | | | | | | ECC | | | Result | |
|---|---|---|---|---|---|---|---|---|---|---|---|---|---|---|---|---|---|---|---|
| | | $d \times b_w$ (mm×mm) | $f_c$ (MPa) | $f_t$ (MPa) | $a/d$ | Bottom bars | Stirrup | $s_f$ (mm) | $t_f$ (mm) | $E_f$ (GPa) | $f_{fu}$ (MPa) | $n_f$ | $A_f$ (mm$^2$) | Type | $t_m$ (mm) | $f_{mt}$ (MPa) | $f_{mc}$ (MPa) | $V_{exp}$ (kN) | Failure mode |
| Guo et al. [171] | EF1S0 | 160×120 | 31.6 | 2.2 | 3.13 | 3ϕ18 | ϕ6@250 | 50 | - | 90 | 900 | 1 | 6.6 | CFRP | 30 | 4.6 | 36.5 | 80.5 | PD |
| | EF′1S0 | | | | | | | 75 | - | | | 1 | | | | | | 76.5 | PD |
| | EF2S0 | | | | | | | 50 | - | | | 2 | | | | | | 83.5 | PD |
| | EF1S1 | | | | 2.81 | | | 50 | - | | | 1 | | | | | | 78 | PD |
| | EF1S2 | | | | 3.44 | | | 50 | - | | | 1 | | | | | | 75 | PD |
| Zheng et al. [169] | SB1 | 260×200 | 32 | 2.2 | 2.40 | 4ϕ20 | ϕ6@200 | 50 | 1 | 52 | 357 | 1 | 3 | BFRP | 60 | 2.7 | 27 | 188 | PD |
| | SB2 | | | | | | | | 3 | 53 | 386 | | 12 | | | | | 224.5 | PD |
| | SB3 | | | | | | | | 5 | 57 | 416 | | 20 | | | | | 235.5 | PD |
| Yang et al. [170] | b-B-E-Pre | 265×150 | 32.7 | 2.2 | 2.26 | 3ϕ20 | - | 50 | - | 80 | 1760 | 1 | 6.34 | BFRP | 40 | 7.2 | 25 | 147.6 | PD |
| | b-C-E-Pre | | | | | | | | - | 100 | 1400 | | 13.2 | CFRP | | | | 142.4 | PD |
| | b-B-E-Cast | | | | | | | | - | 80 | 1760 | | 6.34 | BFRP | | | | 95.5 | DB |
| | c-C-E-Pre | | | | 3.02 | | - | | - | 100 | 1400 | | 13.2 | CFRP | | | | 129 | PD |

Note: $V_{exp}$ — The total shear capacity of strengthened RC beams; PD — The partial debonding; DB — The interfacial debonding. $a$ — The shear span; $d$ and $b_w$ — The effective height and width of the beam; $f_c$ and $f_t$ — The compressive and tensile strength of concrete, respectively; $s_f$ — The spacing of FRP grid; $t_f$ — The nominal thickness of FRP grid; $E_f$ — Elastic modulus of FRP grid; $n_f$ — The number of FRP grid layers; $A_f$ — The cross-sectional area of FRP grids; $f_{fu}$ — The ultimate tensile strength of FRP strip; $t_m$ — The total thickness of ECC; $f_{mt}$ — The tensile strength of the ECC; $f_{mc}$ — The compressive strength of the ECC.

**Table 8.** Existing analysis models for shear-strengthened RC beams using FGRCM

| Reference | Model | Failure mode |
|---|---|---|
| Chen and Teng [173] | Chen and Teng's Model:<br>$V_f = 2f_{fed} n_f t_f \, h_{fe} \, (cot\theta sin\beta + cos\beta) \, \frac{w_f}{s_f}$<br>$f_{fed} = D_f \, f_{fed,max}$<br>$h_{fe} = 0.9d - (h - d_{fb}) - d_{ft}$<br>$f_{fed,max} = 0.427\beta_w\beta_l \sqrt{\frac{E_f\sqrt{f_c}}{t_f}} \le f_{fu}$ (units of MPa and mm)<br>$\beta_w = \sqrt{\frac{2 - \frac{w_f}{(s_f sin\beta)}}{1 + \frac{w_f}{(s_f sin\beta)}}}$<br>$L_e = \sqrt{\frac{E_f t_f}{\sqrt{f_c}}}$ (units of MPa and mm)<br>$\beta_l = \begin{cases} 1 & \lambda \ge 1 \\ sin\left(\frac{\pi\lambda}{2}\right) & \lambda < 1 \end{cases}$<br>$\mathrm{D}_f = \begin{cases} \frac{2}{\pi\lambda}\left[\frac{1 - cos\left(\frac{\pi\lambda}{2}\right)}{sin\left(\frac{\pi\lambda}{2}\right)}\right] & \lambda \le 1 \\ 1 - \frac{\pi - 2}{\pi\lambda} & \lambda > 1 \end{cases}$<br>$\lambda = \frac{L_{max}}{L_e} = \begin{cases} \frac{h_{fe}/sin\beta}{L_e} & \text{for } U - wrapped \text{ FRCM jacket} \\ \frac{h_{fe}/2sin\beta}{L_e} & \text{for } side - bonded \text{ FRCM jacket} \end{cases}$ | Interfacial debonding |
| Tetta et al. [174] | Modified Chen and Teng's Model-version I:<br>It differs from Chen and Teng's model in $f_{fed,max}$<br>$V_f = 2f_{fed} n_f t_f \, h_{fe} \, (cot\theta sin\beta + cos\beta) \, \frac{w_f}{s_f}$<br>$f_{fed,max} = 0.58\beta_w\beta_l \sqrt{\frac{E_f\sqrt{f_c}}{t_f}} \le f_{fu}$ (units of MPa and mm) | Interfacial debonding |

| | | |
|---|---|---|
| Tetta et al. [175] | Modified Chen and Teng's Model-version Ⅱ:<br>It differs from Chen and Teng's model in $f_{fed,max}$ and $L_e$<br>$V_f = 2f_{fed}n_f t_f\, h_{fe}\,(cot\theta sin\beta + cos\beta)\,\frac{w_f}{s_f}$<br>$f_{fed,max} = 8.67\beta_w\beta_l\sqrt{\frac{1000\sqrt{f_c}}{t_f}} \le f_{fu}$ (units of MPa and mm)<br>$L_e = 15\sqrt{\frac{1000t_f}{\sqrt{f_c}}}$ (units of MPa and mm) | Interfacial debonding |
| Tetta et al. [174] | $V_f = 2f_{fu}n_f t_f\, h_{fe}\,(cot\theta sin\beta + cos\beta)\,\frac{w_f}{s_f}$<br>$h_{fe} = 0.9d - (h - d_{fb}) - d_{ft}$ | Fracture of FRP |
| ACI 549.4R-20 [176] | $V_f = 2f_{fv}n_f t_f\, h_{fe}\,\frac{w_f}{s_f}$<br>$f_{fv} = E_f\varepsilon_{fv}$<br>$\varepsilon_{fv}$=$\varepsilon_{fu} \le 0.004$ | - |
| Guo et al. [171] | $V_f = \frac{2E_f(\rho_{ver}\varepsilon_{u,ver} + \rho_{hor}\varepsilon_{u,hor})d}{1.15}$<br>$\varepsilon_{u,ver} = \left(\frac{1}{0.0352\rho_{ver} + 0.0079}\right)^2 \times 10^{-6}$<br>$\varepsilon_{u,hor} = k\varepsilon_{u,ver}$<br>$k = exp[-0.612 \cdot (a/d) + 0.365] \ge 0.23$<br>$\rho_{ver} = \frac{n_f t_f w_f}{s_f}$ | Partial Debonding |
| Cai et al. [177] | $V_f = 2E_f\rho_{ver}\varepsilon_{u,ver}d_f$ $\rho_{ver} = \frac{n_f t_f w_f}{s_f}$<br>$d_f = h_f - d_c$<br>$\varepsilon_{u,ver} = 78\gamma\left(\frac{t_m}{\eta{\rho_{ver}}^2}\right)^{0.70}\left(\frac{a}{d}\cdot\frac{f_{mt}}{f_t}\right)^{0.46} \times 10^{-6} \le 0.7\varepsilon_{fu}$<br>$\gamma = 1.3$ $\eta = 23.4$ | Partial Debonding |

Note: $V_f$ — The contribution of the FGRCM to the shear resistance of the beam; $t_f$ — The nominal thickness of FRP grid; $h_{fe}$ — The effective height of FGRCM jacket; $\theta$ — The angle of critical inclined crack to the member axis; $\beta$ — Inclination angle of fiber with respect to the longitudinal axis of the beam; $w_f$ — The width of FRP grid; $n_f$ — The number of FRP grid layers; $s_f$ — The spacing of grids measured along the longitudinal axis; $h$ — The height of the beam; $d_{fb}$ and $d_{ft}$ — The distance from the top of beam to the bottom and top end of the effective jacket, respectively; $E_f$ — Elastic modulus of FRP grids; $f_c$ — The compressive strength of concrete; $\varepsilon_{fu}$ — The ultimate tensile strain of FRP grids; $a$ and $d$— The shear span and effective depth of beam, respectively; $f_{fu}$ — The ultimate tensile strength of FRP grids; $\rho_{ver}$ and $\rho_{hor}$ — The cross-sectional area of vertical and horizontal grids per unit length, respectively; $f_t$ and $f_{mt}$ — The tensile strength of concrete and ECC, respectively; $h_f$ — The bond depth of the FRP grid; $d_c$ — The thickness of concrete cover.

**Table 9.** The design formulae for shear contribution of ECC and concrete

| Reference | Model |
|---|---|
| JSCE code [178,179] | The shear contribution of concrete:<br>$V_c = 0.2 \cdot \sqrt[3]{f_c} \cdot \sqrt[4]{1000/d} \cdot \sqrt[3]{100\rho_w} \cdot t \cdot d$<br>The shear contribution of ECC matrix:<br>$V_{c,ecc} = 0.7 \times 0.2 \cdot \sqrt[3]{f_{c,ecc}} \cdot \sqrt[4]{1000/d} \cdot \sqrt[3]{100\rho_w} \cdot t \cdot d$ $\rho_w = A_s/(b_w d)$<br>The shear contribution of fiber in ECC:<br>$V_{f,ecc} = \left(f_{t,ecc}/tan\beta_u\right) \cdot t \cdot \frac{d}{1.15}$ ($\beta_u$ =45° is recommended conservatively)<br>The total shear contribution of fiber in ECC:<br>$V_{ecc} = V_{c,ecc} + V_{f,ecc}$<br>$\sqrt[4]{1000/d} \le 1.5; 0.2 \cdot \sqrt[3]{f_{c,ecc}} \le 0.72\text{MPa}; \sqrt[3]{100\rho_w} \le 1.5$ |
| Chinese code [180] | The shear contribution of concrete:<br>$V_c = \frac{1.75}{\lambda+1} f_t b_w d$<br>The shear contribution of ECC:<br>$V_{ecc} = \frac{1.75}{\lambda+1} f_{mt} t d$ |

Note: $V_{ecc}$ — The contribution of ECC layer to the shear resistance of the beam; $V_c$ — The shear contribution of concrete; $f_c$ and $f_{c,ecc}$ — The compressive strength of concrete and ECC, respectively; $f_t$ and $f_{t,ecc}$ — The tensile yield strength of concrete and ECC, respectively; $f_{mt}$ — The tensile strength ECC; $A_s$ — the cross-sectional area of the tension reinforcement; $b_w$ — The width of web; $d$ — The effective depth of beam; $t$ — The total thickness of the ECC; $\beta_u$ — The angle of the diagonal crack surface to the member axis.

**Table 10.** Database for FGREM/FGRUM jacket-confined short cylindrical columns

| Reference | Specimen ID | Column | FRP grid | | | | | | | | Matrix | | | | Result | | |
|---|---|---|---|---|---|---|---|---|---|---|---|---|---|---|---|---|---|
| | | $D$ (mm) | $t_f$ (mm) | $n_f$ | $E_f$ (GPa) | $f_f$ (MPa) | $w$ (mm) | $s$ (mm) | $A_f$ (mm$^2$) | Type | $t_m$ (mm) | $f_{m,c}$ (MPa) | $f_{m,t}$ (MPa) | Type | $f'_{cc}$ (MPa) | $f'_{co}$ (MPa) | $f'_{cc}/f'_{co}$ |
| Yan et al. [64] | N1-t2-C30 | 140 | - | 1 | 230 | 3400 | - | 20 | 1.16 | CFRP | 15 | 32 | 4.3 | ECC | 77.4 | 73.4 | 1.054 |
| | N2-t2-C30 | | - | 2 | | | - | | | | | | | | 83.3 | 73.4 | 1.135 |
| | N3-t2-C30 | | - | 3 | | | - | | | | | | | | 85.5 | 73.4 | 1.165 |
| | N1-t2-C40 | | - | 1 | | | - | | | | | | | | 87.0 | 84.6 | 1.028 |
| | N2-t2-C40 | | - | 2 | | | - | | | | | | | | 92.0 | 84.6 | 1.087 |
| | N3-t2-C40 | | - | 3 | | | - | | | | | | | | 95.4 | 84.6 | 1.128 |
| | N1-t2-C50 | | - | 1 | | | - | | | | | | | | 97.3 | 92.2 | 1.055 |
| | N2-t2-C50 | | - | 2 | | | - | | | | | | | | 100.2 | 92.2 | 1.087 |
| | N3-t2-C50 | | - | 3 | | | - | | | | | | | | 99.4 | 92.2 | 1.078 |
| Tian et al. [50] | T20C1 | 200 | 0.27 | 1 | 167 | 3459 | 3 | 16 | 0.812 | CFRP | 20 | 139.3 | 7.2 | UHPC | 39.0 | 29.3 | 1.331 |
| Chen et al. [181] | ET-C1 | 110 | - | 1 | - | 658.7 | - | 25 | 2.03 | BFRP | 20 | 65 | 3.7 | ECC | 38.8 | 32.2 | 1.205 |
| | ET-C2 | | - | 1 | - | 658.7 | - | 25 | 2.03 | BFRP | | | | | 22.0 | 15.8 | 1.392 |
| Al-Gemeel and Zhuge | C-ECC-TB-O (1) | 110 | - | 1 | - | 658.7 | - | 25 | 2.03 | BFRP | 20 | 65 | 3.7 | ECC | 20.8 | 15.8 | 1.316 |
| | C-ECC-TB-OC (1) | | - | 1 | - | 658.7 | - | 25 | 2.03 | BFRP | | | | | 21.2 | 15.8 | 1.342 |

| | | | | | | | | | | | | | |
|---|---|---|---|---|---|---|---|---|---|---|---|---|---|
| [52] | C-ECC-TB-O (2) | - | 1 | - | 658.7 | - | 25 | 2.03 | BFRP | 37.1 | 32.2 | 1.152 |
| | C-ECC-TB-OC (2) | - | 1 | - | 658.7 | - | 25 | 2.03 | BFRP | 37.8 | 32.2 | 1.174 |

Note: $f'_{cc}$ — The peak stress of the confined column; $f'_{co}$ — The peak stress of the unconfined column; $n_f$ — The number of FRP textile layers; $w$ and $t_f$ — The width and thickness of FRP strip; $E_f$ — The elastic modulus of FRP; $A_f$ — The cross-sectional area of FRP strip; $f_f$ — The tensile strength of FRP strip; $t_m$ — The thickness of the matrix; $f_{m,c}$ and $f_{m,t}$ — The compressive strength and tensile strength of the jacketing matrix, respectively; $D$— The diameter of the core column; $w$ — The width of FRP strip; $s$ — The space between the center of FRP strips.

**Table 11.** Existing strength prediction models of FGRCM-confined short cylindrical columns

| Reference | Model | Illustration |
|---|---|---|
| ACI 549.4R-20 [176] | $f'_{cc} = f'_{co} + 3.1 f_l$<br>$f_l = \frac{2 n_f w t_f E_f \varepsilon_{fe}}{Ds}$<br>$\varepsilon_{fe} = \varepsilon_{fu} \leq 0.012$ | Only accounting for the confinement of FRP |
| Ombres et al. [182] | $\frac{f'_{cc}}{f'_{co}} = 1 + 0.913 \left(\frac{f_l}{f_{c0}}\right)^{0.5}$<br>$f_l = \frac{2 k_e n_f w t_f E_f \varepsilon_{fu}}{Ds}$<br>For FRP grids embedded in mortar, the value of $k_e$ was assumed to be 0.5:<br>$k_e = 0.5$ | Only accounting for the confinement of FRP |
| Chen et al. [181] | $f'_{cc} = f'_{co} + 3.3 f_l$<br>$f_l = \frac{2 k_f n_f w t_f f_f}{Ds} + \frac{2 t_m f_{m,t}}{D}$<br>It is assumed that the FRP grids are fully utilized:<br>$k_f = 1.0$ | Accounting for the confinement of cementitious matrix and FRP |

Note: $f'_{cc}$ — The peak stress of the confined column; $f'_{co}$ — The peak stress of the unconfined column; $n_f$ — The number of FRP textile layers; $t_f$ — The thickness of FRP strip; $E_f$ — The elastic modulus of FRP; $\varepsilon_{fu}$ — The ultimate tensile strain of FRP; $f_f$ — The tensile strength of FRP strip; $t_m$ — The thickness of the matrix; $f_{m,t}$ — The tensile strength of the jacketing matrix; $D$— The diameter of the core column; $w$ — The width of FRP strip; $s$ — The space between the center of FRP strips.

**Table 12.** Results of the peak stress of the confined short cylindrical columns from models and experiments

| Reference | Specimen ID | $f'_{cc}/f'_{co}$ | | | |
|---|---|---|---|---|---|
| | | Experiment | ACI 549.4R-20 [171] | Ombres et al. [177] | Chen et al. [176] |
| Yan et al. [64] | N1-t2-C30 | 1.054 | 1.097 (1.04) | 1.126 (1.07) | 1.168 (1.11) |
| | N2-t2-C30 | 1.135 | 1.193 (1.05) | 1.179 (1.04) | 1.295 (1.14) |
| | N3-t2-C30 | 1.165 | 1.290 (1.11) | 1.219 (1.05) | 1.421 (1.22) |
| | N1-t2-C40 | 1.028 | 1.084 (1.05) | 1.118 (1.09) | 1.146 (1.11) |
| | N2-t2-C40 | 1.087 | 1.168 (1.07) | 1.167 (1.07) | 1.256 (1.16) |
| | N3-t2-C40 | 1.128 | 1.251 (1.11) | 1.204 (1.07) | 1.366 (1.21) |
| | N1-t2-C50 | 1.055 | 1.077 (1.02) | 1.113 (1.05) | 1.134 (1.07) |
| | N2-t2-C50 | 1.087 | 1.154 (1.06) | 1.160 (1.07) | 1.234 (1.14) |
| | N3-t2-C50 | 1.078 | 1.231 (1.15) | 1.195 (1.11) | 1.335 (1.24) |
| Tian et al. [50] | T20C1 | 1.330 | 1.107 (0.83) | 1.158 (0.87) | 1.360 (1.02) |
| Chen et al. [181] | ET-C1 | 1.205 | 1.094 (0.91) | 1.112 (0.92) | 1.238 (1.03) |
| | ET-C2 | 1.392 | 1.191 (0.86) | 1.160 (0.83) | 1.484 (1.07) |
| Al-Gemeel and Zhuge [52] | C-ECC-TB-O (1) | 1.316 | 1.191 (0.91) | 1.160 (0.88) | 1.484 (1.13) |
| | C-ECC-TB-OC (1) | 1.342 | 1.191 (0.89) | 1.160 (0.86) | 1.484 (1.10) |
| | C-ECC-TB-O (2) | 1.152 | 1.094 (0.95) | 1.112 (0.97) | 1.238 (1.07) |
| | C-ECC-TB-OC (2) | 1.174 | 1.094 (0.93) | 1.112 (0.95) | 1.238 (1.05) |

Note: The numbers in brackets mean the ratio of predictive results using models to experimental results.

## FIGURE CAPTIONS

**Fig. 1.** The formation of FRCM composites

**Fig. 2.** Typical tensile stress-strain curve of ECCs

**Fig. 3.** The working mechanism of the fibers in matrix

**Fig. 4.** Relation between fiber volume ratio and compressive and flexural strength of UHPC

**Fig. 5.** Typical tensile stress-strain curve of UHPC

**Fig. 6.** Tensile stress-strain curve of UHPFRCCs: experimental results of UHPC coupons from B.-T. Huang et al. [74] versus experimental results of UHP-ECC coupons from K.-Q. Yu et al. [40]

**Fig. 7.** The bonding strength testing techniques: (a) Slant shear test; (b) Splitting tensile test; (c) Pull-off test; (d) Shear test; (e) Flexural test

**Fig. 8.** The usual bonding form of ECC to existing concrete

**Fig. 9.** Relations between the bond strength of the interface and the roughness/strength of concrete

**Fig. 10.** Effects of different surface preparation methods on the UHPC-to-concrete bond strength

**Fig. 11.** Material properties of ECC/UHPC at different temperatures

**Fig. 12.** The comparison on the freeze-thaw resistances of ECC and UHPC

**Fig. 13.** Four different forms of strengthening schemes using ECC/UHPC layers for RC beams

**Fig. 14.** ECC strengthening systems for RC beams

**Fig. 15.** Typical failure modes of T-sided UHPC layer reinforced RC beams

**Fig. 16.** Typical U-shaped ECC/UHPFRCC permanent formwork for RC beams

**Fig. 17.** Typical ECC permanent formwork for RC columns

**Fig. 18.** Typical UHPC permanent formwork for RC columns

**Fig. 19.** Typical axial load-strain curves of concrete columns confined with UHPC formwork

**Fig. 20.** The ECC/UHPC repairing RC beams

**Fig. 21.** The relation between height replacement ratio and increase in flexure capacity

**Fig. 22.** The comparison on experimental with predictive results of ultimate load capacities

**Fig. 23.** Experimental versus predicted total shear capacities for the: (a) Guo et al.'s model; (b) ACI 549.4R-20.

**Fig. 24.** Typical axial stress-strain curves of columns confined with FRCM

**Fig. 25.** Diagram of a circular cross-section confined with FRP grid reinforced matrix

**Fig. 26.** FRP-ECC/UHPC composite plates

**Fig. 27.** Typical tensile stress-strain curves of FRP grid-reinforced ECC/UHPC composites

**Fig. 28.** Application prospects of FRP-UHPC composites

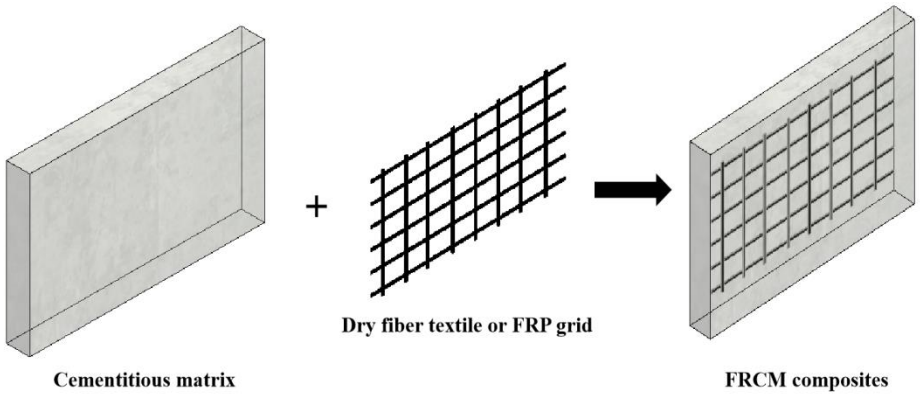



**Fig. 1.** The formation of FRCM composites

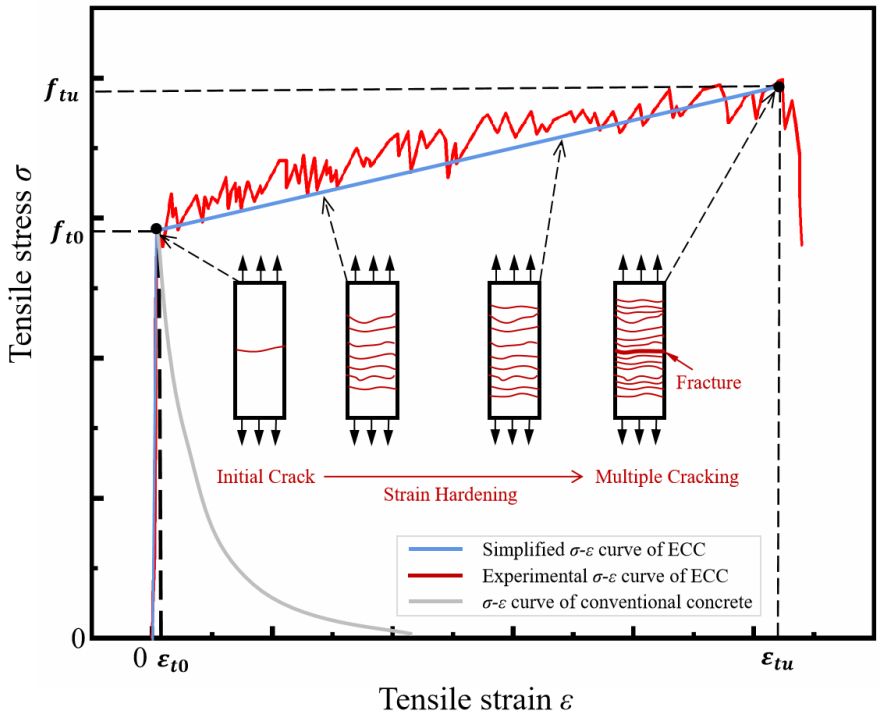
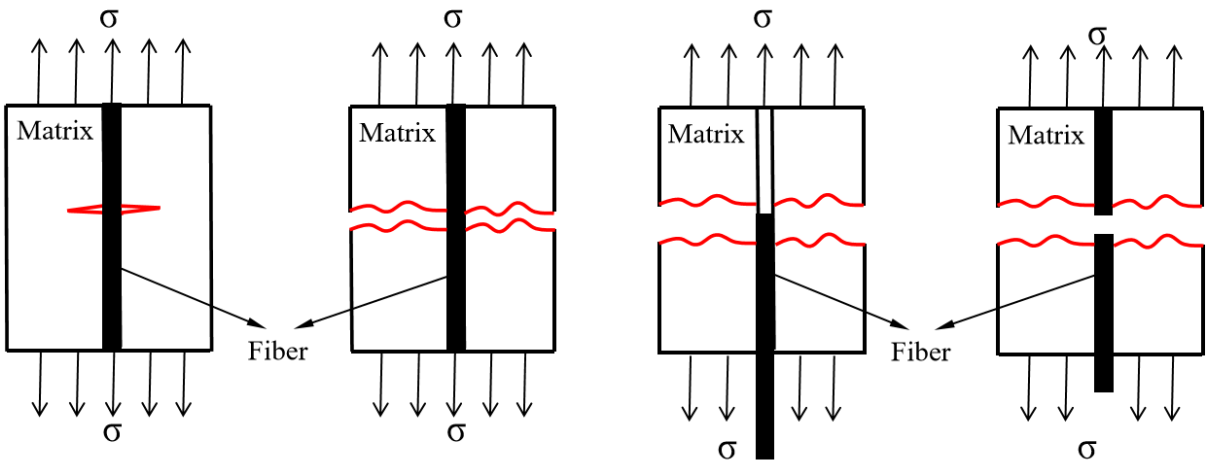
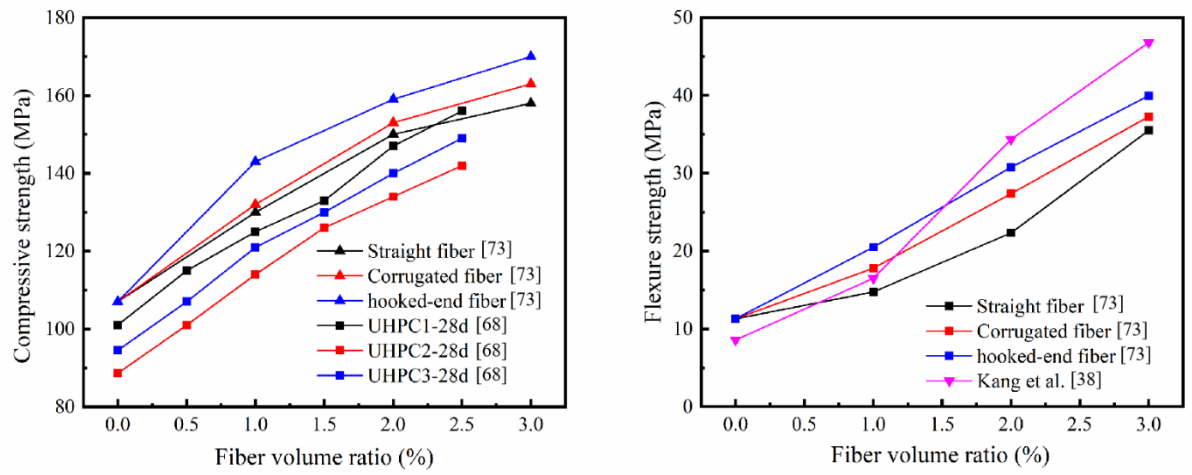



**Fig. 2.** Typical tensile stress-strain curve of ECCs




(a) Fiber debonding (b) Fiber bridging (c) Fiber pullout (d) Fiber rupture

**Fig. 3.** The working mechanism of fibers in matrix




(a) Compressive strength (b) Flexure strength

**Fig. 4.** Relation between fiber volume ratio and compressive and flexural strength of UHPC

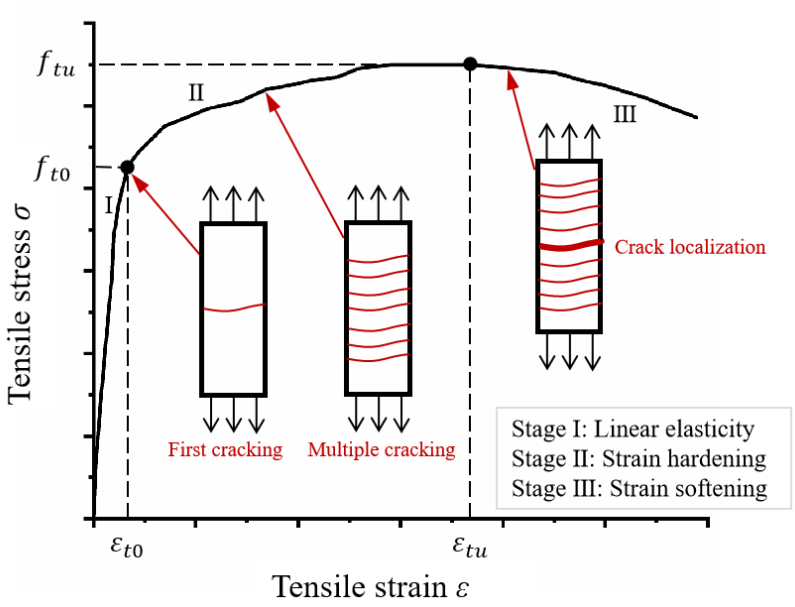



**Fig. 5.** Typical tensile stress-strain curve of UHPC

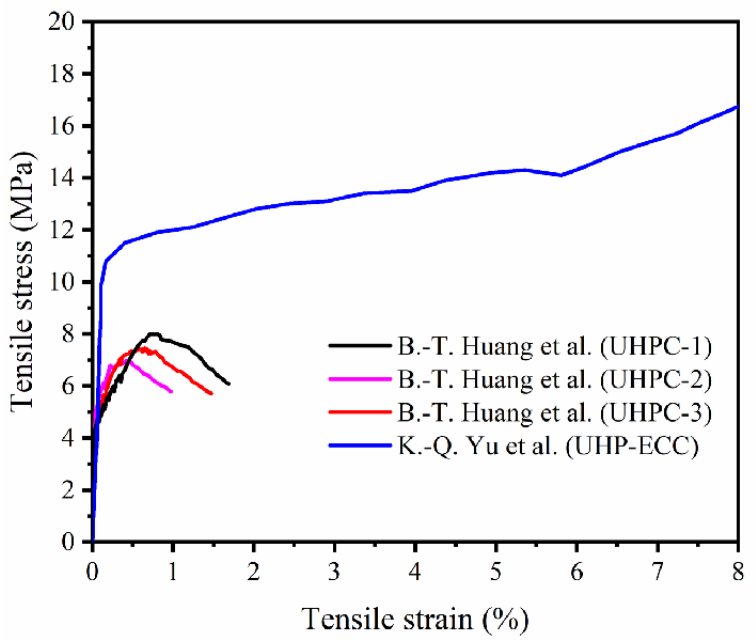



**Fig. 6.** Tensile stress-strain curve of UHPFRCCs: experimental results of UHPC coupons from Huang et al. [74] and experimental results of UHP-ECC coupons from Yu et al. [40]

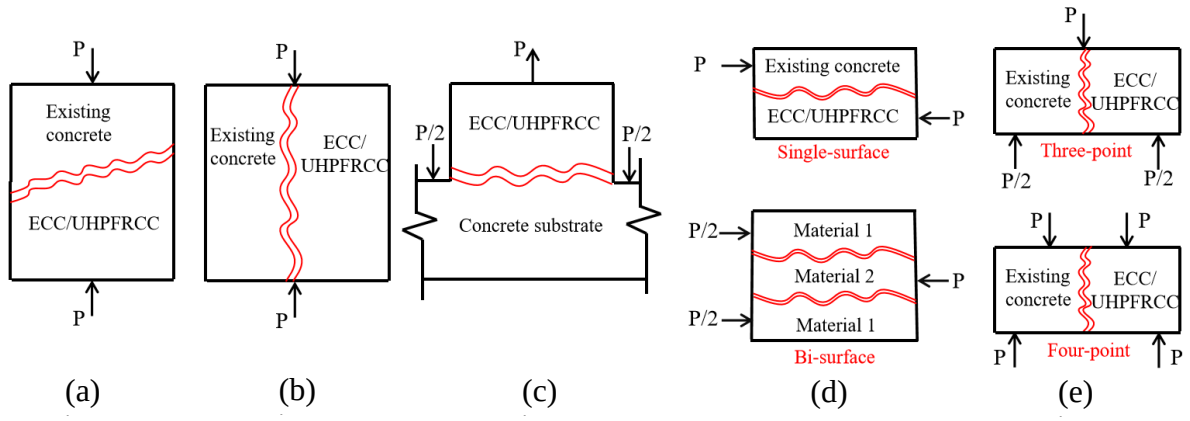



**Fig. 7.** The bonding strength test techniques: (a) Slant shear test; (b) Splitting tensile test; (c) Pull-off test; (d) Shear test; (e) Flexural test

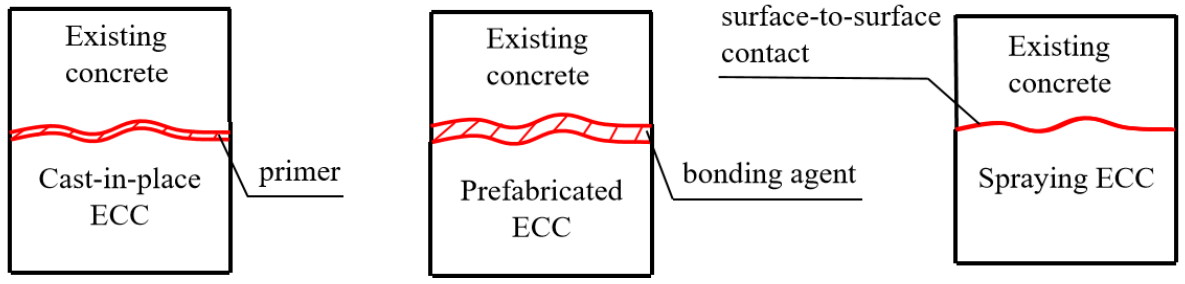
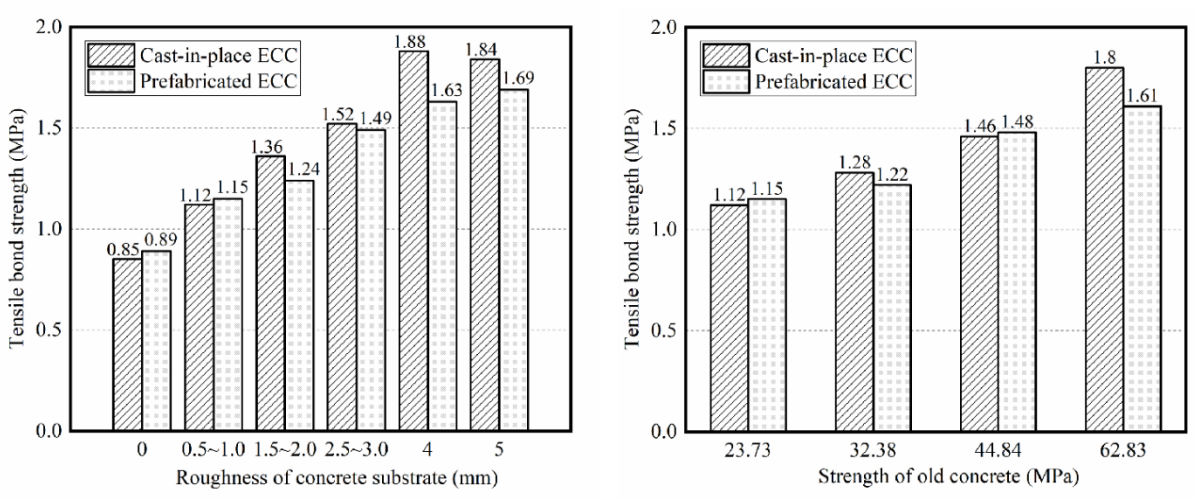
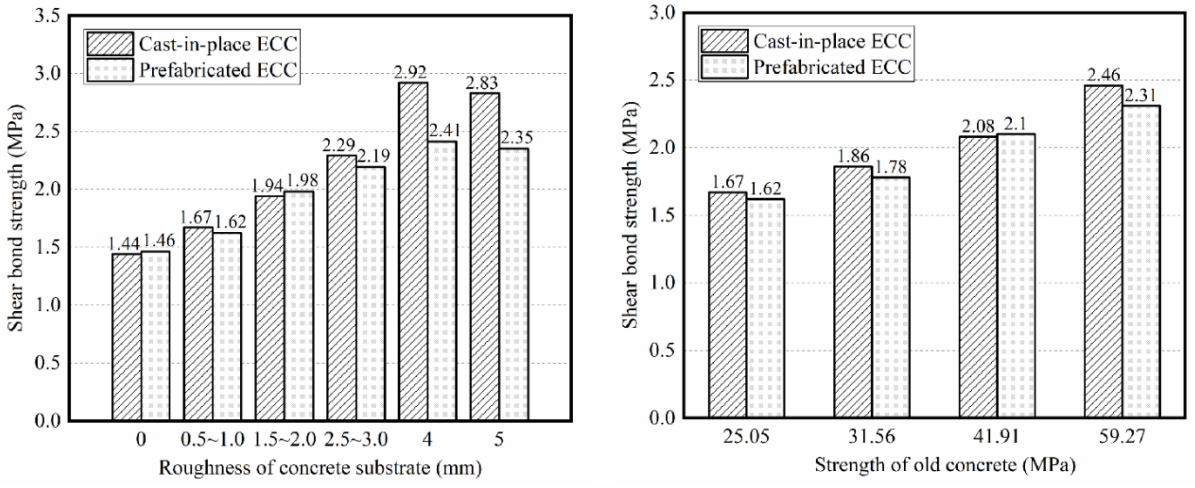


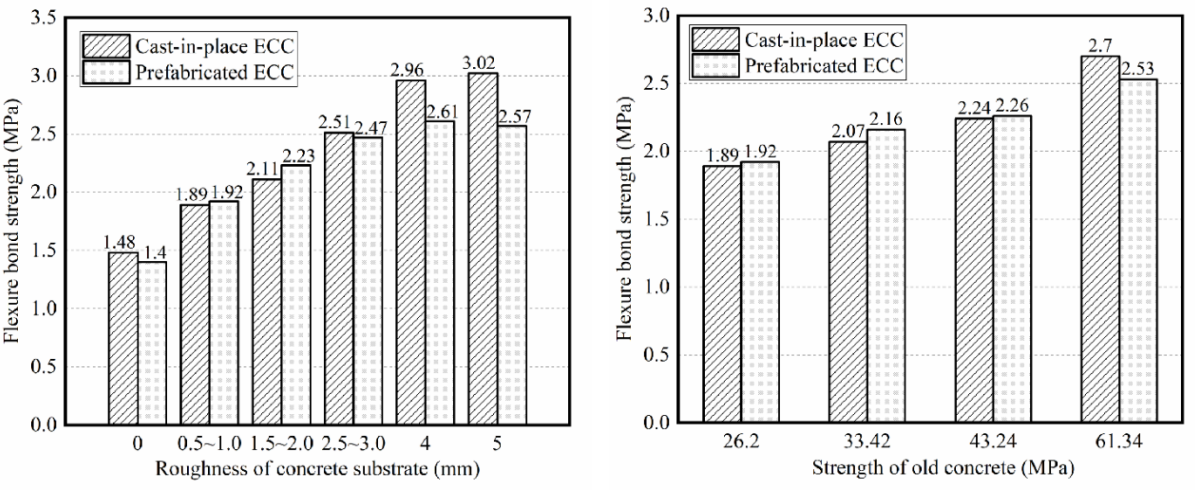

**Fig. 8.** The typical bonding forms of ECC to existing concrete




(a) Pull off tests [83]




(b) Bi-surface shear tests [84]




(c) Four-point flexural tests [82]

**Fig. 9.** Relations between the bond strength of the interface and the roughness/strength of concrete

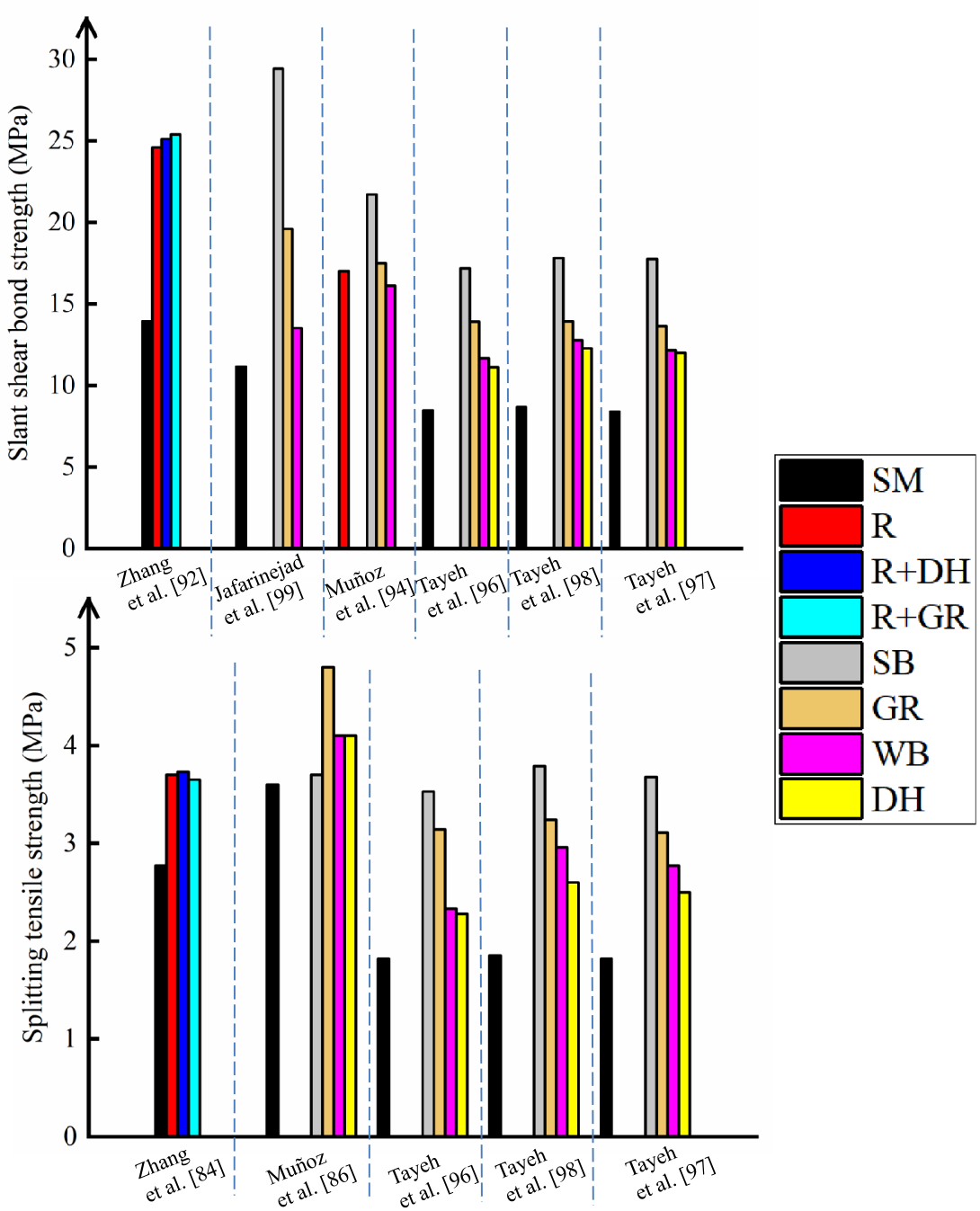
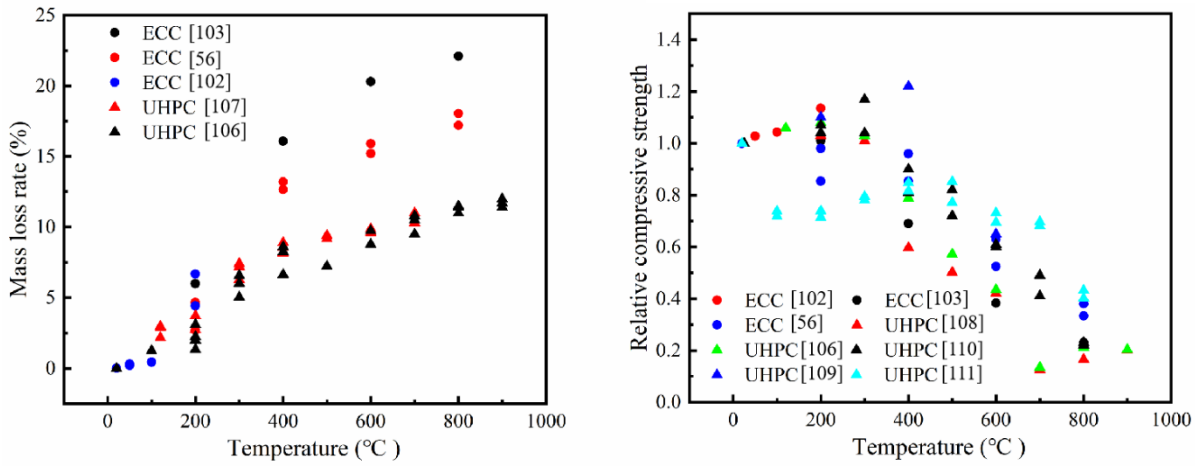
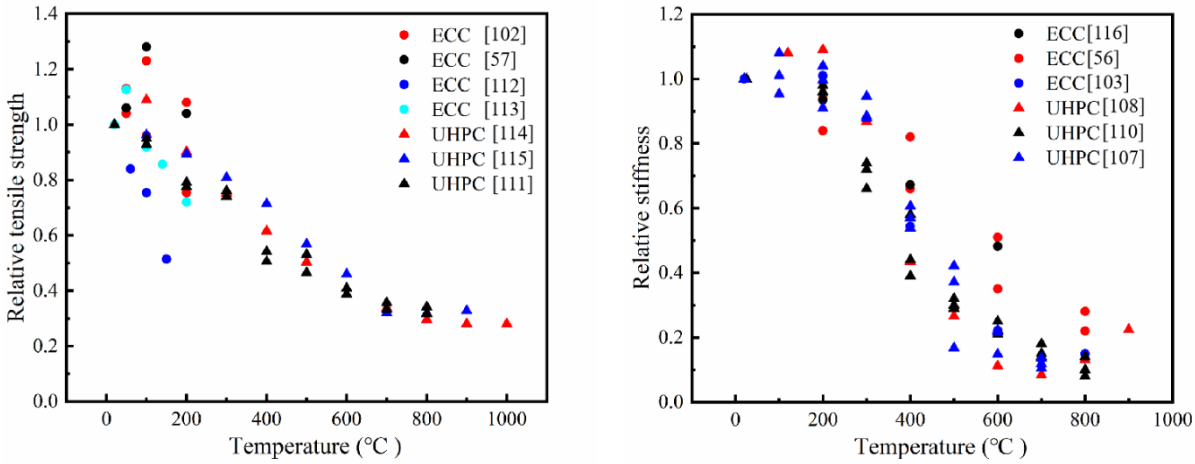



**Fig. 10.** Effects of different surface preparation methods on the UHPC-to-concrete bond strength

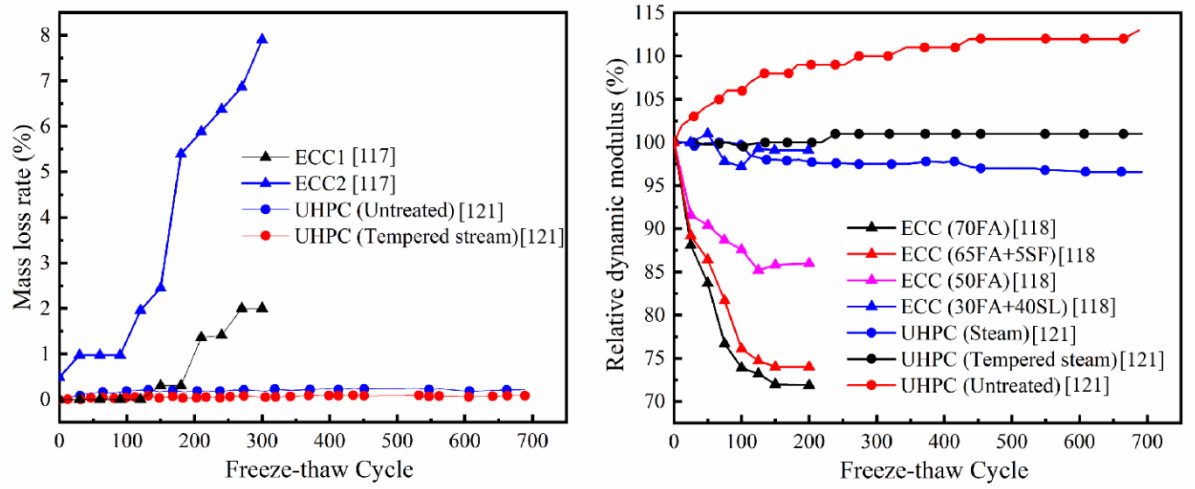



(a) Mass loss rate (b) Relative compressive strength



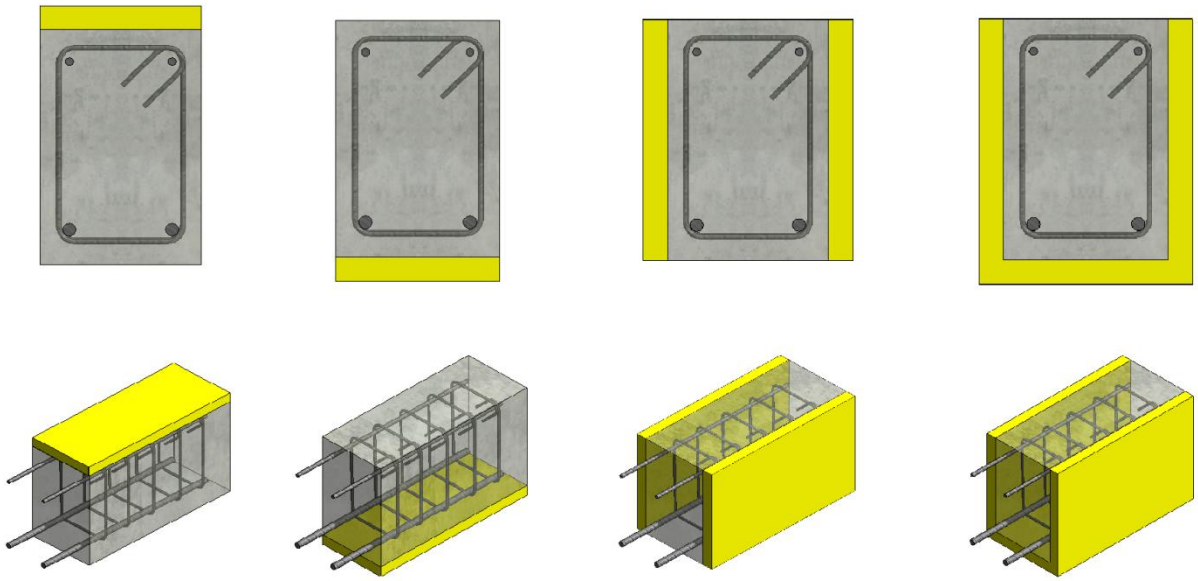

(c) Relative tensile strength (d) Relative stiffness

**Fig. 11.** Material properties of ECC/UHPC at different temperatures



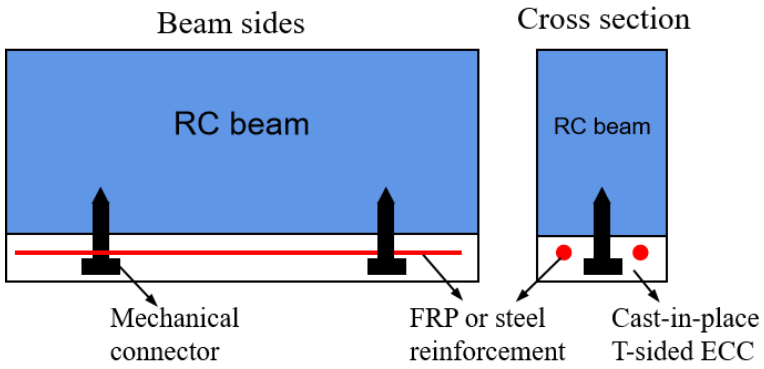

(a) Mass loss rate (b) Relative dynamic modulus

**Fig. 12.** The comparison on the freeze-thaw resistances of ECC and UHPC

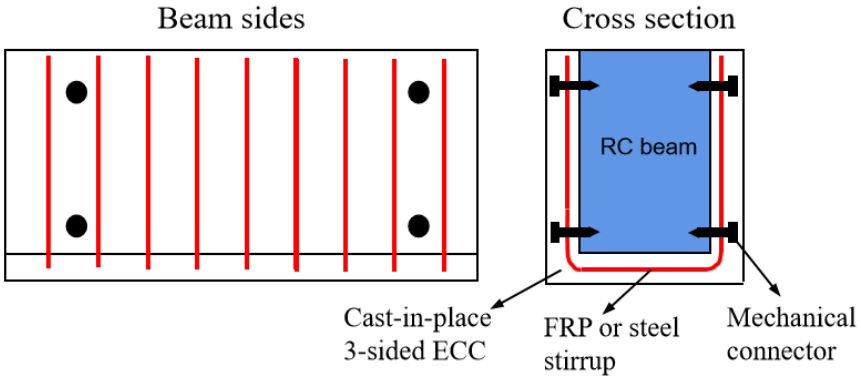


(a) C-sided (b) T-sided (c) 2-sided (d) 3-sided

**Fig. 13.** Four different forms of strengthening schemes using ECC/UHPC layers for RC beams

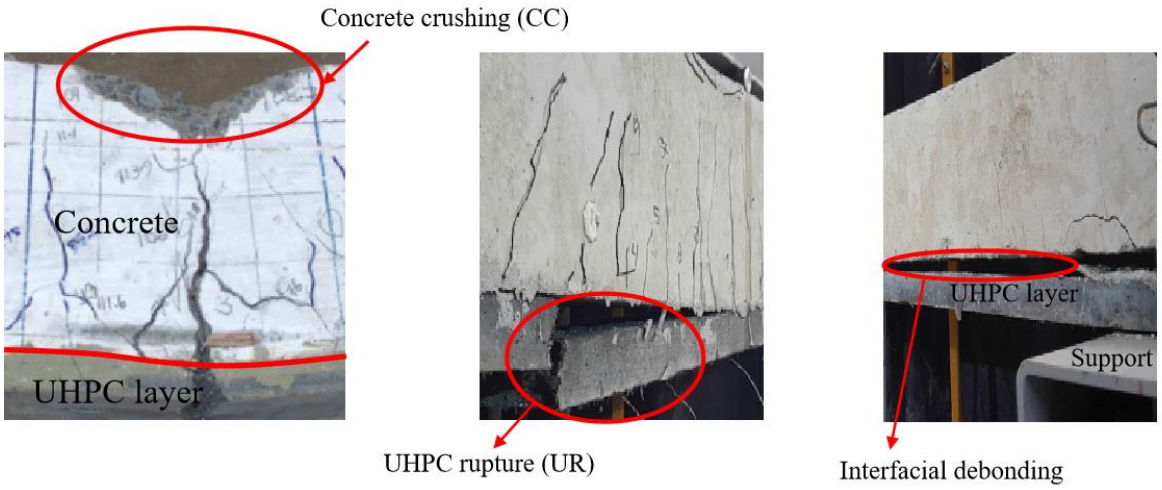



(a) Flexure strengthening



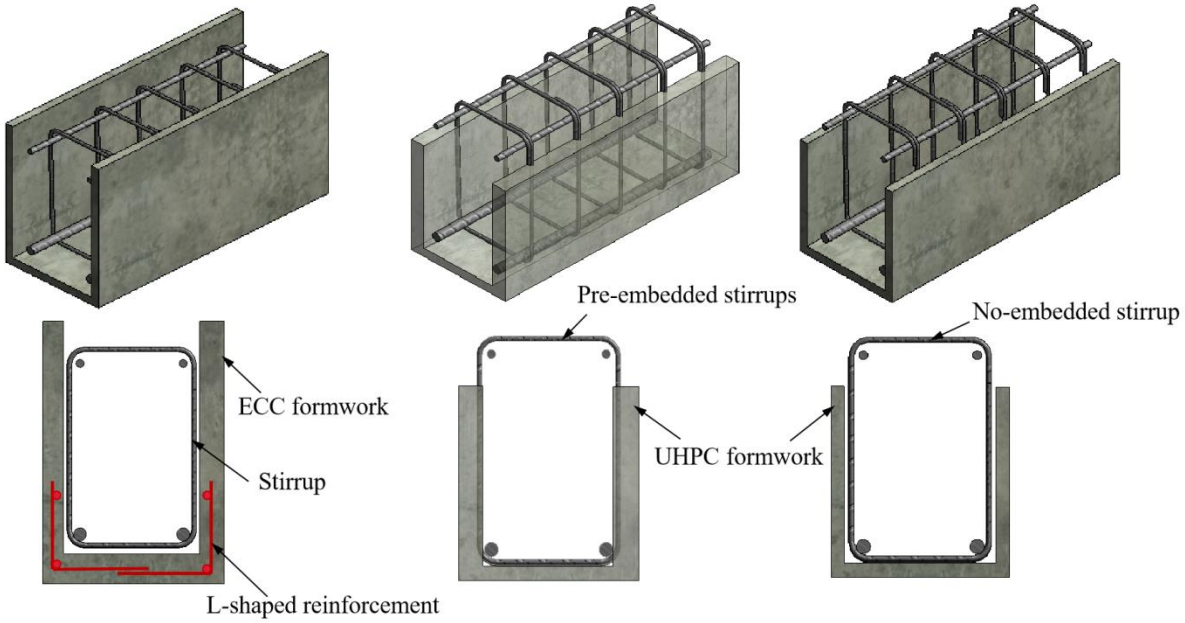

(b) Flexure-shear strengthening

**Fig. 14.** ECC strengthening systems for RC beams




(a) CC failure [140] (b) UR failure [135] (c) Debonding failure [135]

**Fig. 15.** Typical failure modes of T-sided UHPC layer reinforced RC beams




(a) (b) (c)

**Fig. 16.** Typical U-shaped ECC/UHPFRCC permanent formwork for RC beams

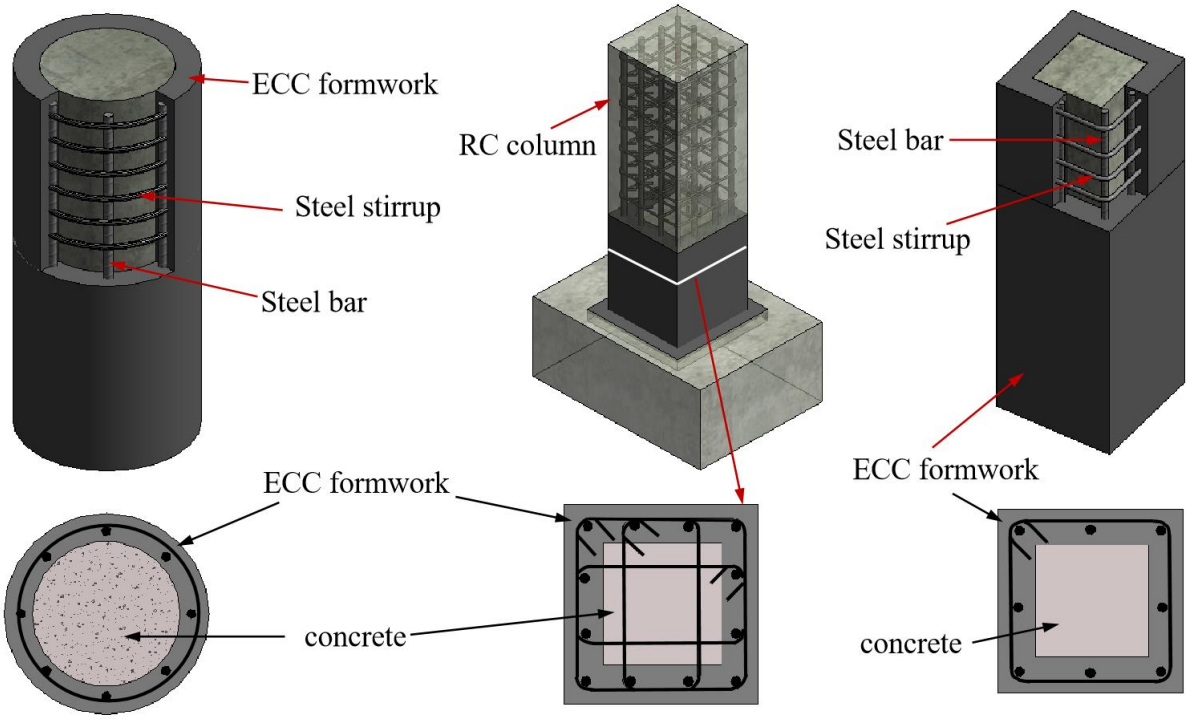



**Fig. 17.** Typical ECC permanent formwork for RC columns

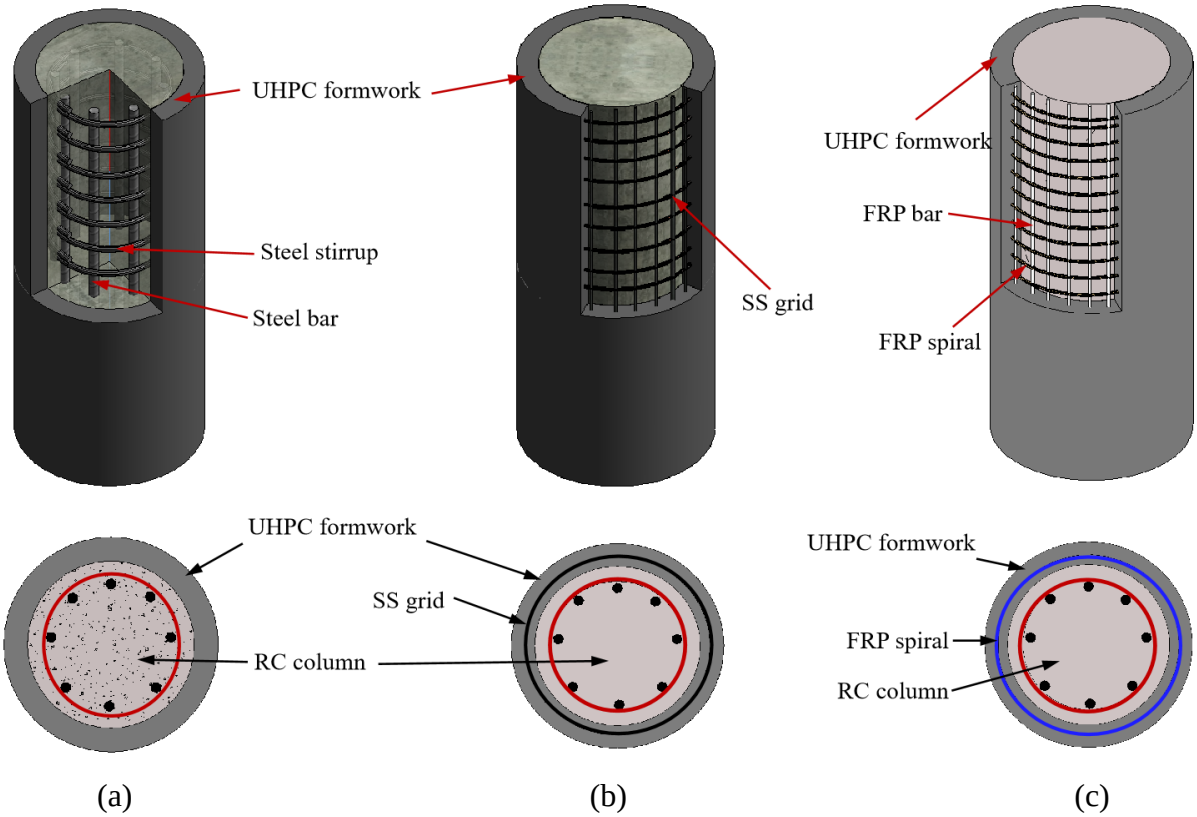
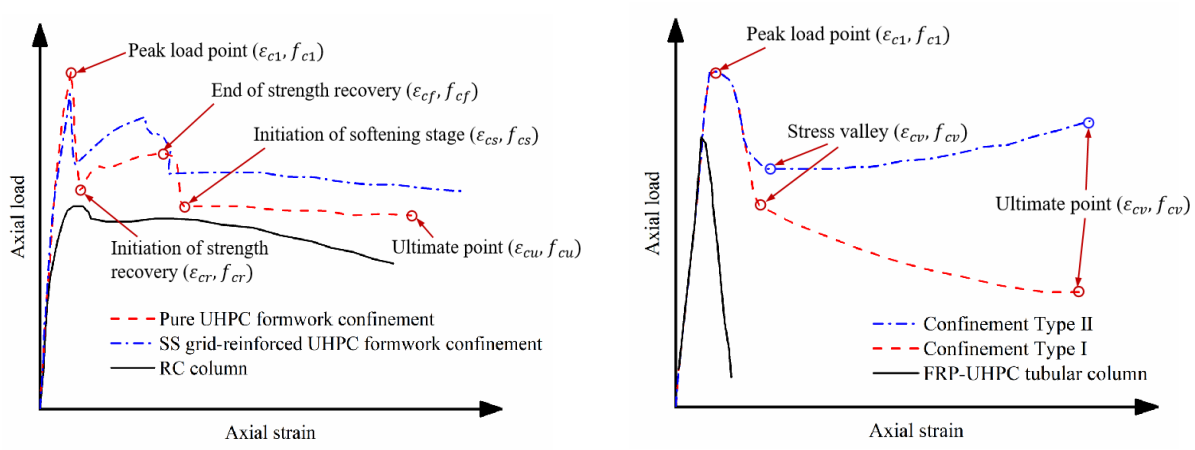



**Fig. 18.** Typical UHPC permanent formwork for RC columns




(a) Pure/SS-grid-reinforced UHPC formwork [50] (b) FRP-UHPC tubular formwork [159]

**Fig. 19.** Typical axial load-strain curves of concrete columns confined with UHPC formwork

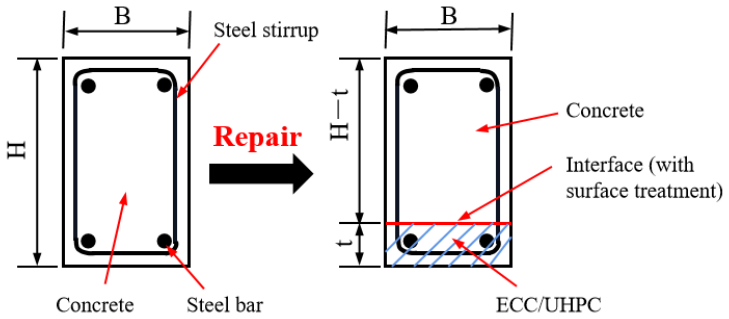
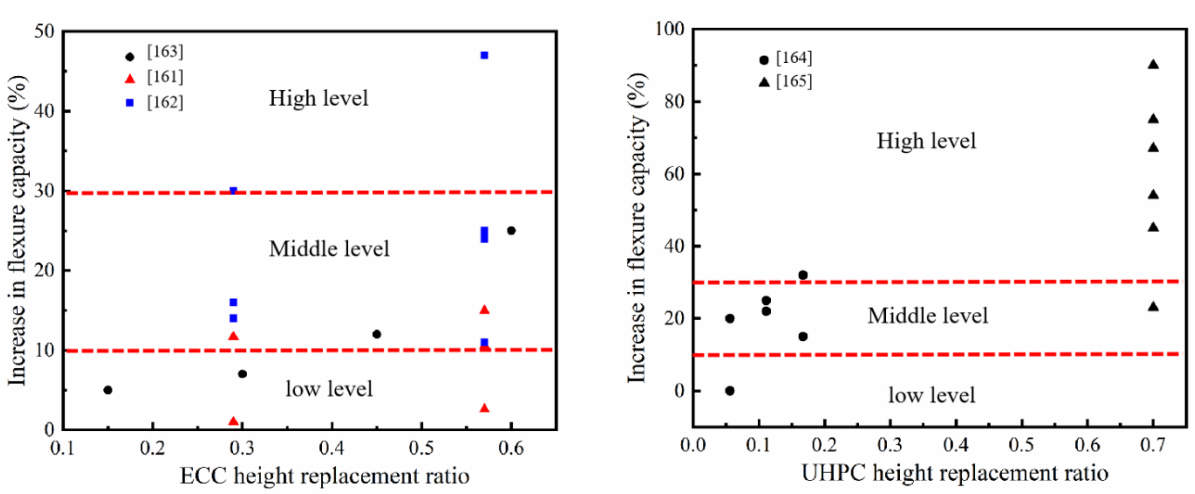



**Fig. 20.** The ECC/UHPC repairing RC beams




(a) ECC-NSC composite beam (b) UHPC-NSC composite beam

**Fig. 21.** The relation between height replacement ratio and increase in flexure capacity

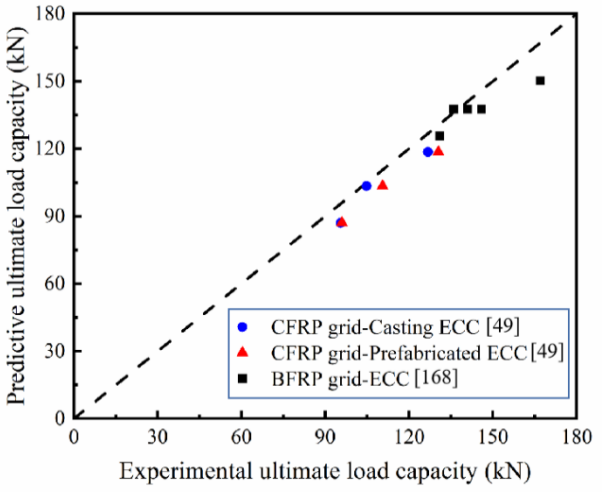



**Fig. 22.** The comparison between experimental results and model predictions for the ultimate load capacities

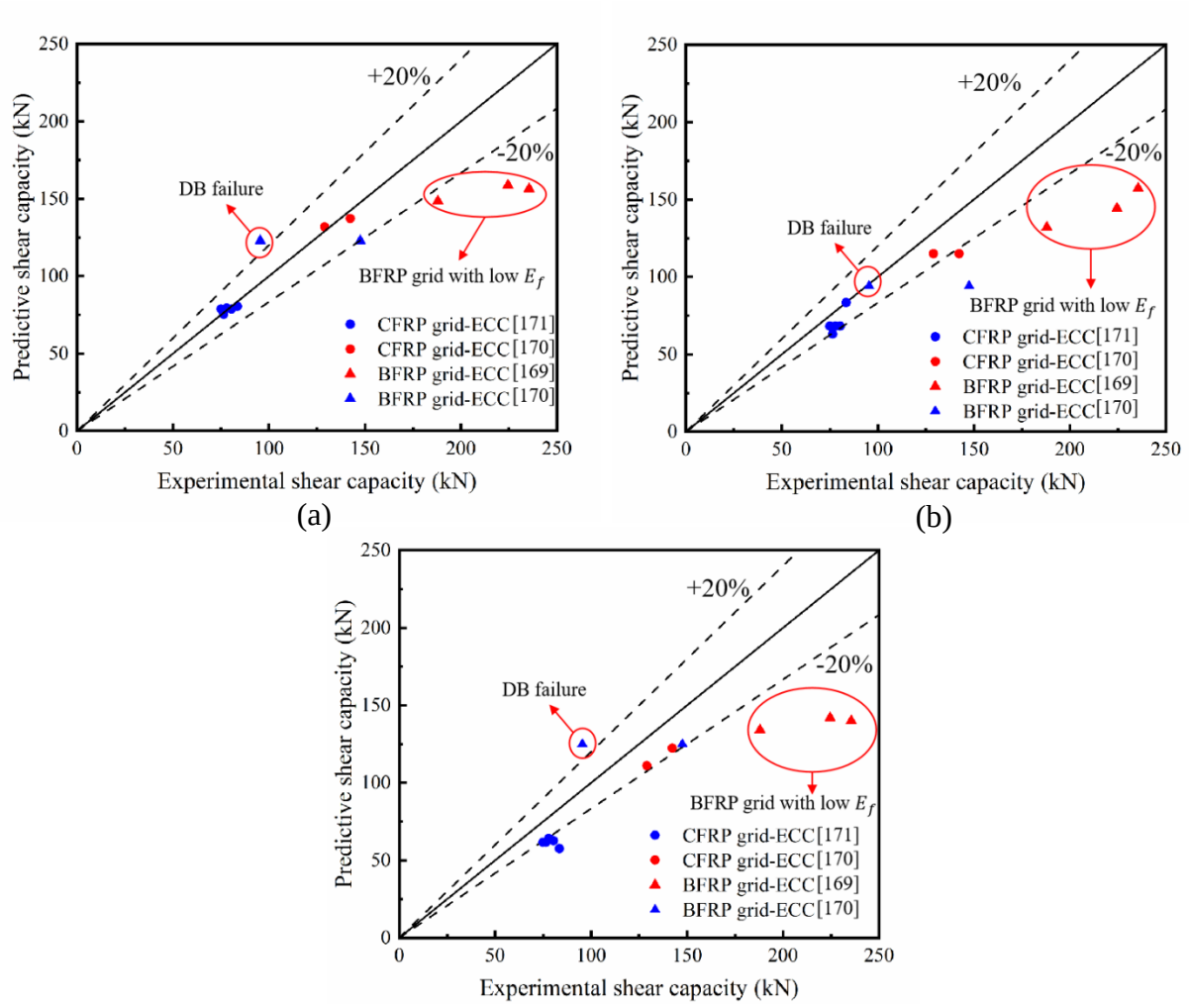



**Fig. 23.** The comparison between experimental results and model predictions for the shear capacity: (a) Guo et al.'s model [171] and JSCE code [178,179]; (b) ACI 549.4R-20 [176]

and JSCE code [178,179]; (b) Cai et al.'s model [177] and Chinese code [180]

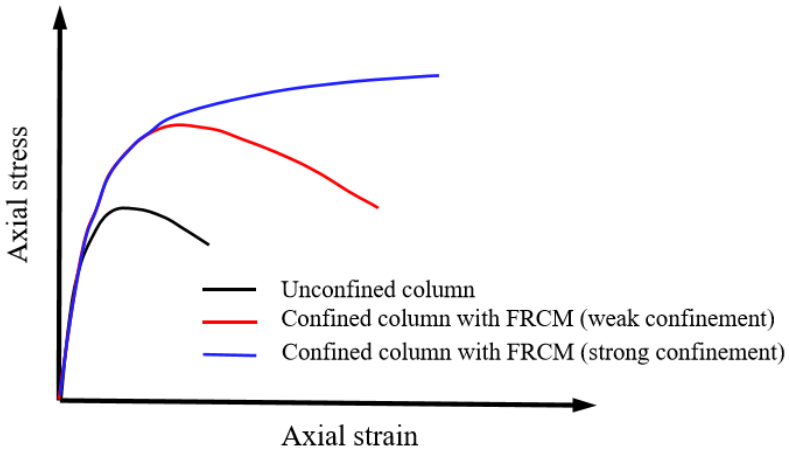



**Fig. 24.** Typical axial stress-strain curves of columns confined with FRCM

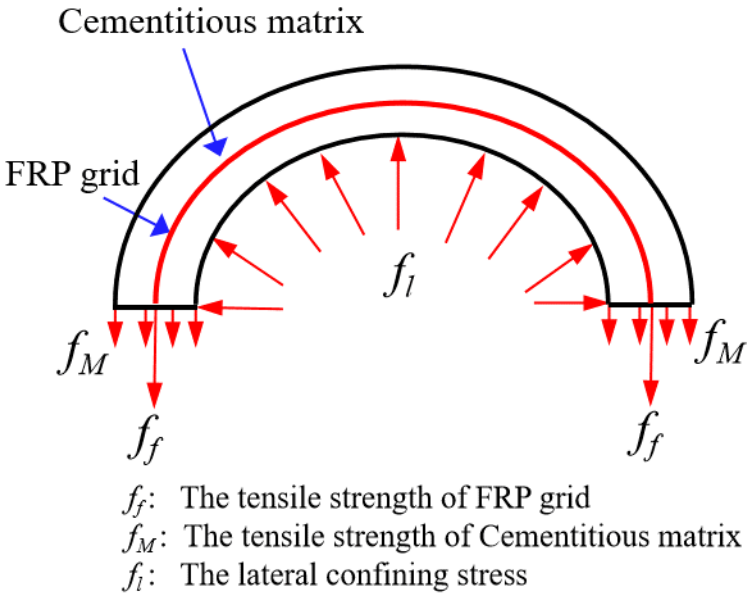



**Fig. 25.** Diagram of a circular cross-section confined with FRP grid reinforced matrix [181]

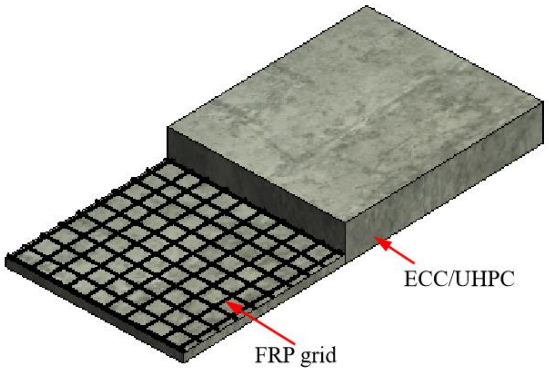
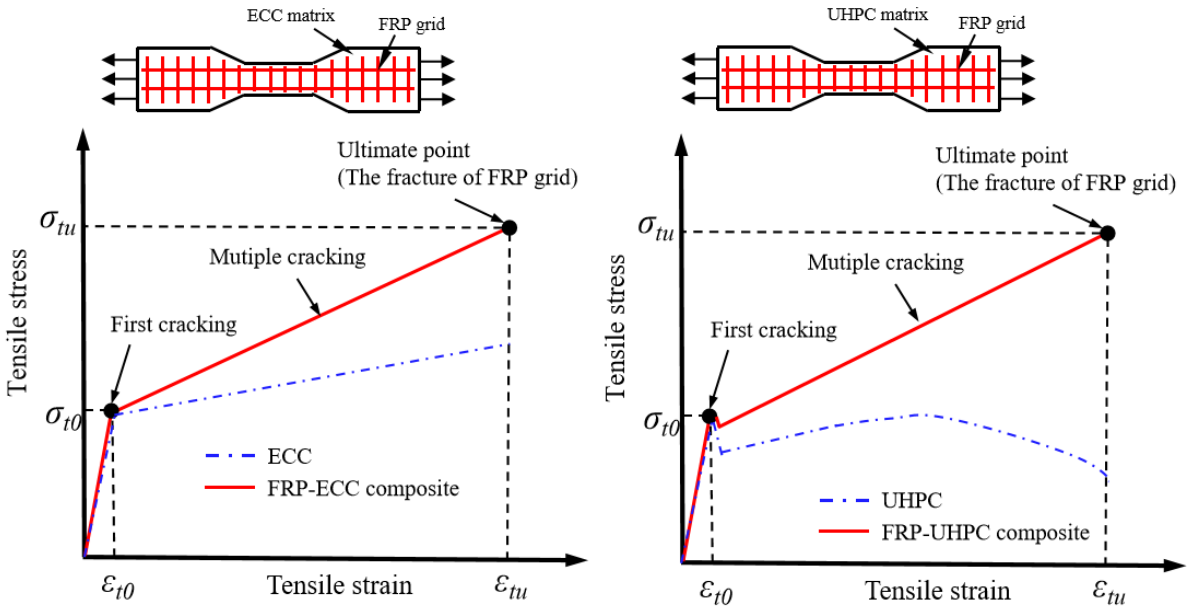



**Fig. 26.** FRP-ECC/UHPC composite plates




(a) FRP-ECC (b) FRP-UHPC

**Fig. 27.** Typical tensile stress-strain curves of FRP grid-reinforced ECC/UHPC composites

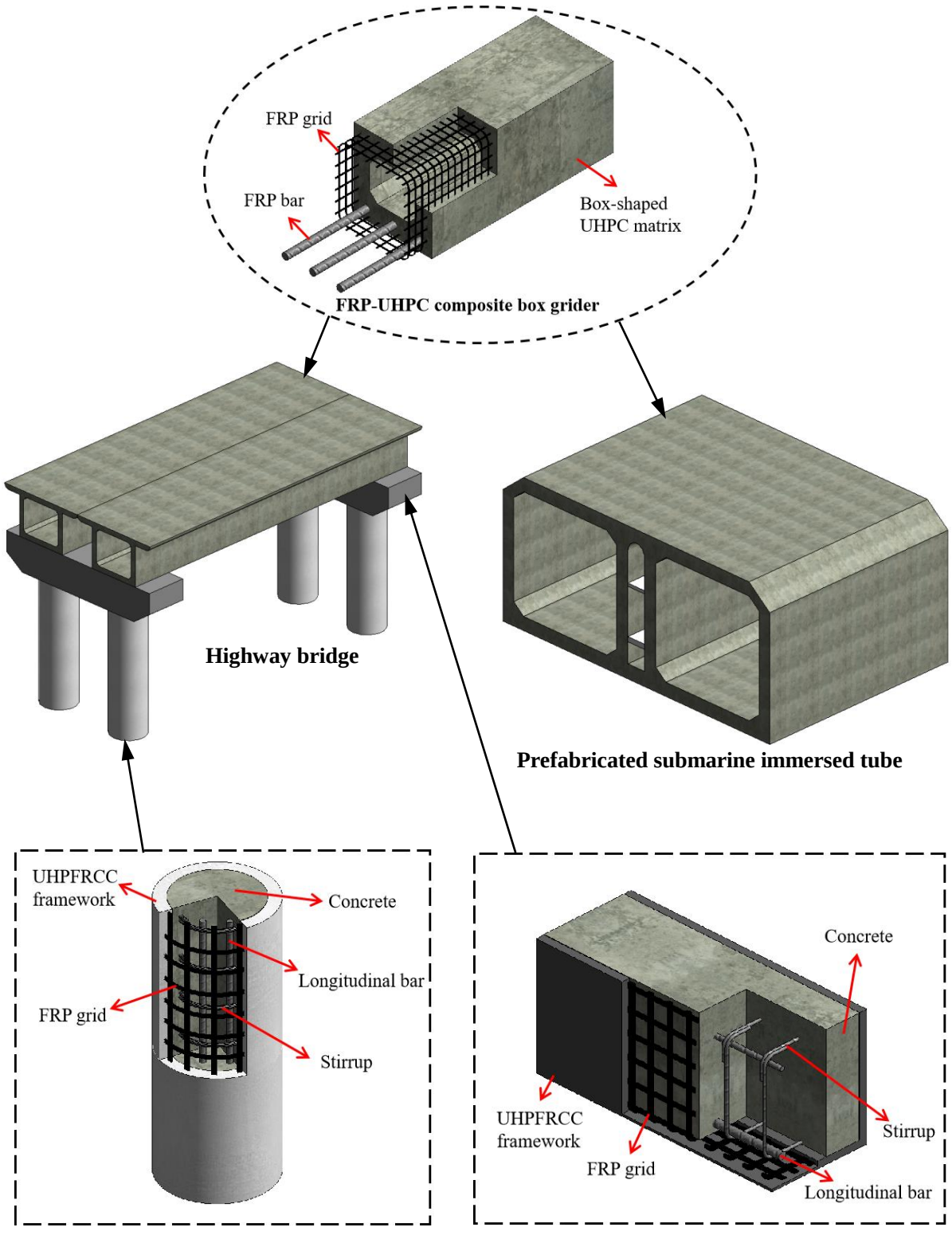



**Fig. 28.** Application prospects of FRP-UHPC composites